19. SITE 731[1]

Shipboard Scientific Party[2]

HOLE 731A

Date occupied: 1 October 1987

Date departed: 4 October 1987

Time on hole: 2 days, 17 hr, 30 min

Position: 16°28.229′N, 59°42.149′E

Water depth (sea level; corrected m, echo-sounding): 2365.8

Water depth (rig floor; corrected m, echo-sounding): 2376.3

Bottom felt (m, drill pipe): 2370.9

Penetration (m): 409.0

Number of cores: 43

Total length of cored section (m): 409.0

Total core recovered (m): 359.28

Core recovery (%): 87.8

Oldest sediment cored:
Depth sub-bottom (m): 409.0
Nature: turbiditic silty clay
Age: early Miocene to late Oligocene (NP25?)
Measured velocity (km/s): 1.67–1.75

HOLE 731B

Date occupied: 4 October 1987

Date departed: 5 October 1987

Time on hole: 1 day, 12 hr, 45 min

Position: 16°28.229′N, 59°42.149′E

Water depth (sea level; corrected m, echo-sounding): 2365.8

Water depth (rig floor; corrected m, echo-sounding): 2376.3

Bottom felt (m, drill pipe): 2370.9

Penetration (m): 457.1

Number of cores: 5

Total length of cored section (m): 48.4

Total core recovered (m): 14.97

Core recovery (%): 31

Oldest sediment cored:
Depth sub-bottom (m): 457.1
Nature: turbiditic silty clay
Age: early Miocene to late Oligocene (NP25?)
Measured velocity (km/s): 1.58

HOLE 731C

Date occupied: 5 October 1987

Date departed: 9 October 1987

Time on hole: 4 days, 3 hr, 15 min

Position: 16°28.229′N, 59°42.149′E

Water depth (sea level; corrected m, echo-sounding): 2365.8

Water depth (rig floor; corrected m, echo-sounding): 2376.3

Bottom felt (m, drill pipe): 2370.9

Penetration (m): 994.2

Number of cores: 24

Total length of cored section (m): 154.7

Total core recovered (m): 59.81

Core recovery (%): 39

Oldest sediment cored:
Depth sub-bottom (m): 994.2
Nature: turbiditic silty clay
Age: early Miocene to late Oligocene (NP25?)
Measured velocity (km/s): 2.24

Principal Results: Site 731 is located in the western Arabian Sea on the Owen Ridge. Scientific objectives for drilling at Site 731 were to recover a continuous Neogene and possibly Paleogene sequence of pelagic and turbiditic sediments from the crest of the Owen Ridge.

The most significant findings at Site 731 are:

1. The thick turbidite sequence from 320 to 994 mbsf, which is characteristic of deep-sea fan deposition from the Indus Fan;
2. The gradual transition from clastic turbiditic depositional mode to pelagic sedimentation in the upper lower Miocene, which marks the uplift of Owen Ridge over the reach of turbidites and above the lysocline;
3. The onset of opaline sedimentation in the upper Miocene concomitant with the onset of cyclic variations in sedimentary properties;
4. The excellent correlation of magnetic susceptibility records between all three sites on the Owen Ridge (721, 722, and 731).

Site 731 penetrated to 994.2 mbsf and recovered sediments that range from possibly Oligocene (NP25) to late Pleistocene in age. The section here and at nearby Sites 721 and 722 provide an excellent record of the onset and evolution of monsoonal upwelling from the late middle Miocene to the Pliocene-Pleistocene. They provide insights into the relationship of orbital changes and the uplift of the Himalaya to the history of monsoon-related upwelling and eolian sedimentation on the Owen Ridge, as well as on tectonic uplift of Owen Ridge and the evolution of Owen Basin.

BACKGROUND AND OBJECTIVES

Site 731 is located at 16°28.229′N and 59°42.149′E in 2366 m water depth, just below the crest of the Owen Ridge. The location of Site 731 is shown in Figure 1, and its depositional and structural setting is shown in Figure 2. The site was selected near the intersection of seismic Lines 35 and 45 collected on the site survey (RC2704). The site is located about 6 km south of DSDP Site 224, which penetrated 792 mbsf to basement. Total sediment thickness at Site 731 is about 1.5 s (about 1800 m) and the target depth was to recover as much of the section as time permitted. The upper 0.42 s of the section (~400 mbsf) is characterized by relatively smooth, low-amplitude parallel reflectors that lie above a prominent but smooth reflector, which was denoted seismic reflector C at Sites 721 and 722. This reflector

[1] Prell, W. L., Niitsuma, N., et al., 1989. *Proc. ODP, Init. Repts.*, 117: College Station, TX (Ocean Drilling Program).

[2] Shipboard Scientific Party is as given in the list of Participants preceding the contents.

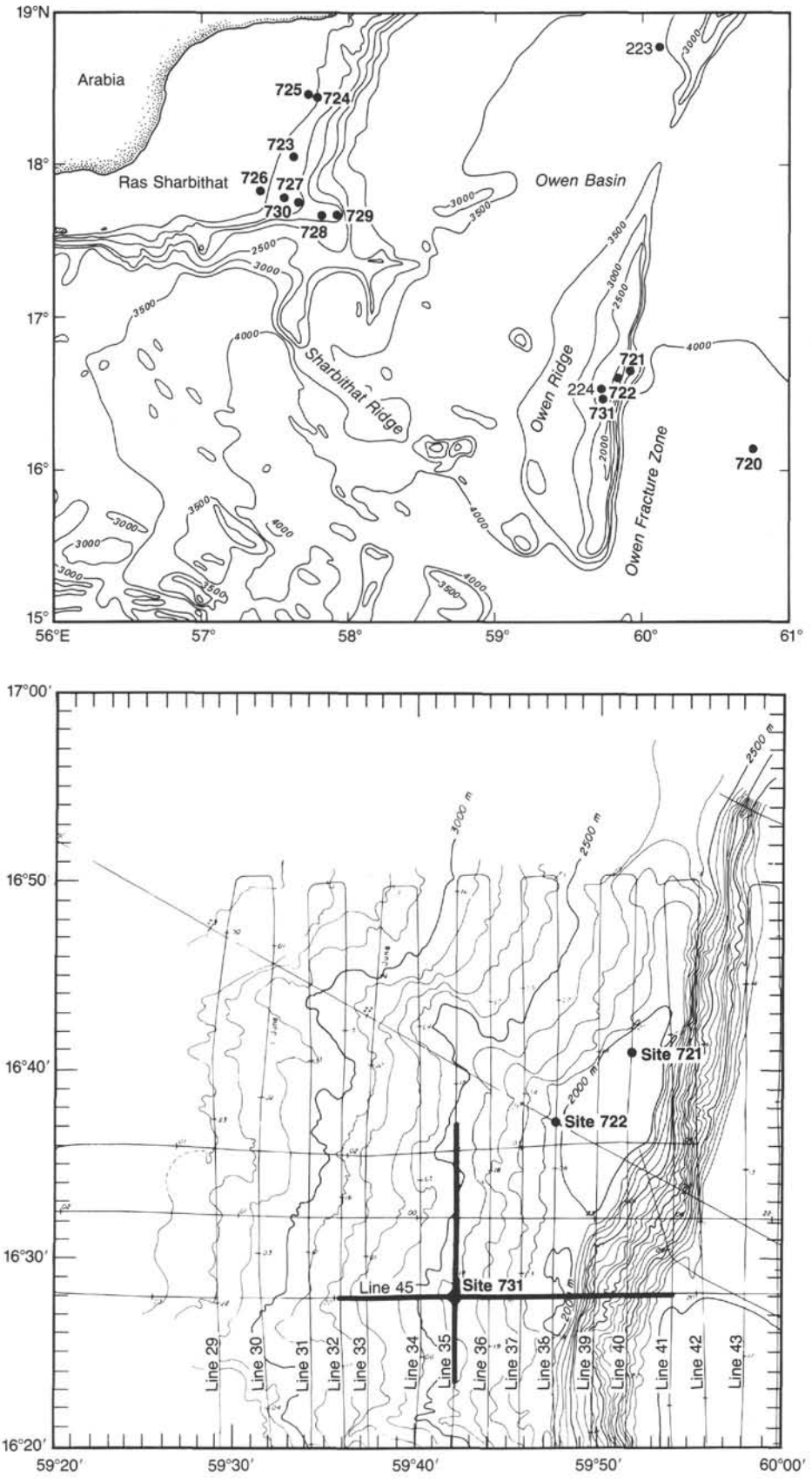

Figure 1. The location of Site 731 on the Owen Ridge. Bathymetry is from the Sea Beam site survey data (Prell, unpubl. data). The portions of RC2704 seismic lines Lines 35 and 45 (shown in Fig. 2) crossing Site 731 are indicated by the heavy lines.

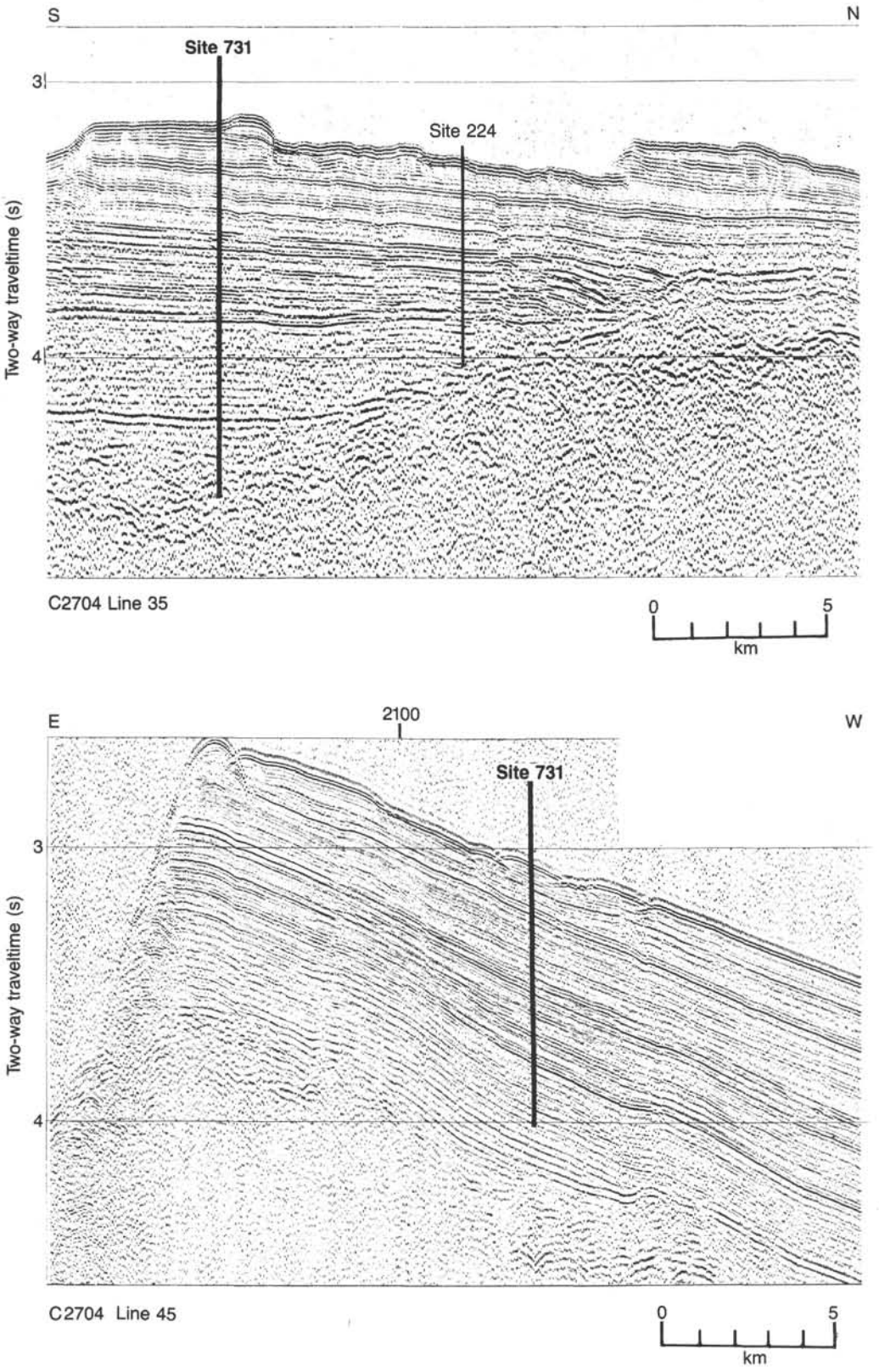

Figure 2. The seismic reflection profiles, Lines 35 and 45 of RC2704, that intersect Site 731. Track lines are shown in Figure 1.

marks the top of the turbiditic sequence that formed the lithologic Unit IV at Sites 721 and 722. The sequence of high-amplitude reflectors extends down to about 0.75 s (~750 mbsf) and onlap onto the basement peak where DSDP Site 224 was cored. This high-amplitude sequence is underlain from 0.75 s to 1.10 s by lower-amplitude reflectors that are parallel and also onlap northward onto basement. Correlation of the sections at DSDP Site 224 and Sites 721 and 722 with the seismic data from the site survey indicates that seismic reflector C, which marks the upper boundary of the turbidites, is of late early Miocene age and that the boundary between the high-amplitude and low-amplitude reflection sequences may be about late Oligocene in age. The age of the lower sequences is unknown, but is expected to postdate the lower Eocene sediments recovered at DSDP Site 224.

OPERATIONS

The seismic survey of Site 731 began at 0600 hr on 1 October after a 13-hr transit from Site 730. By 0730 Site 731 had been located, the beacon was deployed, the seismic gear was retrieved, and the rig was positioned in 2366 m water depth. The position was assessed as 16°28.229′N and 59°42.149′E by Global Positioning Satellite (GPS). After 76 stands of pipe had been tripped, the ship was inclined 5° to perform a bending stress test with bending joint and stress sub incorporated in the string. The test was finished successfully and the mud line of Hole 731A was shot by 2030 hr on 1 October. Hydraulic piston (APC) Cores 117-731A-1H to -7H recovered 102.5% of the interval from 0.0 to 67.0 mbsf, and extended core barrel (XCB) Cores 117-731A-8X through -43X (67.0–409.0 mbsf) yielded 88% of the cored sediments (Table 1). Upon cutting Core 117-731A-43X, the XCB cutting shoe broke, and attempts to dislodge the remnants of the shoe with a center bit failed. The string was pulled to the rig floor, and Hole 731B was spudded after offsetting the rig 10 m north at 0600 on 4 October. The hole was drilled with a polycrystalline diamond drilling bit and a center bit to 408.7 mbsf and coring commenced in XCB mode to Core 117-731B-5X (408.7–457.1 mbsf total depth). The core barrel flared at this depth and after attempts to grind it down had failed, coring in Hole 731B was terminated. Recovery in Hole 731B averaged 31% (Table 1).

Again the rig was offset 10 m to the north, and Hole 731C was spudded with a rotary coring (RCB) assembly at 1815 on 5 October. We drilled and spot-cored through the very thick turbidite sequence previously encountered on Owen Ridge, hoping to reach underlying sediments in the remaining time allocated for Leg 117. At a total depth of 994.2 mbsf, still in lower Miocene to upper Oligocene(?) turbidites, coring was suspended and the hole was prepared for logging. Hole 731C had 111.5 m core recovered, and total recovery during Leg 117 was established at 4367.2 m.

The hole was conditioned for logging, and two logging runs were performed with the bit positioned at 85 mbsf; 14 m of fill was encountered at the bottom of the hole. Two logging strings were run: the first consisted of DIT, BHC, GR, and CAL, while the second combined GST, CNT, NGT, and GPIT. Logging conditions were good, and log quality was excellent.

The ship was underway to Mauritius at 1700 hr on 9 October, 1987.

LITHOSTRATIGRAPHY

Lithologic Units

Sediments recovered at Site 731 range from late Oligocene(?) or early Miocene to late Pleistocene or Holocene in age. Lithologies consist predominantly of nannofossil and marly nannofossil ooze and chalk, fine-grained turbidites, and coarse-grained turbidites; occurrences of foraminifer-nannofossil chalk and siliceous-bearing to diatomaceous marly nannofossil ooze/chalk are locally important. The sedimentary sequence is divided into four lithologic units based on visual core descriptions, smear slide analysis of sediment composition, and calcium carbonate contents (Figs. 3, 4, and 5; Tables 2 and 3). Lithologic Unit I is divided into two subunits. Three lithofacies are identified in lithologic Unit IV.

Table 1. Coring summary, Site 731.

Core no.	Date (Oct. 1987)	Time	Depth (mbsf)	Cored (m)	Recovered (m)	Recovery (m)
117-731A-						
1H	1	2125	0–9.8	9.8	9.87	101.0
2H	1	2155	9.8–19.3	9.5	9.84	103.0
3H	1	2225	19.3–28.8	9.5	9.94	104.0
4H	1	2300	28.8–38.3	9.5	9.77	103.0
5H	1	2340	38.3–47.8	9.5	9.22	97.0
6H	2	0015	47.8–57.3	9.5	9.94	104.0
7H	2	0050	57.3–67.0	9.7	10.10	104.1
8X	2	0235	67.0–76.7	9.7	6.01	61.9
9X	2	0320	76.7–86.4	9.7	8.60	88.6
10X	2	0400	86.4–96.0	9.6	9.65	100.0
11X	2	0440	96.0–105.7	9.7	9.32	96.1
12X	2	0515	105.7–115.4	9.7	9.74	100.0
13X	2	0555	115.4–125.0	9.6	9.17	95.5
14X	2	0635	125.0–134.7	9.7	7.37	76.0
15X	2	0725	134.7–144.4	9.7	9.61	99.1
16X	2	0800	144.4–154.0	9.6	9.68	101.0
17X	2	0835	154.0–163.7	9.7	9.76	100.0
18X	2	0925	163.7–173.4	9.7	9.83	101.0
19X	2	1105	173.4–183.1	9.7	9.77	101.0
20X	2	1145	183.1–192.8	9.7	9.69	99.9
21X	2	1215	192.8–202.5	9.7	8.81	90.8
22X	2	1245	202.5–212.2	9.7	9.60	98.9
23X	2	1315	212.2–221.9	9.7	9.49	97.8
24X	2	1350	221.9–231.6	9.7	8.69	89.6
25X	2	1430	231.6–241.3	9.7	9.78	101.0
26X	2	1610	241.3–250.9	9.6	7.12	74.1
27X	2	1645	250.9–260.6	9.7	9.45	97.4
28X	2	1720	260.6–270.2	9.6	9.70	101.0
29X	2	1810	270.2–279.9	9.7	9.79	101.0
30X	2	1930	279.9–289.6	9.7	9.86	101.0
31X	2	2135	289.6–299.2	9.6	5.22	54.4
32X	2	2210	299.2–308.9	9.7	9.31	96.0
33X	3	0015	308.9–315.5	6.6	4.49	68.0
34X	3	0210	315.5–322.1	6.6	4.12	62.4
35X	3	0355	322.1–331.7	9.6	9.31	97.0
36X	3	0535	331.7–341.3	9.6	0.13	1.4
37X	3	0720	341.3–351.0	9.7	9.63	99.3
38X	3	0850	351.0–360.7	9.7	9.87	102.0
39X	3	1010	360.7–370.4	9.7	5.40	55.7
40X	3	1305	370.4–380.0	9.6	6.69	69.7
41X	3	1505	380.0–389.7	9.7	4.59	47.3
42X	3	1430	389.7–399.4	9.7	1.70	17.5
43X	3	1730	399.4–409.0	9.6	9.65	100.0
				409.0	359.28	

Unit I (Depth: 0–146.5 mbsf; Age: late Miocene to late Pleistocene/Holocene)

Core 117-731A-1H to Section 117-731A-16X-2, 60 cm.

Lithologic Unit I consists of alternating light and dark beds of nannofossil ooze and marly nannofossil ooze, with limited occurrences of foraminifer-nannofossil ooze, diatomaceous foraminifer-nannofossil ooze, and diatomaceous marly nannofossil ooze. Nannofossil-rich calcitic silty clay is present in very minor amounts. These lithologies are interbedded on a scale of 0.05–1.50 m. The relative abundance of diatoms in the upper 66 m of Unit I is used to define lithologic Subunit IA, while Subunit IB contains only trace amounts of diatoms (Fig. 4).

Table 1 (continued).

Core no.	Date (Oct. 1987)	Time	Depth (mbsf)	Cored (m)	Recovered (m)	Recovery (m)
Hole 731B-						
1X	4	2145	408.7–418.3	9.6	0.83	8.6
2X	4	2300	418.3–428.1	9.8	0.95	9.7
3X	5	0030	428.1–437.7	9.6	2.31	24.0
4X	5	0220	437.7–447.4	9.7	6.47	66.7
5X	5	1330	447.4–457.1	9.7	4.41	45.4
				48.4	14.97	
Hole 731C-						
1W	6	0810	351.7–502.4	150.7	2.55	1.7
2R	6	1015	502.4–512.1	9.7	6.35	65.4
3W	6	1300	512.1–560.2	48.1	3.02	6.3
4R	6	1415	560.2–569.9	9.7	1.38	14.2
5W	6	1615	569.9–618.1	48.2	7.22	15.0
6R	6	1730	618.1–627.8	9.7	1.22	12.6
7W	6	2045	627.8–675.9	48.1	4.68	9.7
8R	6	2155	675.9–685.6	9.7	5.77	59.5
9W	7	0025	685.6–733.6	48.0	8.25	17.2
10R	7	0140	733.6–743.3	9.7	2.17	22.4
11W	7	0430	743.3–791.5	48.2	9.65	20.0
12R	7	0555	791.5–801.1	9.6	4.05	42.2
13W	7	0900	801.1–849.4	48.3	9.64	20.0
14R	7	1020	849.4–859.1	9.7	2.18	22.5
15W	7	1315	859.1–907.3	48.2	6.72	13.9
16R	7	1445	907.3–916.7	9.4	3.36	35.7
17R	7	1615	916.7–926.4	9.7	4.98	51.3
18R	7	1755	926.4–936.1	9.7	0.60	6.2
19R	7	1910	936.1–945.7	9.6	4.64	48.3
20R	7	2050	945.7–955.4	9.7	4.97	51.2
21R	7	2220	955.4–965.1	9.7	3.16	32.6
22R	7	2350	965.1–974.8	9.7	4.86	50.1
23R	8	0205	974.8–984.5	9.7	4.77	49.2
24R	8	0415	984.5–994.2	9.7	5.35	55.1
				642.5	111.54	

Subunit IA (Depth: 0–66.3 mbsf)

Subunit IA consists of gradationally interbedded nannofossil ooze, foraminifer-nannofossil ooze, and marly nannofossil ooze. The marly nannofossil oozes commonly grade to foraminifer-bearing or diatomaceous marly nannofossil oozes. Beds range in thickness from 0.05 to 1.50 m, generally with gradational and burrow-mottled contacts. Bioturbation is minor to moderate throughout Subunit IA, although identifiable trace fossils are absent. Light beds range in color from light gray (5Y 7/1, 5Y 7/2) and light greenish gray (10Y 7/2, 10Y 6/2, 5GY 7/1) to light olive gray (5Y 6/2) and pale olive (5Y 6/3). Dark beds range from pale olive (5Y 6/3) to olive (5Y 5/4, 5Y 5/3, 5Y 4/3). Dark beds contain 5%–20% more silty clay and 5%–20% more diatoms than the light beds. The average calcium carbonate content in Subunit IA is 66%, with a range from 48% to 78% (Table 3; Fig. 5). The higher calcium carbonate contents occur in the lighter beds.

Smear slide analysis (Fig. 4) indicates that nannofossils are the dominant sedimentary component in Subunit IA, although clay and detrital calcite abundances equal or exceed nannofossil contents in some of the marly nannofossil ooze beds. Foraminifer abundances exceed 10% in the first two cores at Hole 731A (approximately 0–20 mbsf), but fall below 10% for the remainder of the subunit. Nannofossil abundances range from 25% to 70%, with highest values in the lighter beds. Diatom abundances vary from 0% to 20%, with highest values in a diatomaceous foraminifer-nannofossil ooze in Core 117-731A-2H, a diatomaceous marly nannofossil ooze in Core 117-731A-4H, and a diatomaceous nannofossil-rich silty clay in Core 117-731A-7H. Clays and detrital calcite are the dominant terrigenous components, with abundances ranging from 5% to 30% for each; highest values are found in the darker beds of marly nannofossil ooze and calcitic silty clay. Other minerals present include quartz, mica, volcanic ash, dolomite, and opaque minerals, with abundances generally less than 5%.

Subunit IB (Depth: 66.3–146.5 mbsf)

Subunit IB also consists of alternating light and dark beds of nannofossil ooze and marly nannofossil ooze, but is distinguished from Subunit IA by the decreased abundance or absence of diatoms and foraminifers in smear slides (Fig. 4). Characteristics of the light and dark beds (colors, bedding thickness, and degree of bioturbation) are generally similar to those of Subunit IA, although white (5Y 8/1) nannofossil oozes and olive gray (5Y 4/2) to dark olive gray (5Y 3/2) nannofossil-rich calcitic silty clays are also observed in Subunit IB. Identifiable trace fossils, including *Planolites* and *Zoophycus*, are first identified in Subunit IB. Carbonate contents in Subunit IB average 67% and range from 46% to 85%, similar to the values in Subunit IA (Fig. 5; Table 3).

Smear slide analysis (Fig. 4) indicates that nannofossils remain the dominant sediment component in Subunit IB, with abundances ranging from 35% to 85%. As in Subunit IA, highest nannofossil contents occur in the lightest-colored beds. Foraminifer contents range from 0% to 8%, and average approximately 5%. Diatoms are present at abundances less than 5%, and are absent in much of Subunit IB. Clay contents range from 8% to 30%, averaging approximately 20%. Detrital calcite contents range from 0% to 30%, and average approximately 15%. Quartz abundances range from 0% to 10%, while mica, opaque minerals, and dolomite are present at abundances less than 5%.

Two unconformities are located within Subunit IB, and are tentatively located in Section 117-731A-10X, CC, to Core 117-731A-12X on the basis of nannofossil and radiolarian biostratigraphy (see "Biostratigraphy" section, this chapter). Although these unconformities presently are identified only from paleontological analysis, several lithostratigraphic features within these cores can be proposed as possible locations of the unconformities. The first hiatus superposes upper Pliocene sediments on lower Pliocene deposits, and lies between Sections 117-731A-10X, CC, and -11X-4. In contrast to the overlying beds, sharp contacts were observed at Section 117-731A-11X-1, 70 and 138 cm, while sharp and irregular contacts occurred at Section 117-731A-11X-2, 13, 45, 90, and 105 cm. The superjacent beds in Section 117-731A-11X-2 are distinctive in both color and degree of bioturbation, suggesting that the unconformity (or several smaller unconformities) occurs in that interval. The older unconformity superposes lower Pliocene sediments on upper Miocene deposits, and is located in Core 117-731A-12X. Sharp and irregular contacts occur at Section 117-731A-12X-6, 84-113 cm, while sharp bedding contacts occur at Section 117-731A-12X-7, 6-7 cm. These relationships suggest that the second hiatus at Site 731 is located within one of these intervals. More detailed biostratigraphic study will be required to locate these unconformities more precisely.

Unit II (Depth: 146.5–240.9 mbsf; Age: late Miocene)

Section 117-731A-16X-2, 60 cm, through Section 117-731A-25X-7.

Lithologic Unit II consists of alternating light and dark beds of nannofossil ooze/chalk, marly nannofossil ooze/chalk, diatomaceous marly nannofossil ooze/chalk, diatomaceous nannofossil-rich silty clay/claystone, and nannofossil-rich diatoma-

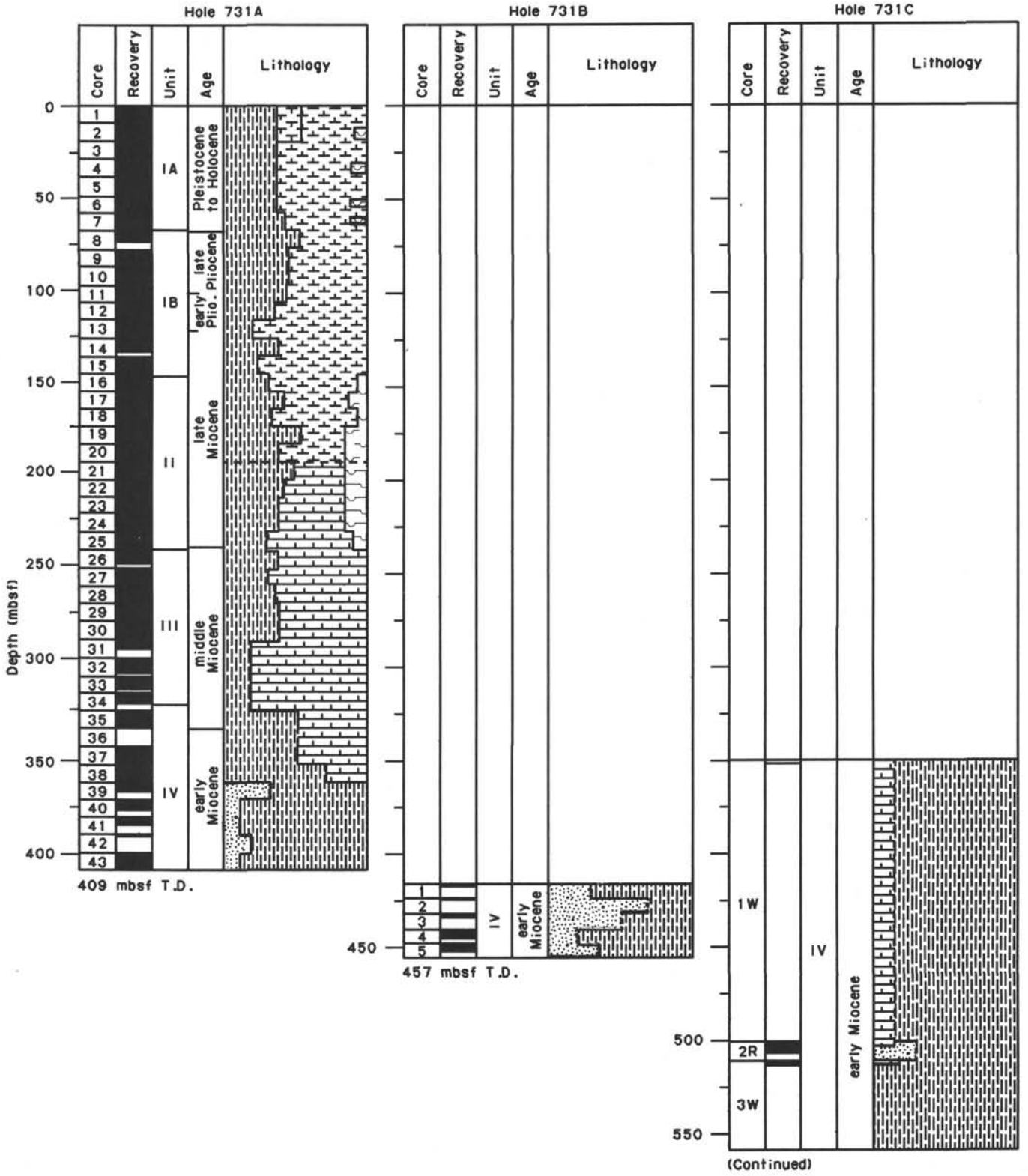

Figure 3. Lithostratigraphic summary, Site 731.

ceous mud/mudstone. Contacts between the light and dark beds are gradational. The transition from soft sediment (ooze/clay/mud) to lithified sediment (chalk/claystone/mudstone) is placed at the top of Core 117-731A-21X (192.8 mbsf). Colors of the light layers include light gray (5Y 7/1, 5Y 7/2, 5Y 6/1), light olive gray (5Y 6/2), light greenish gray (5GY 7/1, 10Y 7/2), and pale olive (5Y 6/3). The darker layers, which contain 20%–40% more terrigenous material and 5%–20% more diatoms than the light layers, are light olive gray (5Y 6/2), olive gray (5Y 5/2, 5Y 4/2), gray (5Y 6/1), olive (5Y 5/3, 5Y 4/3), and dark olive gray

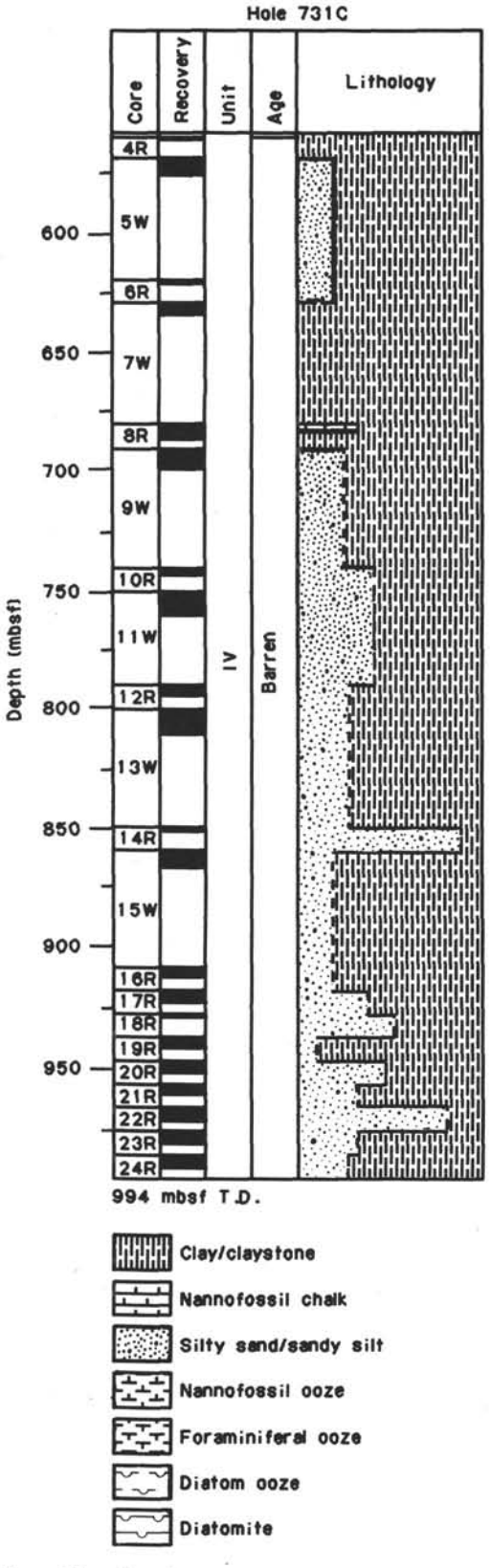

Figure 3 (continued).

(5Y 3/2). The calcium carbonate content (Table 3; Fig. 5) in lithologic Unit II averages 40%, and ranges from 9% to 77%, reflecting the increased, but variable, importance of biogenic silica and detrital components in that unit. Bed thicknesses generally range between 10 cm and 50 cm, with minor to common bioturbation, including *Zoophycus, Chondrites*, and *Planolites*. Purple concentric laminations around large burrows are first observed in Core 117-731A-25X, and are interpreted as redox halos, perhaps formed by the precipitation of dissolved Mn^{2+} or Fe^{2+} at a redox front surrounding the burrow. The concentric halos are best developed in the lighter layers, and become more common in Unit III.

Results of smear slide analyses (Fig. 4) reflect the compositional variability within lithologic Unit II and illustrate the compositional differences between lithologic Units I and II. Nannofossil abundances remain high in the light layers; values range from 50% to 75%. The light layers also contain 3%–7% diatoms, 0%–5% foraminifers, 0%–12% detrital calcite, and 16%–25% clay, so that their compositions are essentially unchanged from those of lithologic Unit I. The dark layers, however, have significantly different compositions, containing only 7%–35% nannofossils, but 10%–35% diatoms, 0%–5% radiolarians, 0%–2% foraminifers, 5%–22% detrital calcite, and 15%–40% clay. Sponge spicules, silicoflagellates, quartz, mica, and opaque minerals are all present in low abundances (0%–5%) throughout lithologic Unit II.

Lithologic Unit II is the youngest/shallowest interval at Site 731 that contains vertical to subvertical sets of parallel, millimeter-width, filled fractures. In some instances, millimeter-scale offsets are visible across these fractures, indicating microfaulting. These structures are well developed in the diatomaceous marly nannofossil chalks and nannofossil-rich diatomaceous mudstones of Cores 117-731A-21X and -24X. Similar features were previously observed at Sites 722 and 730 (see "Lithostratigraphy" sections, "Site 722" and "Site 730" chapters, this volume), also with best development in opal-rich horizons. The fracture sets often are closely associated with slumped intervals. These associations suggest that the fractures may result from volume changes during opal diagenesis, pressure or extension associated with slumping, or other causes. A better understanding of the implications of these structures for diagenetic, tectonic, and sediment loading histories will require more detailed shore-based study.

Although available biostratigraphic data do not indicate that unconformities are present in Core 117-731A-25X, the presence of angular fragments within that interval suggests that slumping probably has influenced that interval to some extent. The fragments are composed of olive (5Y 5/3) diatomaceous marly nannofossil chalk, reach dimensions of approximately 2 cm by 1 cm, and have well-defined edges with angular corners. The fragments are found in beds of light gray (5Y 7/1) nannofossil chalk, generally 5–20 cm above the underlying gradational contact. Burrows within the adjacent nannofossil chalk do not continue through the marly nannofossil chalk fragments. The composition, position, and unburrowed nature of the fragments suggests that they are transported rip-up clasts, while their shape and compositional similarity to underlying beds suggests that the distance of transport was small. Interpretations of the effect of mass movements on this portion of Unit II require further biostratigraphic, sedimentologic, and physical properties data.

Unit III (Depth: 240.9–320.1 mbsf; Age: middle to late Miocene)

Section 117-731A-25X-7, 31 cm, through Section 117-731A-34X-3, 60 cm.

Lithologic Unit III consists of interbedded nannofossil chalk, calcitic marly nannofossil chalk, and limited occurrences of nannofossil-rich calcitic silty claystone. Contacts between these lithologies are gradational. Color variations in the unit are less marked than in Unit II, with light layers ranging from white (5Y

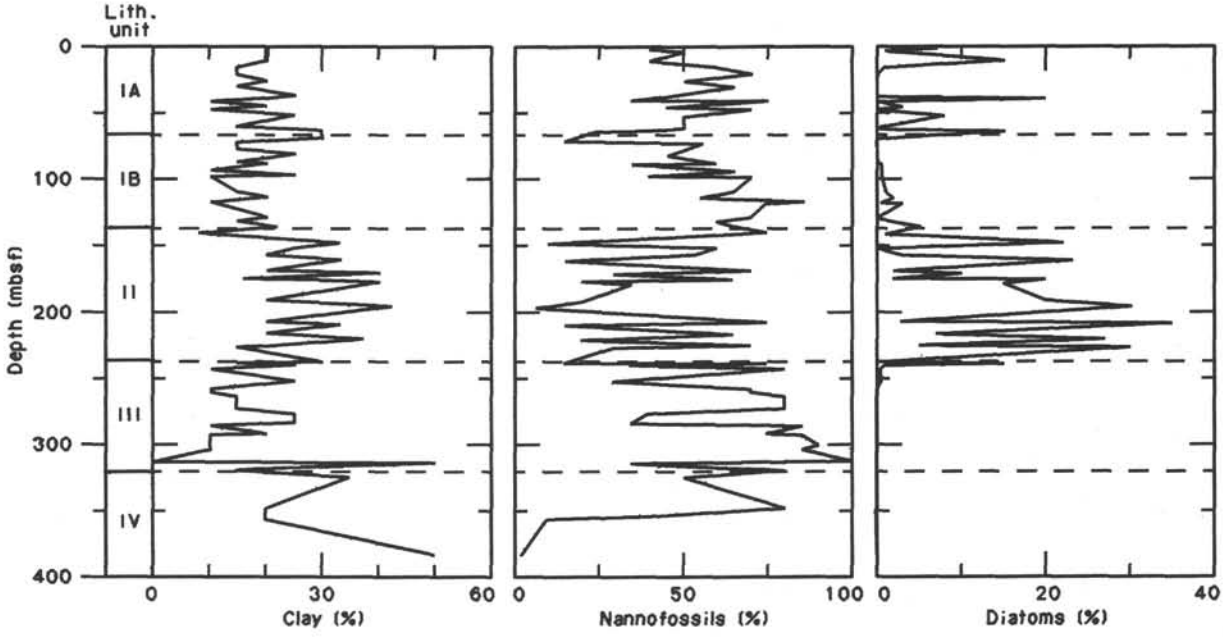

Figure 4. Abundances of clay, nannofossils, and diatoms in smear slides from Hole 731A, illustrating characteristic compositions of lithologic units. Roman numerals indicate lithologic units.

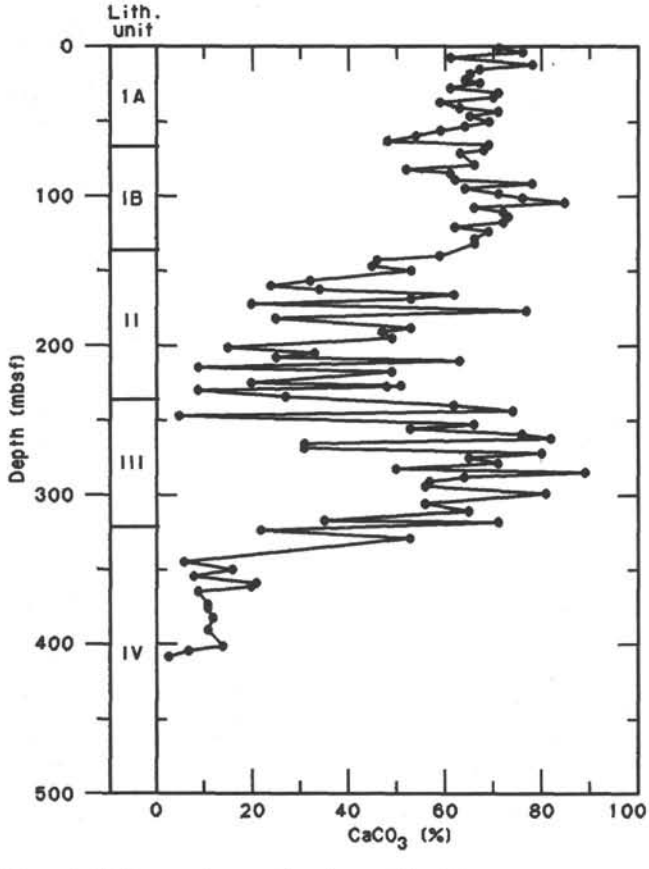

Figure 5. Calcium carbonate abundances, Site 731.

Table 2. Lithostratigraphic summary, Site 731.

Lithologic unit	Cores	Depth (mbsf)	Age
IA Nannofossil ooze, marly nannofossil ooze, nannofossil-foraminifer ooze, diatomaceous marly nannofossil ooze	731A-1H to -7H-6	0.0–66.3	Pleistocene/Holocene
IB Nannofossil ooze, marly nannofossil ooze	731A-7H-6 to -16X-2	66.3–146.5	late Miocene to early Pleistocene
II Nannofossil and marly nannofossil ooze/chalk to *nannofossil-rich* diatomaceous mud/ mudstone	731A-16X-2 to -25X-7	146.5–240.9	late Miocene to middle Miocene
III Nannofossil chalk, marly nannofossil chalk	731A-25X-7 to -34X-3	240.9–320.1	middle Miocene
IV Interbedded siltstones to nannofossil chalk, mud turbidites, sand turbidites	731A-34X-3 to -43X; 731B-1X to -5X; 731C-1W to -24R	320.1–409.0 408.6–457.1 351.7–994.2	late Oligocene(?) to early Miocene

8/1) to light gray (5Y 7/1, 5Y 7/2, N7/), light greenish gray (5GY 7/1, 10Y 7/1, 5G 7/1), pale olive (5Y 6/3), and gray (5Y 6/1). Dark layers range from greenish gray (10Y 6/2, 10Y 5/2, 10Y 4/2, 5G 6/1, 5G 5/1, 5GY 6/1, 5GY 5/1) and gray (5Y 5/1) to olive (5Y 5/3, 5Y 5/4), olive gray (5Y 5/2), and brown (10YR 5/3). Bed thicknesses range from 0.01 m to greater than 1 m, and bioturbation is minor to abundant throughout Unit III. Purple redox(?) halos around large burrows (described for Unit II) are common in Unit III. Average calcium carbonate content in Unit III is 63%, with values ranging from 31% to 89% (Fig. 5; Table 3). The increased carbonate content reflects the absence of biogenic silica, which diluted the carbonate content of Unit II.

Smear slide analyses confirm the carbonate-rich nature of Unit III, with compositional ranges of 30%–90% nannofossils, 0%–30% detrital calcite, 10%–25% clay, 0%–2% foraminifers, and 0%–2% diatoms (Fig. 4). Other minerals are present in only trace amounts. Light layers generally contain 30%–40% more nannofossils than the dark layers, with correspondingly lower abundances of terrigenous material (clays and inorganic calcite).

Vertical to subvertical parallel sets of filled, millimeter-scale fractures and microfaults, described previously for Unit II, are also observed in Cores 117-731A-28X and -29X of Unit III. Unlike most other occurrences, these fracture sets are developed in

Table 3. Calcium carbonate and organic carbon contents, Site 731.

Core, section, interval (cm)	Depth (mbsf)	Total carbon (%)	Inorganic carbon (%)	Organic carbon (%)	$CaCO_3$ (%)
117-731A-					
1H-1, 96–98	0.96	9.95	8.58	1.37	71.5
1H-3, 80–82	3.80		9.12		76.0
1H-5, 80–82	6.80		7.38		61.5
2H-2, 80–82	12.10	9.62	9.36	0.26	78.0
2H-4, 80–82	15.10		8.15		67.9
2H-6, 80–82	18.10		7.83		65.2
3H-2, 80–82	21.60	8.56	7.77	0.79	64.7
3H-4, 80–82	24.60		8.07		67.2
3H-6, 80–82	27.60		7.43		61.9
4H-2, 80–82	31.10	9.03	8.52	0.51	71.0
4H-4, 80–82	34.10		8.40		70.0
4H-6, 80–82	37.10		7.16		59.6
5H-2, 80–82	40.60	7.79	7.58	0.21	63.1
5H-4, 80–82	43.60		8.56		71.3
5H-6, 80–82	46.60		7.84		65.3
6H-2, 80–82	50.10	8.89	8.29	0.60	69.1
6H-4, 80–82	53.10		7.68		64.0
6H-6, 80–82	56.10		7.09		59.1
7H-2, 80–82	59.60	6.73	6.50	0.23	54.2
7H-4, 80–82	62.60		5.81		48.4
7H-6, 80–82	65.60		8.28		69.0
8X-2, 64–66	69.14	8.72	8.22	0.50	68.5
8X-3, 81–83	70.81		7.56		63.0
9X-2, 80–82	79.00	9.50	7.98	1.52	66.5
9X-4, 80–82	82.00		6.32		52.7
9X-6, 39–41	84.59		7.43		61.9
10X-2, 80–82	88.70	8.00	7.50	0.50	62.5
10X-4, 80–82	91.70		9.46		78.8
10X-6, 80–82	94.70		7.68		64.0
11X-2, 92–94	98.42	9.48	8.60	0.88	71.6
11X-4, 92–94	101.42		9.13		76.1
11X-6, 92–94	104.42		10.27		85.6
12X-2, 80–82	108.00	8.39	8.01	0.38	66.7
12X-4, 77–79	110.97		8.73		72.7
12X-6, 77–79	113.97		8.80		73.3
13X-2, 84–86	117.74	8.98	8.70	0.28	72.5
13X-4, 82–84	120.72		7.49		62.4
13X-6, 99–101	123.89		8.30		69.1
14X-3, 77–79	128.77	8.34	8.01	0.33	66.7
14X-5, 75–77	131.75		7.94		66.1
15X-4, 100–101	140.20	7.59	7.16	0.43	59.6
15X-6, 62–64	142.82		5.58		46.5
16X-2, 103–105	146.93	6.15	5.50	0.65	45.8
16X-4, 121–123	150.11		6.36		53.0
17X-2, 125–127	156.75	5.02	3.87	1.15	32.2
17X-4, 123–125	159.73		2.91		24.2
17X-6, 113–115	162.63		4.19		34.9
18X-2, 101–103	166.21	8.15	7.53	0.62	62.7
18X-4, 61–63	168.81		6.41		53.4
18X-6, 100–102	172.20		2.44		20.3
19X-3, 86–88	177.26	9.46	9.27	0.19	77.2
19X-6, 92–94	181.82		3.03		25.2
20X-4, 67–69	188.27	7.13	6.36	0.77	53.0
20X-6, 30–32	190.90		5.73		47.7
21X-2, 56–58	194.86	6.50	5.99	0.51	49.9
21X-6, 48–50	200.78		1.87		15.6
22X-2, 99–101	204.99	4.68	4.01	0.67	33.4
22X-4, 98–100	207.98		3.06		25.5
22X-6, 20–22	210.20		7.60		63.3
23X-2, 70–72	214.40	2.79	1.18	1.61	9.8
23X-4, 70–72	217.40		5.97		49.7
24X-2, 108–110	224.48	3.76	2.47	1.29	20.6
24X-4, 69–71	227.09		6.21		51.7
24X-6, 18–20	229.58		1.14		9.5
25X-2, 90–92	234.00	4.77	3.33	1.44	27.7
25X-4, 94–96	237.02	5.80			48.3
25X-6, 90–92	240.00		7.49		62.4
26X-2, 100–102	243.80	9.00	8.97	0.03	74.7
26X-4, 100–102	246.80		0.68		5.7
27X-2, 79–81	253.19	8.21	8.01	0.20	66.7
27X-4, 52–54	255.92		6.46		53.8
27X-6, 120–122	259.60		9.14		76.1
28X-2, 59–61	262.69	10.07	9.84	0.23	82.0
28X-4, 63–65	265.73		3.77		31.4

Table 3 (continued).

Core, section, interval (cm)	Depth (mbsf)	Total carbon (%)	Inorganic carbon (%)	Organic carbon (%)	$CaCO_3$ (%)
117-731A-					
28X-6, 58–60	268.68		3.77		31.4
29X-2, 80–82	272.50	9.91	9.70	0.21	80.8
29X-4, 91–93	275.61		7.81		65.1
29X-6, 92–94	278.62		8.54		71.1
30X-2, 71–73	282.11	6.28	6.08	0.20	50.7
30X-4, 76–78	285.16		10.71		89.2
30X-6, 116–118	288.56		7.74		64.5
31X-2, 51–53	291.61	7.06	6.95	0.11	57.9
31X-CC, 18–20	294.53		6.74		56.1
32X-1, 28–30	299.48	9.83	9.78	0.05	81.5
32X-5, 46–48	305.66		6.77		56.4
33X-2, 25–27	310.65	7.93	7.88	0.05	65.6
34X-1, 73–75	316.23	4.26	4.22	0.04	35.2
34X-2, 69–71	317.69		8.62		71.8
35X-1, 78–80	322.88	2.73	2.68	0.05	22.3
35X-5, 37–39	328.47		6.42		53.5
37X-3, 25–27	344.55	0.87	0.80	0.07	6.7
37X-6, 84–86	349.64		1.93		16.1
38X-3, 31–33	354.31	1.10	1.00	0.10	8.3
38X-6, 67–69	359.17		2.61		21.7
39X-1, 48–50	361.18	2.55	2.46	0.09	20.5
39X-3, 111–113	364.81		1.18		9.8
40X-2, 137–139	373.27	1.64	1.43	0.21	11.9
40X-4, 91–93	375.81		1.43		11.9
41X-2, 90–92	382.40	1.73	1.53	0.20	12.7
42X-1, 68–70	390.38	1.61	1.42	0.19	11.8
43X-2, 52–54	401.42	1.84	1.76	0.08	14.7
43X-4, 79–81	404.69		0.93		7.8
43X-6, 92–94	407.82		0.38		3.2
117-731B-					
1X-1, 17–19	408.77		1.43		11.9
2X-1, 34–36	418.64		1.11		9.3
3X-1, 80–82	428.90		1.60		13.3
4X-1, 80–82	438.50		1.63		13.6
4X-3, 47–49	441.17		1.22		10.2
5X-1, 40–43	447.80		1.36		11.3
117-731C-					
2R-2, 76–78	504.66		1.37		11.4
2R-3, 121–123	506.61		0.72		6.0
4R-1, 36–38	560.56		1.36		11.3
5W-4, 74–76	575.14		1.19		9.9
6R-1, 94–96	619.04		1.05		8.8
7W-1, 53–55	628.33		1.20		10.0
8R-1, 62–64	676.52		1.20		10.0
8R-4, 26–28	680.66		1.20		10.0
10R-1, 22–24	733.82		0.02		0.2
10R-2, 3–5	735.13		1.33		11.1
10R-2, 43–45	735.53		1.79		14.9
11W-5, 137–139	750.67		1.68		14.0
12R-1, 94–96	792.44		1.10		9.2
12R-2, 137–139	794.37		1.34		11.2
12R-3, 95–97	795.45		1.64		13.7
14R-1, 39–41	849.79		1.61		13.4
14R-2, 53–55	851.43		1.19		9.9
16R-1, 137–139	908.67		1.18		9.8
16R-2, 60–62	909.40		1.32		11.0
16R-3, 6–8	910.36		1.45		12.1
17R-2, 142–145	919.62		1.20		10.0
17R-4, 2–4	921.22		1.53		12.7
19R-1, 141–143	937.51		1.65		13.7
19R-3, 8–10	939.18		1.64		13.7
20R-1, 34–36	946.04		1.29		10.8
20R-3, 1–63	949.31		1.34		11.2
20R-4, 20–22	950.40		1.44		12.0
21R-1, 17–19	955.57		1.43		11.9
21R-2, 121–123	958.11		1.54		12.8
22R-2, 82–84	967.42		1.49		12.4
23R-2, 83–85	977.13		1.40		11.7
24R-2, 136–138	987.36		1.51		12.6

sediments that lack biogenic silica, suggesting that processes other than diagenetic volume changes of opal (see "Lithostratigraphy" section, "Site 722" chapter, this volume) can produce these structures. Angular clasts of marly nannofossil chalk, similar to those described at the base of Unit II, also occur in Section 117-731A-25X-5. This suggests that episodic slumping occurred throughout deposition of the sediments at the Unit III/Unit II transition. However, neither the clast occurrences nor the fracture development in Unit III provide further insight to the depositional, diagenetic, or deformational implications of these two types of features.

Unit IV (Depths: Hole 731A, 320.1–409.0 mbsf; Hole 731B, 408.6–457.1 mbsf; Hole 731C, 351.7–994.2 mbsf; Age: late Oligocene(?) to early Miocene)

Section 117-731A-34X-3, 60 cm, through Core 117-731A-43X; Core 117-731B-1X through 117-731B-5X; Cores 117-731C-1W through 117-731C-24R.

The top of lithologic Unit IV is defined by the top of the uppermost (youngest) clastic-based turbidite, based on criteria used at Site 721 and 722 (see "Lithostratigraphy" sections, "Site 721" and "Site 722" chapters, this volume). Although Unit IV is dominated by turbidites, the relative abundances of biogenic carbonate, coarse detrital components, and fine-grained detrital components can be used to distinguish three separate lithofacies. These are characterized as follows:

1. Mixed turbidite-carbonate lithofacies: The mixed turbidite-carbonate lithofacies is best-developed at the top of Unit IV, where it forms a transitional zone between the carbonate chalks of Unit III and the terrigenous turbidites that occur below 360 mbsf (Section 117-731A-38X-6, 95 cm). This lithofacies also occurs in Cores 117-731C-1W to -3W, -7W, -8R, and -13W as thin (<20 cm thick) intervals; upper and lower contacts of these occurrences are generally obscured or destroyed by drilling disturbance. This lithofacies is characterized by clayey siltstones/silty claystones interbedded with nannofossil chalk, forming beds that grade from basal terrigenous sediments to biogenic carbonate caps. The silty claystones to clayey siltstones are generally sharp-based and thin (<10 cm), with colors of greenish gray (5GY 5/1, 5G 6/1, 5BG 5/1), gray (5Y 5/1), olive gray (5Y 4/2), dark gray (N4/) and dark greenish gray (5GY 4/1). The carbonate caps are bioturbated nannofossil chalks to marly nannofossil chalks, with colors of olive gray (5Y 5/2) and gray (5Y 6/1) to light gray (10YR 7/1), or brown (10YR 5/3) and grayish brown (10YR 5/2) to light grayish brown (10YR 6/2). Complete gradational sequences range from 10 cm to approximately 60 cm in thickness. Calcium carbonate contents in the lithofacies average 21%, but vary from 6% in a basal turbidite to 53% in a carbonate cap (Table 3; Fig. 5). Smear slide analyses also reflect this compositional variability, with one basal turbidite containing 10% nannofossils, 40% quartz, 20% clay, and 30% detrital calcite (Fig. 4). One carbonate cap, however, contains 80% nannofossils and 20% clay.

2. Mud turbidite lithofacies: The second lithofacies in Unit IV occurs below 360 mbsf, and consists of gradationally interbedded clayey siltstones or siltstones and silty claystones. The interbedded lithologies form fining-upward beds 3–30 cm thick; they generally begin with a sharp-based or scoured contact and parallel-laminated siltstone or clayey siltstone, and grade upward to uniform silty claystone (Fig. 6). The upper 1–5 cm of the beds is commonly bioturbated. Ripple cross-lamination and low angle cross-stratification are observed in a few of the basal siltstones, and slumping and dewatering structures are rarely present in the silty claystones. The fining-upward beds are commonly stacked, forming intervals of repeated mud turbidites as thick as 3 m. Colors are relatively uniform through this lithofacies, including dark gray (N4/, 5Y 4/1, 10YR 4/1), dark greenish gray (5BG 4/1, 5GY 4/1, 5B 4/1, 5G 4/1), dark brown (10YR 4/3, 10YR 3/3), dark grayish brown 10YR 4/2, 10YR3/2), and very dark gray (5Y 3/1). Calcium carbonate contents are low below 360 mbsf, and average approximately 10% (Fig. 5; Table 3), with detrital calcite providing most of the carbonate seen in Unit IV. Smear slide analyses indicate that quartz, clay, and detrital calcite are the dominant constituents of the mud turbidite lithofacies. Abundances range from 15% to 50% quartz, 10%–70% clay, and 10%–30% detrital calcite. Quartz and detrital calcite are generally enriched in the siltstone and clayey siltstone intervals, while clays dominate in the silty claystones. Feldspar, mica, volcanic ash, heavy minerals, and opaque minerals are present at abundances of 0%–5% each.

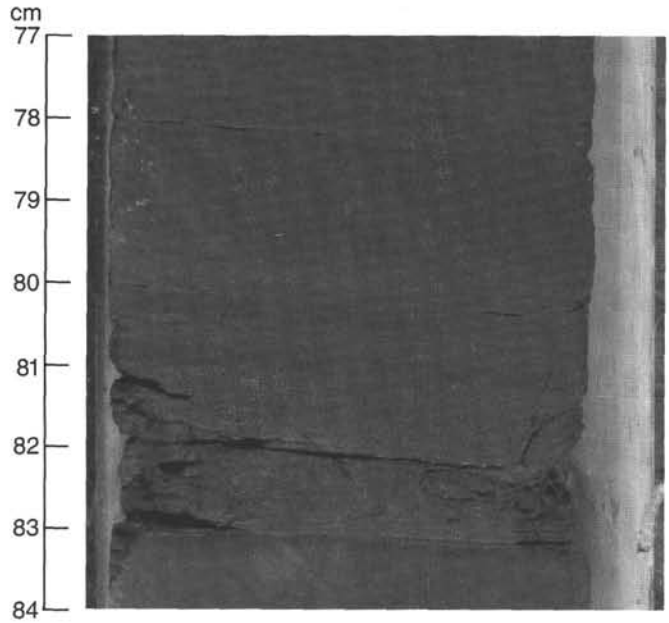

Figure 6. Photograph of the mud turbidite lithofacies in Unit IV, showing a stacked sequence of fining-upward, siltstone to claystone beds (Section 117-731C-12R-2, 77–84 cm).

3. Coarse-grained turbidite lithofacies: The third lithofacies in Unit IV is characterized by significant amounts of coarse-grained clastics, including silty sandstones/sandy siltstones and sandstones. These coarser clastics occur in two modes: either as the coarse-grained base of a fining-upward sequence, which can extend into a siltstone or a thin silty claystone cap, or as a discrete, ungraded to slightly fining-upward, coarse-grained bed, generally with sharp upper and lower contacts. Bed thicknesses range from approximately 10 cm to as much as 150 cm in both modes of occurrence. Primary sedimentary structures are rare to absent in the coarse-grained turbidites, with a diffuse parallel lamination as the most common structure. The sandstones and siltstones are dominated by quartz and detrital calcite, with feldspars, amphiboles, pyroxenes, mica, and opaque minerals also present. Rock fragments, including chert and chlorite-rich schist, are present in trace amounts. The sandstones in the coarse-grained turbidite lithofacies are commonly poorly cemented and friable; locally, however, the sandstones are heavily cemented with calcite. The cemented intervals show no significant difference in grain composition from the weakly cemented sandstones.

Within Unit IV, the mixed turbidite-carbonate lithofacies is generally restricted to depths shallower than 360 mbsf. The mud turbidite lithofacies and the coarse-grained turbidite lithofacies, however, are not depth-restricted in the interval from 360 to 994 mbsf. The relative abundances of these two lithofacies are generally represented by the proportions of coarse clastics and fine clastics shown in Figure 3. The data from Hole 731C suggest a general downhole increase in the importance of coarse clastics, which is supported by the results of downhole logging (see "Downhole Measurements" section, this chapter). The lithologic summary from Hole 731B, however, indicates that coarse clastics are also important within the upper portions of Unit IV.

Discussion

Site 731

The sequence of lithostratigraphic units at Site 731 records the tectonic evolution of the Owen Ridge and variations in marine planktonic productivity, dissolution, and terrigenous sediment supply from the Oligocene to the Holocene. Deposition at Site 731 during the late Oligocene(?) to early middle Miocene was dominated by terrigenous turbidites, and coarse-grained and fine-grained sediments apparently were supplied by distinct depositional processes. The intervals of stacked mud turbidites represent deposition by repeated low-velocity events (predominantly from suspended load), perhaps either downfan from distributary channels or in overbank regions away from leveed distributaries. The interbedded coarse-grained turbidite lithofacies, however, indicates that coarse clastic input to Site 731 was sustained episodically, perhaps by distributary channel migration or by sand transport to distal lobe depocenters during early stages of Indus Fan construction (predominantly by bed-load transport).

The coarse-grained turbidite and the mud turbidite lithofacies are interbedded throughout the interval from 360 to 994 mbsf, so that no large-scale fining-upward trend is evident in sediments recovered from that portion of Unit IV. The absence of such a trend indicates that both bed-load and suspended load depositional processes were active into the middle Miocene at Site 731; this suggests that relatively stable depositional conditions were maintained until that time. Turbidite influence decreased and pelagic carbonate deposition was periodically important at Site 731 during the late early to middle Miocene, producing the mixed turbidite-carbonate lithofacies at the top of Unit IV. This transition in depositional style reflects the tectonic uplift of the Owen Ridge, which moved Site 731 above the level of turbidite deposition during the middle Miocene. Owen Ridge uplift, however, began in the early Miocene (Whitmarsh, 1974), indicating that Site 731 was not affected by the first stages of uplift. The relatively rapid change from interbedded coarse-grained and mud turbidites to the mixed carbonate-turbidite lithofacies suggests that uplift at Site 731, once initiated, quickly influenced deposition at that site. The relatively thin transitional zone (the mixed turbidite-carbonate lithofacies) may record relatively rapid uplift of Site 731 through the zone of episodic turbidite suspended-load deposition.

During the middle Miocene, Site 731 was uplifted above the zone of turbidite influence, and pelagic deposition became dominant. The decrease in turbidite supply is recorded by a decrease in sedimentation rate above 305 mbsf (see "Accumulation Rates" section, this chapter). Because of the loss of turbidite input, the major controls on sedimentation became the rates of supply and preservation of biogenic calcium carbonate and biogenic silica, and the rate of terrigenous supply, which was probably dominated by eolian processes (Kolla et al., 1981).

During the middle Miocene, carbonate was the dominant biogenic constituent, producing the nannofossil chalks and marly nannofossil chalks of Unit III. Abundant bioturbation in Unit III records the presence of oxygenated bottom waters throughout this time. Relatively low organic carbon contents in Unit III (see "Organic Geochemistry" section, this chapter) indicate conditions of low productivity and/or significant organic matter recycling in the water column and surface sediments.

The planktonic productivity/preservation signal changed at approximately the beginning of the late Miocene, however, with the onset of significant biosiliceous sedimentation in Unit II. Smear slide data show that diatom abundances reach their maximum within 20 m of the base of Unit II, and gradually decrease above that level. Diatom-poor nannofossil oozes/chalks and marly nannofossil oozes/chalks are interbedded throughout Unit II, recording repeated fluctuations in the biogenic carbonate vs. biogenic silica production/preservation balance through the late Miocene. Organic carbon contents are generally high but variable in Unit II, perhaps recording both increased productivity and enhanced preservation at this time. Bioturbation in Unit II again records the presence of oxygenated bottom waters, but an increased sedimentation rate (observed above 205 mbsf; see "Accumulation Rates" section, this chapter) may have enhanced both organic carbon and opal preservation at that time.

Biogenic carbonate also dominates pelagic input from the upper Miocene to the Holocene, producing the nannofossil oozes and marly nannofossil oozes of Unit I. More variable conditions of production and preservation are indicated by Subunit IA, with its variable biosiliceous and organic carbon contents (see "Organic Geochemistry" section, this chapter).

Reduced sedimentation rates and/or the presence of unconformities through the Pliocene section at Site 731 may limit its usefulness for high resolution studies. The enhanced record of biogenic silica production and preservation in Units IA and II at Site 731, however, will provide data for valuable comparisons with the correlative records at Sites 721 and 722.

BIOSTRATIGRAPHY

Introduction

Site 731 was the third site drilled on the crest of the Owen Ridge after Sites 721 and 722. Planktonic microfossil biostratigraphy has been established for this site and is depicted in Figures 7, 9, and 10. Planktonic foraminifers are abundant to common with good preservation in the five uppermost core-catcher samples (down to 47.8 mbsf) in Hole 731A. Below this interval down to 308.9 mbsf, the planktonic foraminifers are rare and the preservation is poor; sediments below 308.9 mbsf are barren of planktonic foraminifers. Benthic foraminifers are abundant down to 86.4 mbsf, common from this level down to 154.0 mbsf, and rare to few from this level down to 299.2 mbsf. Below 299.2 mbsf, benthic foraminifers are few with poor preservation.

Throughout the length of Hole 731A, preservation states of the calcareous nannofossils show many changes, but they remain abundant down to 289.6 mbsf. From this level down to the bottom of the hole abundance varies from barren to abundant. Preservation of the nannofossils is poor below 370.1 mbsf. All five samples in Hole 731B were barren of nannofossils. Nannofossils range from abundant to barren throughout Hole 731C, but the preservation is poor, with all of the specimens being heavily overgrown.

Radiolarians are present in Hole 731A down to 279.9 mbsf but below this level the sediments are barren of radiolarians. Few specimens are present in the two uppermost core catcher samples, and the preservation is moderate to good. From 28.8 to 192.8 mbsf there is an increase in the abundance and the state of preservation of the radiolarians, while from 202.5 mbsf to 221.9 mbsf we noted a slight decrease in the abundance and

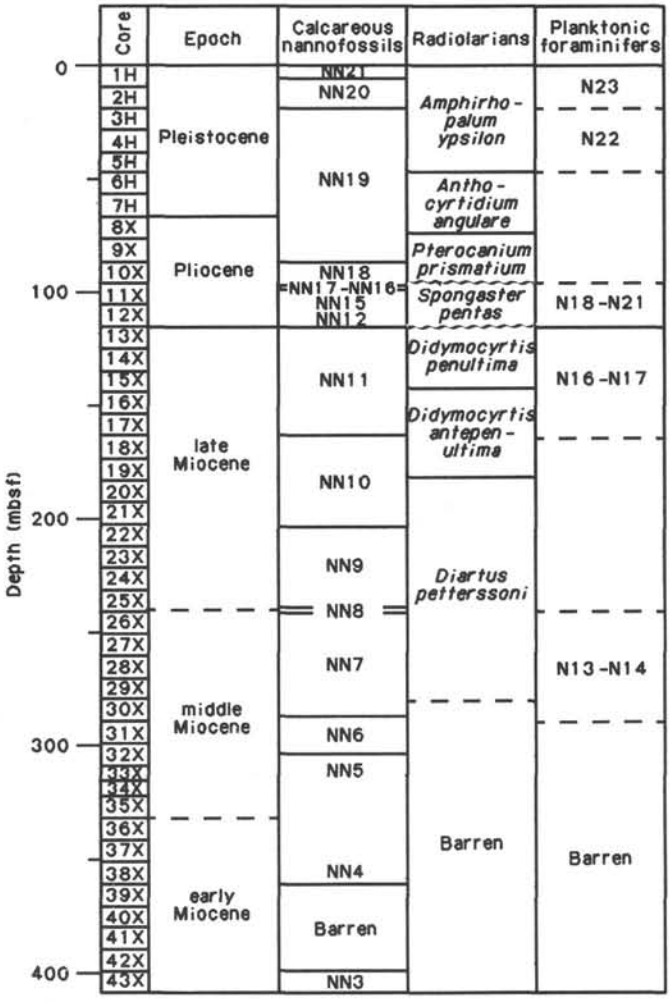

Figure 7. Correlation of planktonic microfossil groups in Hole 731A.

state of preservation of radiolarians. In 117-731A-28X, CC, and -29X, CC (270.2–279.9 mbsf), radiolarians are rare and many have been pyritized. Diatoms are common from 154.0 mbsf to 260.6 mbsf. Holes 731B and 731C are barren of siliceous microfossils.

Two hiatuses have been recognized based on the radiolarian data. Some of the middle Pliocene (2.4 Ma to less than 3.4 Ma) and lowermost Pliocene to uppermost Miocene (around 4.3 Ma to 6.1 Ma) sediments appear to be missing at this site. The calcareous nannofossil zonal markers are missing in this part of the sequence so it is nearly impossible to recognize a hiatus in Hole 731A. A plot of faunal datum levels and paleomagnetic reversals vs. depth below sea level is presented in Figure 8; for a detailed listing see Table 4.

Planktonic Foraminifers

The drilled sequence in Hole 731A contains abundant to common and well-preserved planktonic foraminifers in the interval from 9.8 to 47.8 mbsf (Samples 117-731A-1H, CC, through 117-731A-5H, CC), which is composed of Pleistocene marly-nannofossil oozes. Rare and poorly preserved specimens were found in Samples 117-731A-6H, CC, through 117-731A-32X, CC (57.3–308.9 mbsf). This part of the sequence ranges from the Pliocene to the middle Miocene. The underlying sediments, which are comprised of sandy turbidites, did not yield planktonic foraminifers.

The first appearance of *Globigerinella calida calida* was noted in Sample 117-731A-2H, CC (19.3 mbsf), which marks the lower limit of Zone N23. The lower boundary of Zone N22, which is based on the first appearance (FA) of *Globorotalia truncatulinoides*, was found in Sample 117-731A-5H, CC (47.8 mbsf). However, the boundary is not reliable because this species is very rare in this area. Other foraminifers are also rare, and thus the Pleistocene/Pliocene boundary could not be approximated.

A Pliocene foraminiferal assemblage was noted in Sample 117-731A-11X, CC (105.7 mbsf), which was assigned to Zones N19 to N21. A substantial hiatus occurs somewhere in this interval because the Pliocene is too condensed (see "Calcareous Nannofossils" and "Radiolarians" discussions below).

Upper Miocene sediments range from Sample 117-731A-13X, CC, through 117-731A-17X, CC (125.0–163.7 mbsf), pointed out by *Globorotalia tumida merotumida* and *Globorotalia tumida plesiotumida* (Zones N16–N17). The lower limit of this zone is not its true boundary as the underlying sediments are barren of planktonic foraminifers.

The presence of *Globorotalia mayeri* and the lack of *Globorotalia fohsi* in Samples 117-731A-26X, CC, through 117-731A-30X, CC (250.9–289.6 mbsf), indicate middle Miocene sediments (Zones N13–N14). The remainder of the section does not contain planktonic foraminifers.

Benthic Foraminifers

The benthic foraminiferal fauna of Site 731 was studied in the core catchers of Hole 731A. Benthic foraminifers are abundant and well-preserved in the upper part of the sequence (Samples 117-731A-1H, CC, through -9X, CC; 9.8–86.4 mbsf). Below 86.4 mbsf, benthic foraminifers are common and moderately well preserved. Below Sample 117-731A-16, CC (154.0 mbsf), the benthic foraminifers are few to rare and poorly preserved. Samples below Sample 117-731A-31X, CC (299.2 mbsf), are essentially barren with only a few poorly preserved specimens in some of the samples. The core catchers of Hole 731B and 731C were all within the turbiditic sequence and were barren. The preservation is good in the upper 115 m below which it becomes moderate to poor. Pyritized benthic and planktonic foraminiferal tests are abundant throughout the sequence studied.

The P/B (planktonic/benthic) ratio is above 90% in the uppermost seven samples (down to 67.0 mbsf); it decreases and remains low (0%–25%), with the exception of a few excursions at around 105 and 145 mbsf, down to Sample 117-731A-25X, CC (241.3 mbsf). Below 241.3 mbsf, the P/B ratio increases to more than 75% and is continuously high down to the level where both benthic and planktonic foraminifers disappear (299.2 mbsf).

The benthic foraminiferal fauna can be divided into three slightly different assemblages. Assemblage I is present in the uppermost seven samples (9.8–67.0 mbsf) and is characterized by high relative abundances of *Cassidulina carinata, Chilostomella oolina, Epistominella exigua, Globocassidulina subglobosa*, and *Pullenia subcarinata*. Additional species are *Ehrenbergina trigona, Melonis barleeanum, Pullenia bulloides, Sigmoilinopsis schlumbergeri*, and *Uvigerina peregrina*.

Assemblage II dominates the fauna in the interval 76.7–115.4 mbsf and is characterized by high relative abundances of *Melonis pompilioides*. Additional species are *Eggerella bradyi, Pullenia bulloides, Quadrimorphina laevigata* A, *Sigmoilopsis schlumbergeri*, and *Uvigerina spinicostata*.

Assemblage III is present below 125.0 mbsf and is characterized by high relative abundances of *Cibicidoides wuellerstorfi, Melonis pompilioides*, and *Pullenia bulloides*. Species present in lower relative abundances are *Eggerella bradyi, Globocassidulina subglobosa, Laticarinina halophora*, and *Melonis barleeanum*.

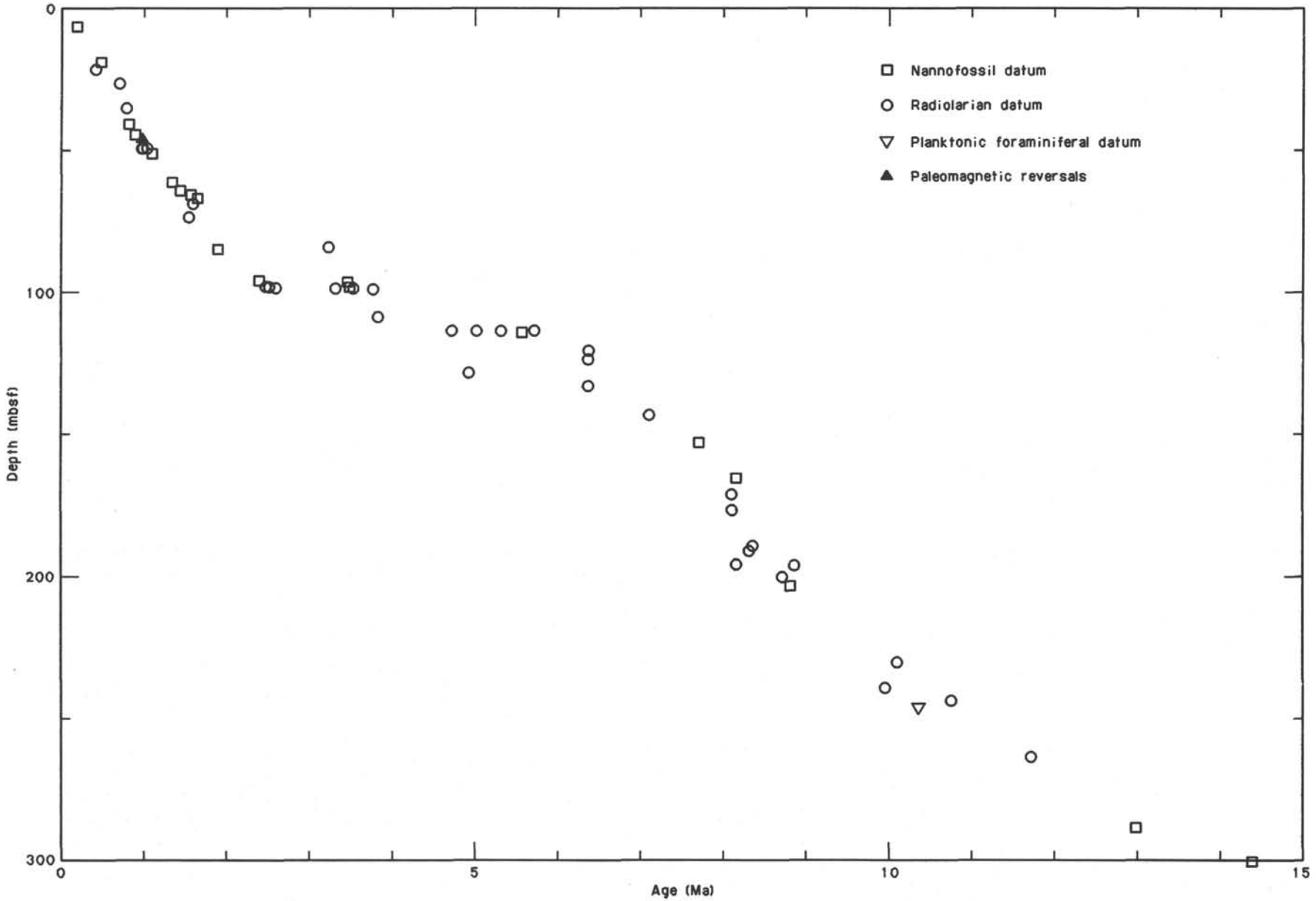

Figure 8. Age-depth plot for Hole 731A. For a detailed listing of events see Table 4.

Table 4. Stratigraphic listing of faunal events and paleomagnetic reversals for Hole 731A.

Event	Core level	Depth (mbsf)	Age (Ma)	Source of age	Notes
B *Emiliania huxleyi*	1H-4, 115–117	5.62	0.19	3	
	1H-5, 115–117	7.15			
T *Pseudoemiliania lacunosa*	2H-6, 115–117	18.45	0.49	3	
	2H-CC	19.30			
T *Stylatractus universus*	2H-CC	19.30	0.37–0.46	1	Cores MD81-369, RC14-22 and VM34-35; DSDP 214 data probably less accurate.
	3H-4, 85–87	24.65			
T *Anthocyrtidium nosicaae*	3H-4, 85–87	24.65	0.66–0.76	1	
	3H-CC	28.80			
B *Pterocorys hertwigii*	4H-4, 85–87	34.15	0.76–0.84	1	
	4H-CC	38.30			
T *Reticulofenestra* sp. A (acme)	5H-2, 115–117	40.95	0.82	3	
	5H-3, 115–117	42.45			
B *Gephyrocapsa parallela*	5H-4, 115–117	43.95	[a]0.89	4	
	5H-5, 115–117	45.45			
B Jaramillo	5H-5, 115–117	45.45	0.98	6	
	5H-6, 45–47	46.25			
T *Anthocyrtidium angulare*	5H-CC	47.80	0.94–1.04	1	
	6H-4, 85–87	53.15			
B *Lamprocyrtis nigriniae*	5H-CC	47.80	1.02–1.07	1	
	6H-4, 85–87	53.15			
T *Lamprocyrtis neoheteroporos*	5H-CC	47.80	0.94–1.04	1	
	6H-4, 85–87	53.15			
T *Gephyrocapsa* "large"[b]	6H-3, 115–117	51.95	[a]1.10	4	
	6H-4, 115–117	53.45			
T *Helicosphaera sellii*	6H-6, 115–117	56.45			No good published ages; event may be diachronous.
	6H-CC	57.30			
B *Gephyrocapsa* "large"[b]	7H-3, 115–117	61.45	[a]1.36	4	
	7H-4, 115–117	62.95			
T *Calcidiscus macintyrei*	7H-5, 115–117	64.45	1.45	6	
	7H-6, 115–117	65.95			
B *Gephyrocapsa oceanica*	7H-6, 115–117	65.95	[a]1.57	4	
	7H-CC	67.00			
B *Gephyrocapsa caribbeanica*	7H-CC	67.00	[c]1.66	4,8	
	8X-1, 115–117	68.15			
B *Anthocyrtidium angulare*	7H-CC	67.00	1.52–1.64	1	
	8X-4, 85–87	72.35			
T *Pterocanium prismatium*	8X-4, 85–87	72.35	1.52–1.56	1	
	8X-CC	76.70			
T *Phormostichoartus fistula*	9X-4, 85–87	82.05	3.26–3.28	1	? Too high; possible reworking.
	9X-CC	86.40			
T *Discoaster brouweri*	9X-5, 115–117	83.85	1.9	6	
	9X-CC	86.40			
T *Discoaster pentaradiatus*	10X-CC	96.00	2.4	6	
	11X-1, 115–117	97.15			
T *Sphenolithus abies*	10X-CC	96.00	3.47	6	
	11X-1, 115–117	97.15			
B *Theocalyptra davisiana*	10X-CC	96.00	2.42–2.44	1	
	11X-4, 85–87	101.35			
B *Lamprocyrtis neoheteroporos*	10X-CC	96.00	2.51–2.53	1	
	11X-4, 85–87	101.35			
T *Stichocorys peregrina*	10X-CC	96.00	2.62–2.64	1	
	11X-4, 85–87	101.35			
T *Lychnodictyum audax*	10X-CC	96.00	3.33–3.35	1	
	11X-4, 85–87	101.35			
T *Phormostichoartus doliolum*	10X-CC	96.00	3.53–3.55	1	
	11X-4, 85–87	101.35			
B *Amphirhopalum ypsilon*	10X-CC	96.00	3.77–3.79	1	
	11X-4, 85–87	101.35			
T *Didymocyrtis penultima*	10X-CC	96.00			
	11X-4, 85–87	101.35			
T *Reticulofenestra pseudoumbilica*	11X-1, 115–117	97.15	3.5	6	
	11X-2, 116–118	98.66			
T *Spongodiscus ambus*	11X-4, 85–87	101.35			
	11X-CC	105.70			
B *Spongaster tetras tetras*	11X-CC	105.70	3.83–3.85	1	
	12X-4, 85–87	111.05			
T *Spongaster berminghami*	11X-CC	105.70			
	12X-4, 85–87	111.70			
T *Stichocorys johnsoni*	12X-4, 85–87	111.05	5.7–5.8	[d]2	
	12X-CC	115.40			
T *Solenosphaera omnitubus*	12X-4, 85–87	111.05	4.7–4.8	2	
	12X-CC	115.40			
T *Acrobotrys tritubus*	12X-4, 85–87	111.05	5.3–5.4	2	Rare in Site 731.
	12X-CC	115.40			
T *Siphostichartus corona*	12X-4, 85–87	111.05	5.0–5.1	2	
	12X-CC	115.40			

Table 4 (continued).

Event	Core level	Depth (mbsf)	Age (Ma)	Source of age	Notes
T *Stichocorys delmontensis*	12X-4, 85–87	111.05			
	12X-CC	115.40			
T *Discoaster quinqueramus*	12X-5, 115–117	112.85	5.6	6	Age appears to be erroneous.
	12X-6, 115–177	114.35			
B *Spongodiscus ambus*	12X-CC	115.40			
	13X-4, 85–87	120.70			
S. delmontensis → *S. peregrina*	12X-CC	115.40	6.1–6.7	2	
	13X-CC	125.00			
T *Calocycletta caepa*	13X-4, 85–87	120.70	[e]6.2–6.6	2	
	13X-CC	125.00			
T *Botryostrobus bramlettei*	13X-CC	125.00	4.9–5.0	2	Should be higher.
	14X-4, 85–87	130.35			
B *Stichocorys peregrina*	13X-CC	125.00			
	14X-4, 85–87	130.35			
T *Didymocyrtis antepenultima*	14X-4, 85–87	130.35			
	14X-CC	134.70			
B *Solemosphaera omnitubus*	14X-4, 85–87	130.35	6.3–6.5	2	
	14X-CC	134.70			
T *Diartus hughesi*	15X-4, 85–87	140.95	7.1–7.2	2	
	15X-CC	144.40			
T *Dictyocoryne ontongensis*	16X-4, 85–87	149.75			
	16X-CC	154.00			
B *Acrobotrys tritubus*	16X-4, 85–87	149.75	7.7–7.8	2	Rare in Site 731.
	16X-CC	154.00			
B *Discoaster quinqueramus*	17X-CC	163.70	8.2	6	
	18X-1, 135–137	165.05			
T *Botryostrobus miralestensis*	18X-4, 85–87	169.05	8.1–8.2	2	
	18X-CC	173.40			
T *Diartus petterssoni*	18X-CC	173.40	8.1–8.2	2	
	19X-4, 85–87	178.75			
T *Didymocyrtis laticonus*	19X-4, 85–87	178.75			
	19X-CC	183.10			
D. petterssoni → *D. hughesi*	19X-4, 85–87	178.75	8.3–8.5	2	
	21X-4, 85–87	198.15			
T *Stichocorys wolffii*	20X-4, 85–87	188.45	[e]8.1–8.2	2	
	20X-CC	192.80			
B *Spongaster berminghami*	20X-CC	192.80	7.9–8.0	2	
	21X-4, 85–87	198.15			
B *Botryostrobus bramlettei*	20X-CC	192.80	8.8–9.0	2	
	21X-4, 85–87	198.15			
B *Diartus hughesi*	21X-4, 85–87	198.15	8.7–8.8	2	
	21X-CC	202.50			
T *Discoaster hamatus*	21X-CC	202.50	8.85	6	
	22X-1, 129–131	203.79			
T *Cyrtocapsella japonica*	24X-4, 85–87	227.25	10.0–10.3	2	
	24X-CC	231.60			
B *Discoaster hamatus*	25X-5, 115–116	238.75	10.0	6	
	25X-6, 115–116	240.25			
T *Globorotalia mayeri*	25X-CC	241.30	10.4	[f]6	
	26X-CC	250.90			
B *Catinaster coalitus*	25X-CC	241.30	10.8	6	
	26X-3, 117–119	245.47			
T *Lithopera thornburgi*	27X-4, 85–97	256.27			
	27X-CC	260.60			
T *Cyrtocapsella cornuta*	27X-CC	260.60	11.6–11.9	2	
	28X-4, 85–87	265.96			
B *Discoaster kugleri*	30X-5, 115–116	287.05	13.1	6	
	30X-CC	289.60			
T *Sphenolithus heteromorphus*	31X-CC	299.20	14.4	6	
	32X-1, 115–116	300.35			

Note: T = upper limit, B indicates lower limit, and → = an evolutionary transition. Sources of ages are: 1 = Johnson et al., in press; 2 = Johnson and Nigrini, 1985; 3 = oxygen isotope data for Site 723 (N. Niitsuma, unpubl. data); 4 = Takayama and Sato, 1987; 6 = Berggren et al, 1985; and 8 = Sato et al., in press.

[a] North Atlantic data.
[b] Long axis greater than 6 μm.
[c] North Atlantic age consistent with Italian-type section.
[d] *E.* cf. *diaphanes* cited in this source.
[e] Age in western Pacific.
[f] *G. siakensis* cited in this source.

Calcareous Nannofossils

Hole 731A

Sample 117-731A-1H-5, 115–117 cm (5.62 mbsf), contains *Emiliania huxleyi* and is assigned to Pleistocene-Holocene Zone NN21. Samples 117-731A-1H-5, 115–117 cm (7.15–18.45 mbsf) contain neither *Emiliania huxleyi* nor *Pseudoemiliania lacunosa*, and are therefore assigned to Pleistocene Zone NN20 (Fig. 9). Sediments from 19.3 mbsf down to 83.85 mbsf (Samples 117-731A-2H, CC through 117-713A-9X-5, 115–117 cm) contain *P. lacunosa*, but no discoasters and are assigned to Zone NN19 (uppermost Pliocene to Pleistocene). In Samples 117-731A-7H, CC (67.0 mbsf), and -8X, CC (76.6 mbsf), we recognized some reworked Miocene and Pliocene species such as *Cyclicargolithus floridanus, Discoaster brouweri, D. quinqueramus, Reticulofenestra pseudoumbilica*, and *Sphenolithus moriformis*.

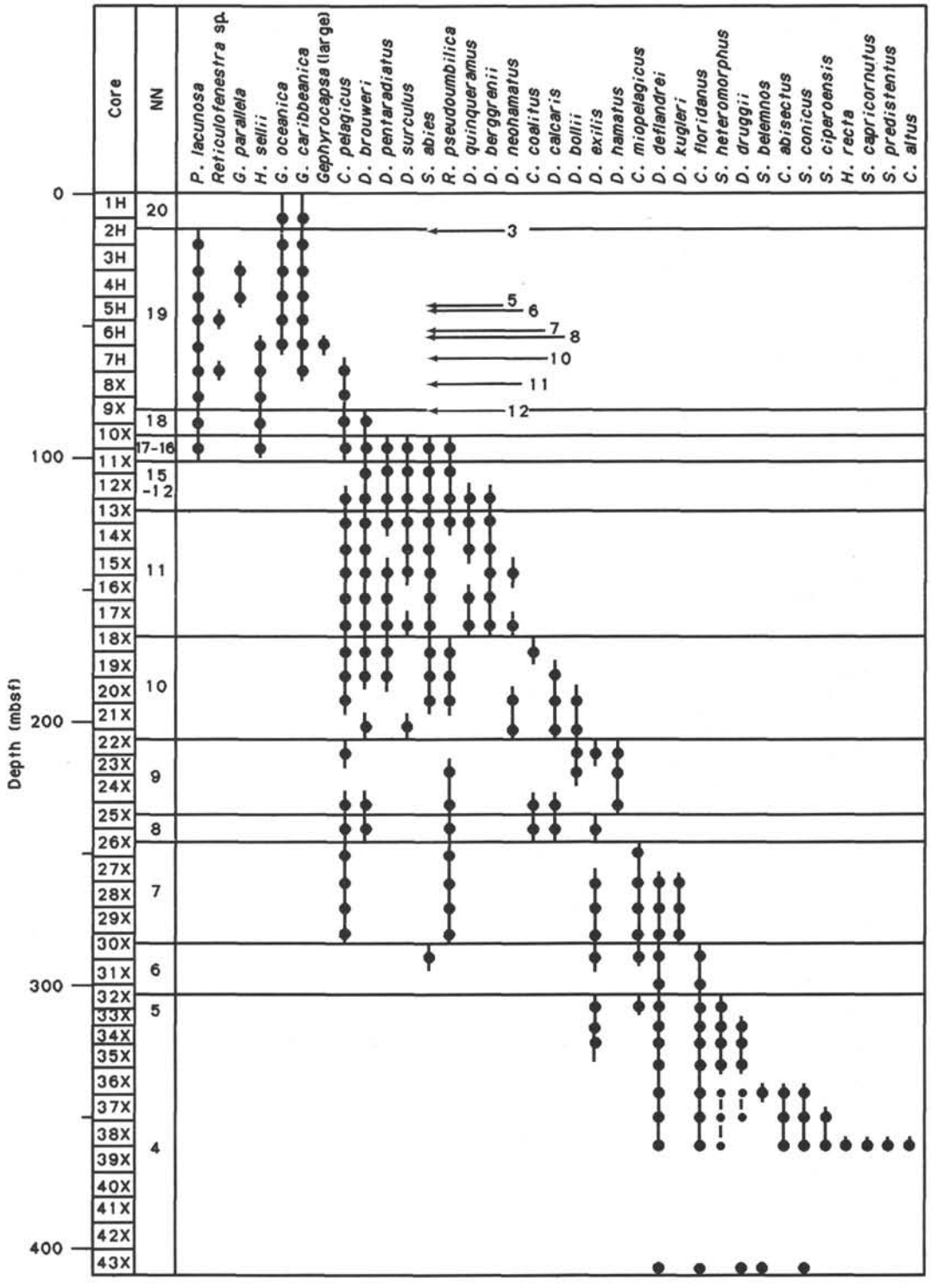

Figure 9. Distribution of selected calcareous nannofossil species in Hole 731A.

Nannofossils are abundant throughout this sequence with moderate to good preservation down to 38.3 mbsf. The preservation is poor throughout the remainder of Zone NN19.

The approximate position of the Pliocene/Pleistocene boundary is between Samples 117-731A-7H, CC, and 117-731A-8X-1, 115–117 cm (67.0–68.15 mbsf). Samples 117-731A-9X, CC (86.4 mbsf) and 117-731A-10X, CC (96.0 mbsf) contain rare specimens of *Discoaster brouweri*, but no specimens of *D. pentaradiatus* and is assigned to upper Pliocene Zone NN18. Nannofossils are abundant but poorly preserved.

Samples 117-731A-10X, CC (96.0 mbsf), through 117-731A-11X-1, 115–117 cm (97.15 mbsf), contain abundant nannofossils having moderate preservation. The assemblage contains *Discoaster brouweri, D. pentaradiatus*, and a few *D. surculus* and is assigned to Zone NN17.

As has been the case at the other sites of this leg, the zonal markers *Amaurolithus tricorniculatus* and *Ceratolithus rugosus* are missing and we must combine Zones NN15 through NN12. Samples 117-731A-11X-2, 116–118 cm, and -12X-5, 115–117 cm (98.66–112.85 mbsf), are given such a zonal assignment. Nannofossils having moderate to good preservation are abundant within these zones. The length of these zones is somewhat abbreviated, but without the ability to recognize these as four distinct zones, it is impossible to determine if a hiatus is present or a slow rate of sedimentation is responsible for this thin sedimentary section.

Samples 117-731A-12X-6, 115–117 cm, through -17X, CC (114.35–163.7 mbsf), contain *D. quinqueramus* and are assigned to Zone NN11 (upper Miocene). A diverse assemblage of discoasters is found in this zone, which in addition to *D. quinqueramus*, include: *D. berggrenii, D. brouweri, D. challengeri, D. neohamatus, D. neorectus, D. pentaradiatus, D. surculus, D. triradiatus*, and *D. variabilis*. Nannofossils are abundant with moderate preservation throughout this zone.

Neither *Discoaster hamatus* nor *D. quinqueramus* was found in Samples 117-731A-18X-1, 135–137 cm, through -21X, CC (165.05–202.5 mbsf), and so this interval can be assigned to upper Miocene Zone NN10. Nannofossils are abundant, and the preservation ranges from moderate to poor. The lowermost sample in this zone contains a few reworked specimens of *D. hamatus*.

D. hamatus is present in Samples 117-731A-22X-1, 129–131 cm, through 117-731A-25X-5, 115–116 cm (203.79–238.75 mbsf). These sediments are assigned to Zone NN9. Sample 117-731A-25X, CC (241.3 mbsf), lacks *D. hamatus* but contains *Catinaster coalitus* and is, therefore, assigned to Zone NN8 (middle to upper Miocene). Zone NN7 is characterized by the presence of *Discoaster kugleri* and the absence of *C. coalitus*. Samples 117-731A-26X-3, 117–119 cm, through 117-731A-30X5, 115–116 cm (245.47–287.05 mbsf) are assigned to this zone. Abundant, moderately well-preserved nannofossils are found in Zones NN9 through NN7.

Preservation becomes poor, specifically the nannofossils are heavily overgrown, and hinders a confident identification of the nannofossils in Samples 117-731-30X, CC, and -31X, CC (289.6–299.2 mbsf). Specimens tentatively identified as *Cyclicargolithus floridanus* were noted. The last appearance datum (LAD) of this species is used as one of the criteria for recognizing the top of Zone NN6. No *Sphenolithus heteromorphus* specimens were recognized which is consistent with the NN6 zonal assignment.

Sediments below Sample 117-731A-32X-1, 115-116 cm (300.35 mbsf) contain *S. heteromorphus. Helicosphaera ampliaperta*, whose LAD is used to define the top of Zone NN4, is not present in this region and so it is necessary to combine Zones NN5 and NN4. Nannofossils are abundant, but poorly preserved in Cores 117-731A-32X, CC, through -34X, CC; rare in 117-731A-35X, CC, and -36X, CC, and the preservation is moderate; abundant in 117-731A-37X, CC, and common in -38X, CC, and the preservation is moderate. Reworked Paleogene species are common. These include: *Chiasmolithus altus, Cyclicargolithus abisectus, Discoaster barbadiensis, Helicospheara recta, S. capricornutus, S. ciperoensis, S. conicus*, and *S. predistentus*.

Sample 117-731A-40X-1, 69 cm (371.1 mbsf), contains *S. belemnos* and *Discoaster druggii* and is assigned to lower Miocene Zones NN3 to NN2. Nannofossils are abundant, but the sphenoliths and asteroliths are strongly overgrown. Sample 117-731A-39X, CC (370.4 mbsf), was barren of nannofossils. Sample 117-731A-40X-1, 81 cm, contains rare, poorly preserved nannofossils, but it can be placed somewhere in the early Miocene. Samples 117-731-40X, CC, through -42X, CC (380.0–399.4 mbsf), are barren of nannofossils. Sample 117-731A-43X, CC (409.0 mbsf), contains abundant, poorly preserved nannofossils including *S. belemnos* and *D. druggii* and can be placed in lower Miocene Zone NN3. Drilling in Hole 731A stopped at a depth of 409.0 mbsf due to mechanical problems.

Hole 731B

Coring at Hole 731B commenced at 408.7 mbsf after the overlying section had been drilled and washed. Only five XCB cores were recovered from this hole before it, too, was abandoned because of mechanical problems. All five core-catcher samples (418.3–457.1 mbsf) are barren of nannofossils.

Hole 731C

Hole 731C was drilled down to a depth of 351.7 mbsf. At this point, washing commenced and continued to 502.4 mbsf. Sample 117-731C-1W-2, 39 cm, contains *S. heteromorphus* and *D. druggii* in an abundant, moderately preserved assemblage. A zonal assignment of NN5–NN4 (lower to middle Miocene) is given to this sample (Fig. 10). Sample 117-731C-1W, CC (502.4 mbsf), is barren of nannofossils. A rotary core was taken immediately below the washed core. Sample 117-731C-2R, CC (512.1 mbsf), contains abundant, well-preserved nannofossils. *Sphenolithus belemnos, S. dissimilis*, and *Cyclicargolithus abisectus* are present. This sample is assigned to Zone NN2. Washing of the hole continued from 512.1 to 560.1 mbsf. Within this interval, Sample 117-731C-3W-2, 80 cm, was found to contain *D. druggii, C. abisectus, Triquetrorhabdulus carinatus*, and *S. belemnos*, in an abundant but poorly preserved assemblage, and can be assigned to lower Miocene Zone NN2. Sample 117-731C-3W, CC (560.2 mbsf), contains rare nannofossils with moderate to poor preservation. Age-diagnostic taxa are not recognizable, but a presumably reworked specimen of the Eocene genus *Chiasmolithus* was noted. Core 117-731C-4R was taken immediately below the washed interval, but the core catcher was barren of nannofossils. Hole 731C was washed from 569.9 mbsf to 618.1 mbsf. The core catcher of -5W contains rare, poorly preserved nannofossils which are not age-diagnostic. Core 117-731C-6R, was taken immediately below the washed interval. Sample 117-731C-6R, CC, contains rare, poorly preserved, non-age-diagnostic forms. Core 117-731C-7W is from the washed interval between 627.8 mbsf and 675.9 mbsf. An abundant, but poorly preserved, nannofossil flora is contained in Sample 117-731C-7W-2, 83–84 cm. This assemblage is composed of *C. abisectus, Dictyoccites bisectus*, and *Coccolithus eopelagicus* together with long-ranging species such as *Cyclicargolithus floridanus* and *S. moriformis*. Therefore, this sample is referred tentatively to upper Oligocene Zone NP25. Below this, sediments down to the bottom of the hole are all barren or have so few nannofossils that they should be considered barren. The one and only brief flicker of hope was in Sample 117-731C-13W-5, 75 cm (Core 13W spanned from 801.1 to 849.4 mbsf). An abundant, yet poorly preserved nannofossil assemblage which includes *Cycli-*

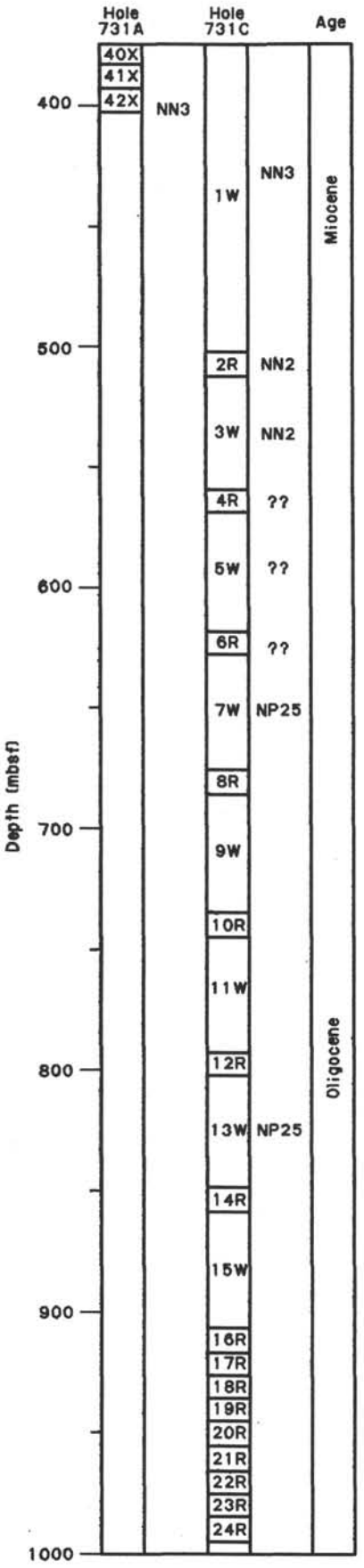

Figure 10. Distribution of selected calcareous nannofossil zones in Hole 731C.

cargolithus abisectus, C. floridanus, Discoaster deflandrei, Helicosphaera euphratis, H. recta, Sphenolithus ciperoensis, and *S. dissimilis*. A zonal assignment of NP25 (upper Oligocene) has been given to this sample.

Radiolarians

In Hole 731A all samples from Cores 117-731A-1H, CC, through 117-731A-29X (9.8–279.9 mbsf) contain radiolarians. Below this level all samples are barren. Diatoms are a common component of the siliceous fauna between Samples 117-731A-16X, CC (154.0 mbsf), and 117-731A-27X, CC (260.6 mbsf). No siliceous microfossils occur in any of the material recovered at Holes 731B or 731C.

Samples 117-731A-1H, CC (9.8 mbsf) and 117-731A-2H, CC (19.3 mbsf) contain a few, moderately well-preserved radiolarians which appear to belong to the *Amphirhopalum ypsilon* Zone. Both preservation and abundance improve below Sample 117-731A-3H-4, 85–87 cm (24.65 mbsf), and remain relatively good through Sample 117-731A-20X, CC (192.8 mbsf). The *A. ypsilon/Anthocyrtidium angulare* zonal boundary lies between Samples 117-731A-5H, CC (47.8 mbsf), and 117-731A-6H-4, 85–87 cm (53.15 mbsf). Based on a single fragment of *Pterocanium prismatium*, Sample 117-731A-8X, CC (76.7 mbsf), has been placed in the *P. prismatium* Zone. *P. prismatium* is also very rare in samples from Cores 117-731A-9X and 117-731A-10X, but they are, nevertheless, placed in the *P. prismatium* Zone because *Stichocorys peregrina* is also absent. A hiatus probably occurs in the upper part of Core 117-731A-11X, because Sample 117-731A-11X-4, 85–87 cm (101.35 mbsf), belongs to the lower part of the *Spongaster pentas* Zone; *Lychnodictyum audax, Phormostichoartus fistula*, and *Phormostichoartus doliolum* are all present. Another hiatus lies within Core 117-731-12X, as the *Stichocorys peregrina* Zone is entirely missing. Sample 117-731A-12X, CC (115.4 mbsf), lies within the *Didymocyrtis penultima* Zone which continues through Sample 117-731A-15X-4, 85–87 cm (140.5 mbsf). The LAD of *Diartus hughesi* in Sample 117-731A-15X, CC (144.4 mbsf), denotes the top of the *Didymocyrtis antepenultima* Zone and its transition from *Diartus petterssoni* between Samples 117-731A-19X-4, 85–87 cm (178.75 mbsf), and 117-731A-19X, CC (183.1 mbsf), marks the boundary with the *D. petterssoni* Zone. The remainder of the radiolarian bearing sediment apparently belongs to this zone. Samples from Cores 117-731A-21X through 117-731A-23X show a slight decrease in radiolarian abundance and preservation; Samples 117-731A-28X, CC (270.2 mbsf), and 117-731A-29X, CC (279.9 mbsf), contain only rare radiolarians and many of those in 117-731A-29X, CC, have been pyritized.

Paleoenvironmental Implications

As with planktonic foraminifers, calcareous nannofossils attain their maximum diversity in tropical areas. According to McIntyre and Bé (1967), tropical and subtropical assemblages contain over three times more species than subarctic and subantarctic assemblages and thus, conform to present ideas on latitudinal changes in diversity. Many species such as *Coccolithus pelagicus* are obviously controlled by temperature; this species seems to be extremely rare or absent in tropical waters. In contrast with this, most species of *Sphenolithus*, some species of *Helicosphaera*, and probably all species of *Scyphosphaera* are absent in boreal waters (Martini, 1970).

Roth (1974) superimposed the paleotemperature curve based on planktonic foraminiferal assemblages on the stratigraphic changes of the nannofossil diversity values from DSDP Site 167 (Magellan Rise, central Pacific Ocean) and suggested that the species diversity of nannofossils was highest during times of warm temperatures and lowest during times of low temperatures.

Figure 11 shows the calcareous nannofossil species diversity in the operations area of Leg 117 (northwest Indian Ocean) compared to the typical tropical region (for example the tropical Pacific) in each calcareous nannofossil one. For example, in the the sediments referred to Zone NN5 (lower middle Miocene) in the tropical region, about 17 species commonly occur. These are: *Coccolithus miopelagicus, C. pelagicus, Cyclicargolithus floridanus, Calcidiscus leptoporus, C. macintyrei, Discoaster aulakos, D. deflandrei, D. exilis, D. variabilis, Helicosphaera granulata, H. carteri, Reticulofenestra pseudoumbilica, Sphenolithus abies, S. heteromorphus, S. moriformis, Triquetrorhabdulus rugosus*, and *Coronocyclus* sp. During Leg 117, we recognized common occurrences of all but the last two species mentioned above in Zone NN5 in both the Owen Ridge sites and the Oman margin sites. This means that about 88% of the total tropical flora was recognized in the area studied on this leg. This assemblage is considered to be similar to the tropical flora. The species diversity, however, gradually decreases upward and in Zone NN8 the nannofossil assemblage is about 64% of the tropical one. In Zone NN9 the flora is again "subtropical" (about 85%) and then rapidly becomes less diversified until Zone NN12 (about 36%). After that the diversity is around 50%, although it increases slightly upward. Based on this rough estimation, we can conclude that the calcareous nannofossils in this area were first affected by upwelling in the early late Miocene (about 9.5 Ma).

PALEOMAGNETISM

Magnetic Measurements

Paleomagnetic measurements were made on discrete specimens using the MINISPIN spinner magnetometer after alternating field (AF) demagnetization using the Schonstedt demagnetizer. Figure 12 shows the combined data from Holes 731A and 731C after AF demagnetization at 5 or 10 mT (depending on the initial intensity) and removal of points with circular standard deviations greater than 40°. Figure 13 shows the distributions of intensities (plotted on a logarithmic scale) for the pelagic sediments (above around 300 mbsf) and the turbiditic sediments (below around 300 mbsf), respectively. Intensities in the pelagic oozes average around 0.2 mA/m; significantly higher values (around 6.3 mA/m) occur in the turbidites. The inclination data for the relatively weakly magnetized pelagic oozes and chalks are significantly more scattered in comparison with the correlative intervals at the other Owen Ridge sites (Sites 721 and 722); this is partly a result of weaker intensities at Site 731, but may also reflect instrumental problems (increased noise level of the MINISPIN because of irregular spinning) during occupation of the site.

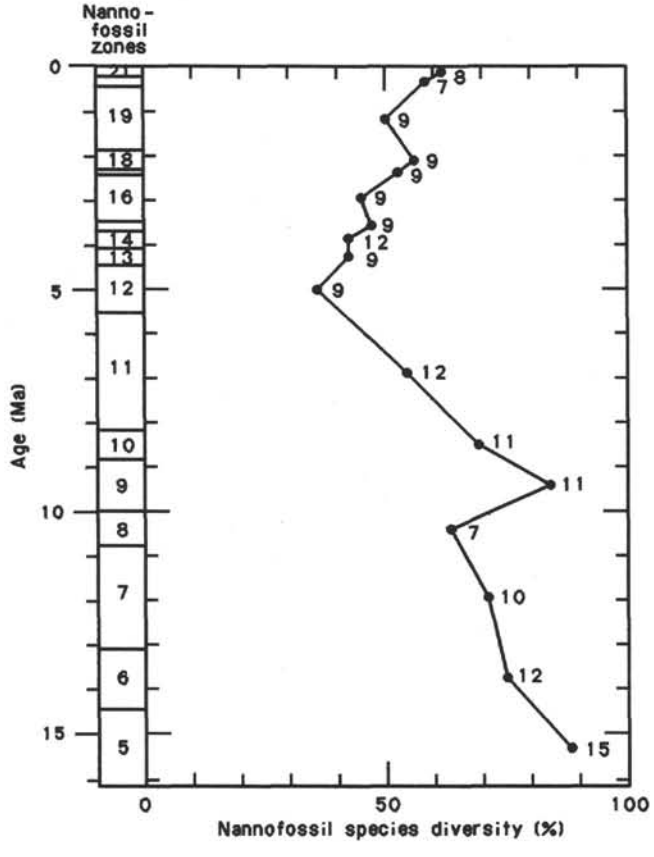

Figure 11. Calcareous nannofossil species diversity for Zones NN5 through NN21. Number is number of species occurring.

Because the AF demagnetization behavior of the Pleistocene and Pleistocene oozes on the Owen Ridge was relatively well-documented from efforts at previous Leg 117 sites, we confined such studies to specimens from the turbidite sequence. They showed variable behavior during demagnetization. The Zijderveldt plot for specimen from Core 117-731A-37X (Fig. 14) shows an example of a specimen which shows no sign of univectorial decay of the magnetization toward the origin, together with evidence of possible acquisition of anhysteretic remanent magnetization (ARM) above 25 mT. The Zijderveldt plots in Figures 15–16 of specimens from Cores 117-731A-40X and -43X show removal of a low coercivity overprint, followed by apparently univectorial decay toward the origin; however, they then exhibit increasing intensity (probably ARM acquisition) at fields greater than 30 mT. We are uncertain whether this behavior reflects intrinsic properties of the sediments or inadequacies of the shipboard AF demagnetizer. More careful AF and thermal demagnetization experiments will be performed on turbidite samples during post-cruise studies.

Magnetostratigraphy

Biostratigraphic datums of calcareous nannoplankton (see "Biostratigraphy" section, this chapter) were used in assignment of the polarity intervals above 100 mbsf. The top of acme *Reticulofenestra* sp. A and the first appearance datum of *Gephyrocapsa parallela* occur within Core 117-731A-5H. These datums occur between the Chron C1/C1r (Brunhes/Matuyama Chronozone) boundary and Subchron C1r-1 (Jaramillo Subchronozone). The last appearance datum of *Helicosphaera sellii* occurs in Core 117-731A-6H, and this datum predates Subchron C1r-1. In the shipboard results (Fig. 12), the uppermost reverse-to-normal transition was found at around 50 mbsf. Shore-based remeasurements with 15 mT AF demagnetization indicate that the boundary occurs between Samples 117-731-5H-5, 115 cm, and -5H-6, 45 cm. This suggests that, as at almost all of the other Oman margin and Owen Ridge sites, the Brunhes/Matuyama boundary has not been recorded clearly and that this first transition is the older Jaramillo boundary. Between this transition and the top of the turbidite sequence, a significant number of points were eliminated from the data set because of high circular standard deviations. Moreover, many of the remaining points do not accord with the expected axial dipole inclination for the site latitude (30.6°), as is reflected in Figure 13C. Therefore, we are reluctant to make any further correlations with the polarity time-scale on the basis of the shipboard data. Shore-based study of additional samples may significantly improve the paleomagnetic record over this interval.

Within the turbidite sequence the inclinations are consistently shallower (generally less than 10°) than in the pelagic sediments (Figs. 13C and -D). This implies that Site 731 was located significantly closer to the equator during the period of turbidite de-

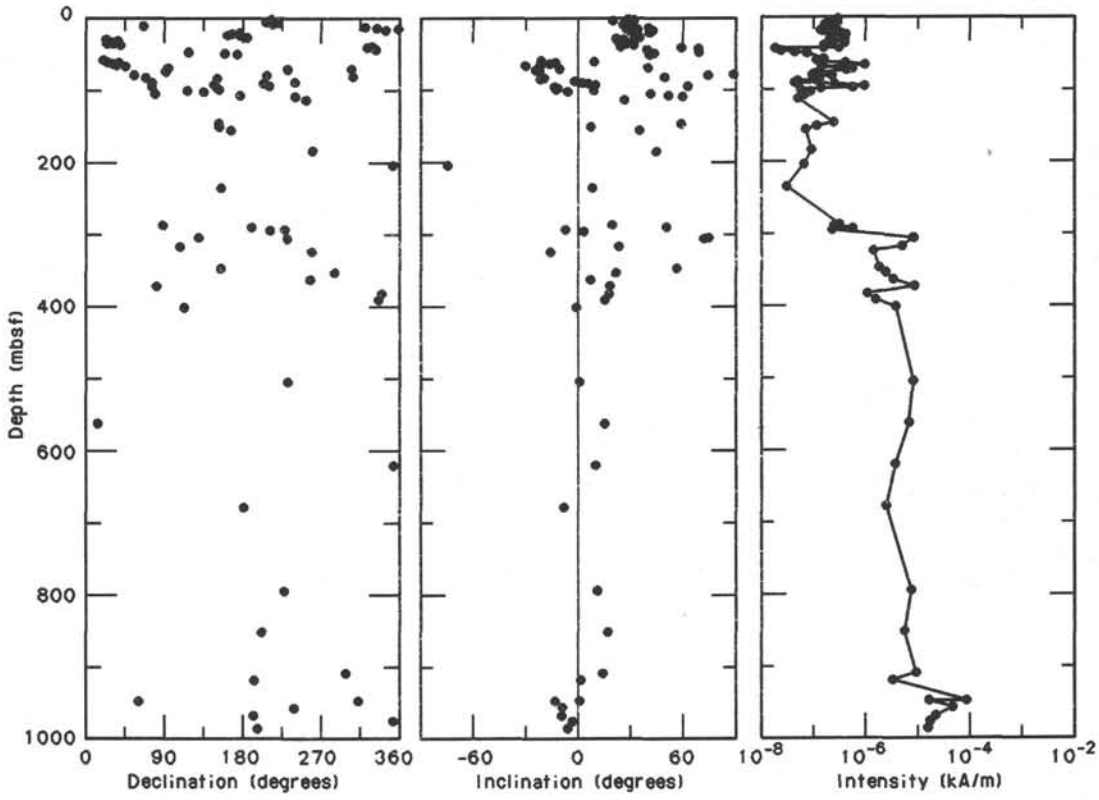

Figure 12. Plots of magnetic declination (relative values), inclination, and intensity vs. depth of Holes 731A and 731C, obtained after AF demagnetization at 5 or 10 mT and filtering circular standard deviation values greater than 40°.

position than at the present day. The mean of the absolute inclinations, excluding anomalously high values from Cores 117-731A-32X and -37X, is 11.0°, giving a paleolatitude of 5.6°. Some caution is required in using these data for quantitative estimation of paleolatitude because of the possibility of inclination error in what may be possibly rapidly deposited and nonbioturbated sediments; also no precise age control is available at present for the turbidites.

Magnetic Susceptibility

The volume magnetic susceptibility of Hole 731A sediments was measured using the Bartington Instruments' whole-core sensor at the 0.1 sensitivity and low-frequency (0.47 kHz) settings. Measurements were made at 5-cm intervals for a total of about 6800 measurements.

Four lithologic units were recognized at Hole 731A (see "Lithostratigraphy" section, this chapter). Lithologic Subunit IA (0–66.3 mbsf) is comprised of a marly nannofossil ooze with minor biosiliceous components. Unit I exhibits regular susceptibility fluctuations of ~1 m wavelength and about 30–100 × 10^{-6} volume SI units amplitude. The Hole 731A susceptibility record of Subunit IA can be correlated on a virtual point-for-point basis with Sites 721 and 722 which are also from the Owen Ridge (Fig. 17). Susceptibility fluctuations of ~2–3 m and ~4-5 m wavelengths are also apparent. If ~40 m/m.y. is used for the sedimentation rate of Site 731, these wavelengths correspond roughly to the ~19–23 k.y, ~41 k.y., and ~100 k.y. Milankovitch orbital isolation periodicities.

Lithologic Subunit IB (66.3–146.5 mbsf) is also a marly nannofossil ooze, but with no significant biosiliceous material. The susceptibility data representative of Unit IB are not significantly different in character from the data of Subunit IA (Fig. 18). However, pipe rust contamination of the upper ~1 m of the XCB cores did obscure many of the correlatable features which were apparent at Sites 721 and 722.

Lithologic Unit II (146.5–240.9 mbsf) consists of a marly diatom-rich nannofossil ooze. The susceptibility data from this unit are slightly lower in value than Unit I but a regular cyclicity of about ~1 m is apparent, despite XCB-coring disturbance and pipe rust contamination. The depression of susceptibility values near ~220 mbsf is coincident with increases in sediment porosity and biosiliceous (diatom) components, which suggests that this interval of low values may be due to dilution by biogenic sediment (Fig. 18). Flux data for the different components are required to say this with confidence, however.

Lithologic Unit III (240.9–320.1 mbsf) consists of nannofossil chalks without biosiliceous components. Susceptibility data in the lower part of this unit are generally higher and more variable than the overlying units (Fig. 19). The higher values reflect an increase in terrigenous component supply which was noted in the visual core descriptions of Unit III sediments.

Lithologic Unit IV (320.1–409.0 mbsf in Hole 731A) consists of numerous turbidite layers which are intercalated with higher carbonate pelagic layers. As with Sites 721 and 722, the turbidite layers are indicated by high susceptibility values, which presumably reflects the increased grain size and concentration of ferrimagnetic particles.

ACCUMULATION RATES

Sedimentation rates for the top 300 m of Site 731 are based on the mean depth and age of magneto- and biostratigraphic datum levels identified in Holes 731A (Table 5 and Fig. 20). Because of uncertainties in the shipboard paleomagnetic data (see "Explanatory Notes" chapter, this volume), we favor the nannofossil biostratigraphic datums for the determination of the sedimentation rates at Leg 117 sites. For the interval from 0 to 2.4

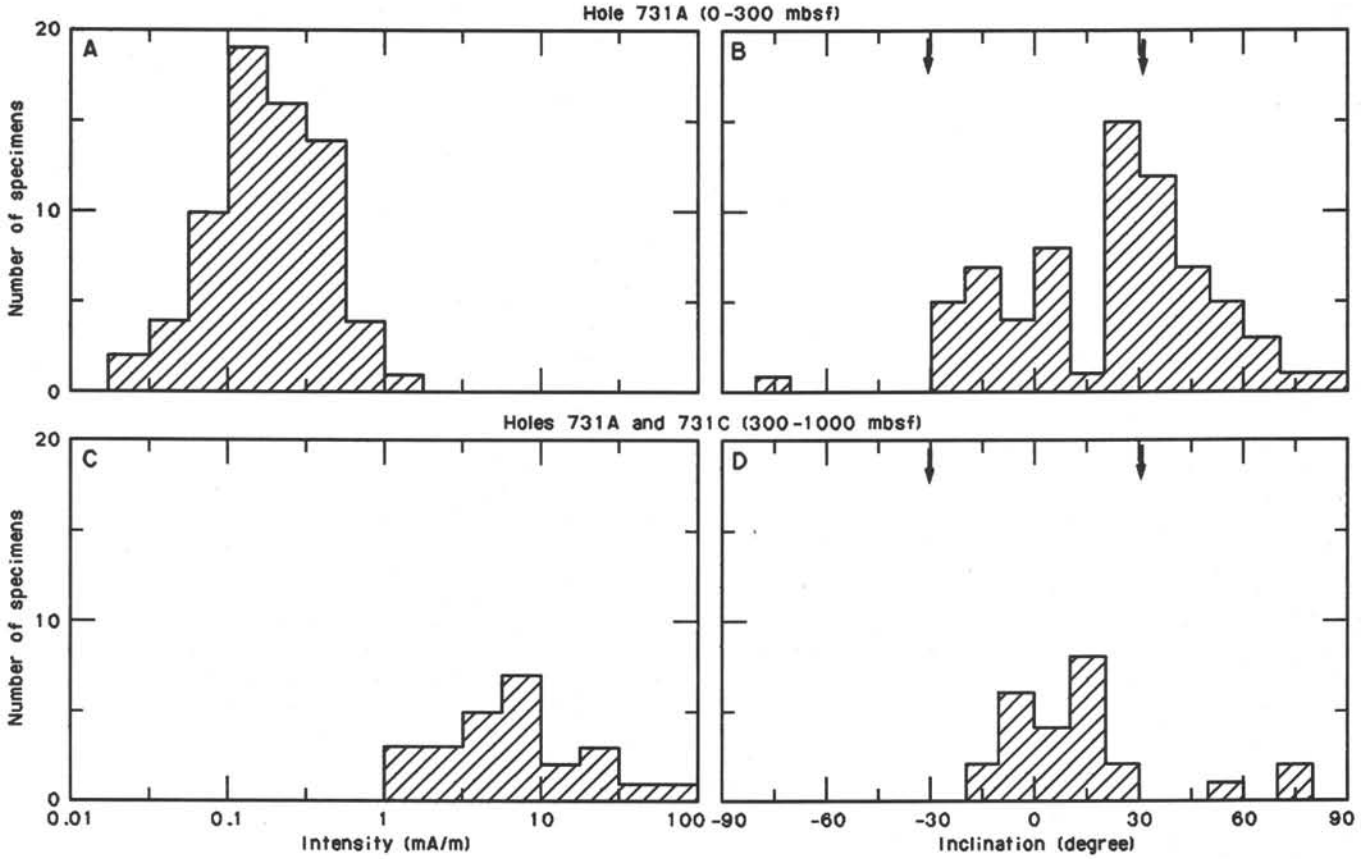

Figure 13. Histograms of magnetic inclination and intensity values from the interval above 300 mbsf of Hole 731A (A and B) and below 300 mbsf of Holes 731A and 731C (C and D). Arrows show the inclination values expected from the geocentric axial dipole field (30.6°).

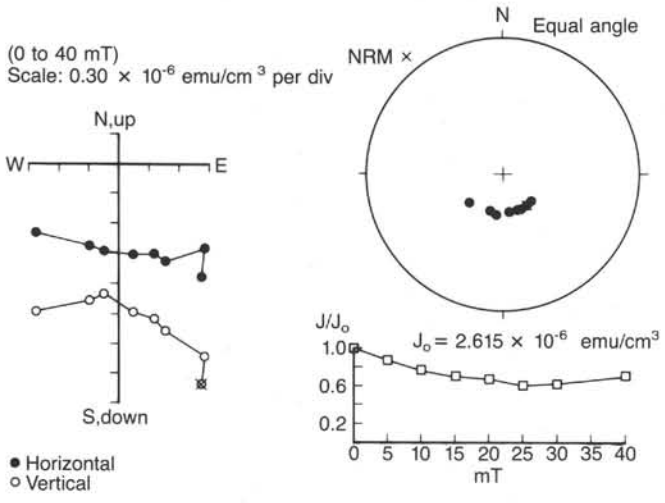

Figure 14. Result of stepwise AF demagnetization for Sample 117-731A-37X-3, 137–139 cm.

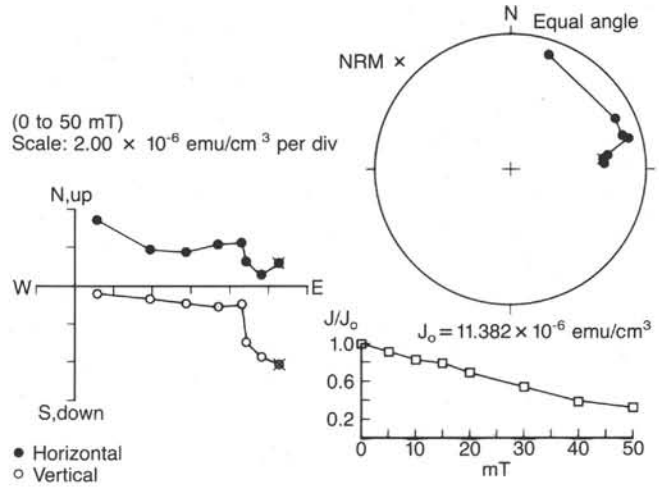

Figure 15. Result of stepwise AF demagnetization for Sample 117-731A-40X-1, 32–34 cm.

m.y., we used six nannofossil datums with ages based on oxygen isotope stratigraphy (N. Niitsuma, unpubl. data) and from Berggren et al. (1985) to determine variations in the mean sedimentation (Tables 4 and 5). These same biohorizons are used to determine the mean sedimentation rate at other Leg 117 sites to permit the comparison of sediment accumulation of hemipelagic deposits on the Oman margin and the pelagic sediments on the Owen Ridge.

Site 731 encountered the same sedimentary sequence as in nearby Sites 721 and 722, and the same four lithologic units are identified at all three sites. These lithologic units reflect the changing depositional environment of the site due to the uplift of the Owen Ridge, and variations in surface plankton activity. At Site 731, one or more gaps in sediment accumulation are evident between 97 and 115 mbsf. These gaps represent a hiatus that spans more than 3 m.y. The comparable section at Site 722

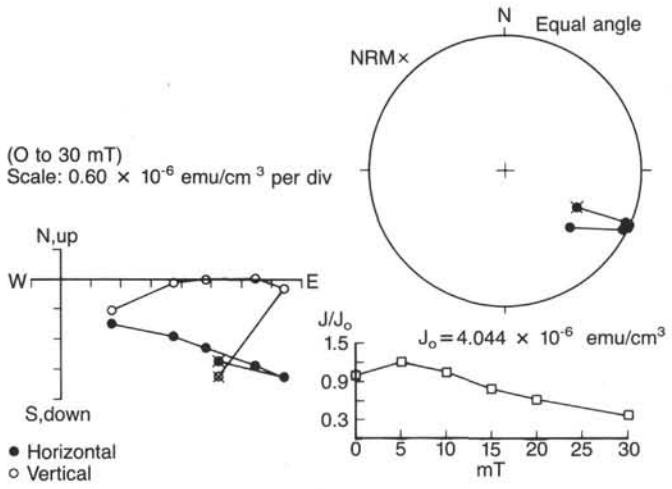

Figure 16. Result of stepwise AF demagnetization for Sample 117-731A-43X-1, 22–24 cm.

appears complete and undisturbed. Because of poor age control in the turbidite sequence of lithologic Unit IV, no estimate of sedimentation rate can be made at this time.

Lithologic Unit III, a nannofossil chalk deposited in the middle Miocene, is characterized by relatively low mean sedimentation rates of 9–30 m/m.y. These low rates reflect pelagic sedimentation above the zone of turbidite deposition but still in waters corrosive to calcium carbonate. The transition from Unit III to II is identified by an increase in opal-rich sediments which characterize lithologic Unit II. Sedimentation rates which average 30–35 m/m.y. are associated with the upper Miocene opal-rich sediments of lithologic Unit II (Fig. 20 and Table 5).

The nannofossil oozes/chalks of lithologic Unit I ranging from late Miocene to Holocene were deposited at mean rates of 20–69 m/m.y., but sedimentation is interrupted by the hiatus noted above (Fig. 20 and Table 5). The Pleistocene sedimentation rates at Site 731 are similar to, but slightly higher than, those at Owen Ridge Sites 721 and 722. However, further downhole the rates at Site 731 are lower than at Sites 721 and 722.

The mass accumulation of calcium carbonate, noncarbonate (100 − $CaCO_3$), and organic carbon are calculated from the average values between selected datums (Table 5 and Fig. 21). These data allow independent examination of the temporal variability in each component. The accumulation rates of calcium carbonate and noncarbonate at Site 731 mostly mirror the sedimentation rate, and calcium carbonate accumulation is generally twice that of noncarbonate in Pliocene to Pleistocene deposits. These rates are characteristic of areas having a high production of calcium carbonate shells of coccolithophores and foraminifers with minimal postdepositional dissolution.

PHYSICAL PROPERTIES

Introduction

Physical properties measured on discrete samples of sediment from Site 731 include index properties (wet-bulk density, porosity, water content, and grain density), compressional-wave velocity, thermal conductivity, and vane shear strength. The properties determined for Holes 731A, 731B, and 731C are listed in Tables 6, 7, and 8, respectively. The GRAPE and *P*-wave logging systems were used to measure the wet-bulk density and compressional-wave velocity of all whole-round sections that substantially filled the core liner and were longer than 80 cm. All techniques and equipment used are described in the "Explanatory Notes" chapter (this volume).

The pattern of variation of physical properties at Site 731 is similar to the patterns displayed at the other Owen Ridge sites, Sites 721 and 722. Transitions in the physical properties profiles mark the boundaries between the four lithologic units at Site 731 in a manner similar to that at Sites 721 and 722.

Index Properties

Lithologic Unit I

The nannofossil ooze and marly nannofossil ooze of lithologic Unit I (0–146.5 mbsf) display normal trends of decreasing porosity and water content and increasing wet-bulk density with increasing burial depth. In lithologic Unit I, porosity decreases from 75% to 61%, water content decreases from 52% to 37%, and wet-bulk density increases from 1.49 to 1.67 g/cm³ (Fig. 22). Grain density exhibits no consistent change downsection and varies about an average value of 2.57 g/cm³. Lithologic Subunit IA (0–66.3 mbsf), which is characterized by intermittent biosiliceous intervals, is distinguished from Subunit IB (66.3–146.5 mbsf) by a greater variability in porosity, water content, and wet-bulk density (Fig. 22).

The uppermost sediments of lithologic Unit I are characterized by higher porosity and water content and lower wet-bulk density than sediments near the seafloor at Sites 721 and 722. These differences are attributed to the siliceous-microfossil-rich intervals which are present in Subunit IA at Site 731 but do not occur at the other Owen Ridge sites. The values for porosity, water content, and wet-bulk density at the base of lithologic Unit I at Site 731 are comparable to those values at similar depths at Sites 721 and 722.

Lithologic Unit II

Downsection trends of index properties present in lithologic Unit I are reversed in lithologic Unit II (146.5–240.9 mbsf) reflecting the greater abundance of biogenic silica in the nannofossil oozes and diatomaceous marly nannofossil oozes of this unit. With increasing depth in lithologic Unit II, porosity increases from 63% to 66%, water content increases from 39% to 43%, grain density decreases from 2.68 to 2.52 g/cm³, and wet-bulk density decreases from 1.67 to 1.57 g/cm³ (Fig. 22). Variation of index properties in lithologic Unit II correlates well with the concentrations of organic carbon, calcium carbonate, and siliceous microfossils (see "Lithostratigraphy" section, this chapter). Sediments with a low concentration of calcium carbonate and high concentrations of organic carbon and biogenic silica are characterized by high porosity and water content and low grain and wet-bulk density.

Lithologic Unit III

Index properties in lithologic Unit III (240.9–320.1 mbsf) display a rapid and uniform change from the properties that characterize the nannofossil and marly nannofossil chalks at the base of lithologic Unit II and the terrigenous turbidites of lithologic Unit IV. A pronounced break in slope in the profiles of porosity, water content, and wet-bulk density occurs at 295 mbsf. This depth coincides with reductions in the concentrations of both calcium carbonate and organic carbon (see "Lithostratigraphy" section, this chapter). Between 240.9 and 294.5 mbsf porosity decreases from 66% to 49%, water content decreases from 43% to 27%, and wet-bulk density increases from 1.57 to 1.88 g/cm³ (Fig. 22). Below 295 mbsf, gradients in the porosity, water content, and wet-bulk density profiles are sharply reduced as porosity and water content decrease to 46% and 24%, respectively, and wet-bulk density increases to 1.97 g/cm³. The grain density

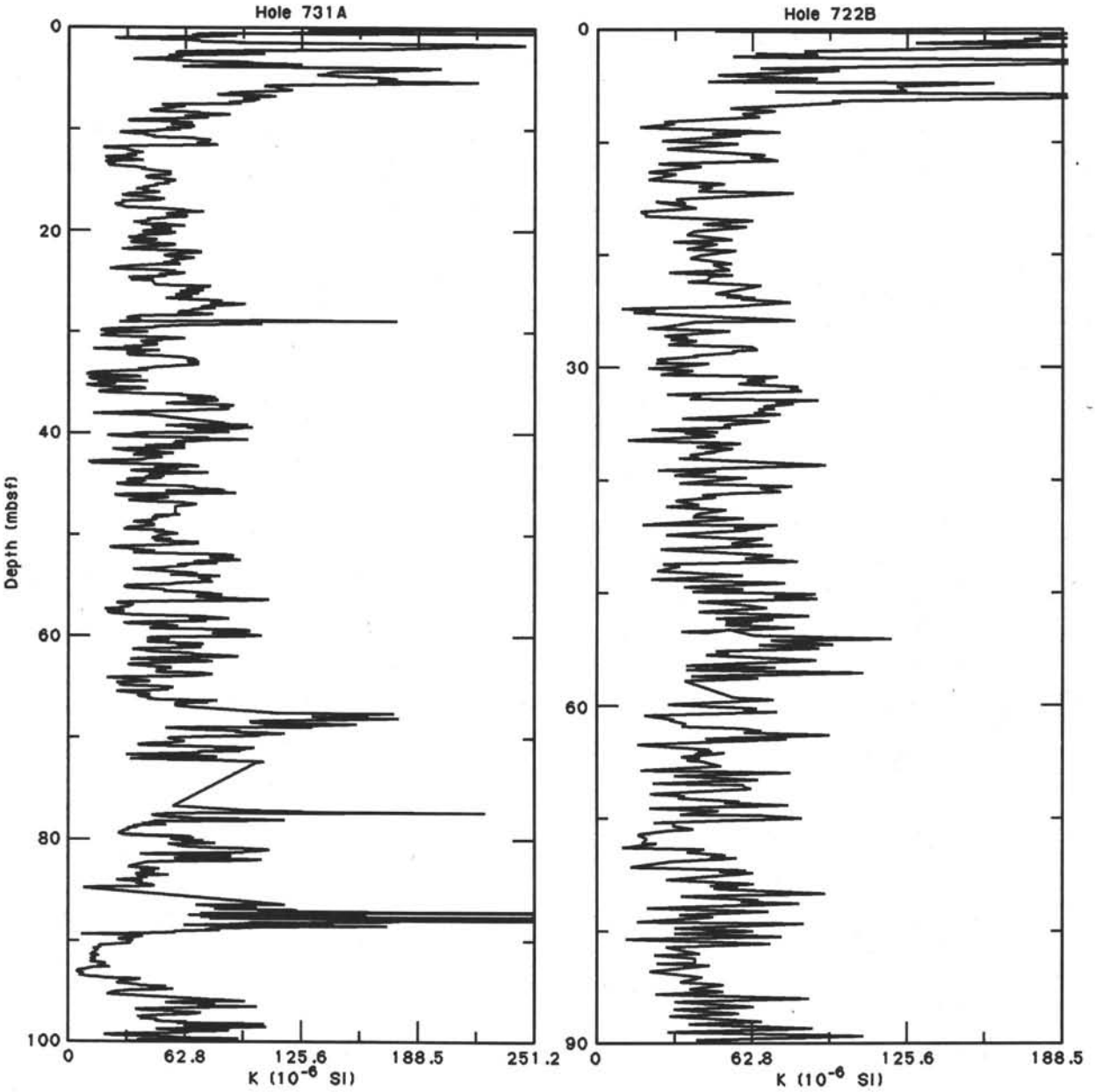

Figure 17. Volume magnetic susceptibility of Hole 731A (0–100 mbsf) compared to Hole 722B (0–90 mbsf), also from the Owen Ridge.

profile does not display a distinct gradient change in lithologic Unit III. Overall there is an increase in grain density from 2.52 g/cm^3 at 240.9 mbsf to 2.63 g/cm^3 at 320.1 mbsf (Fig. 22).

Lithologic Unit IV

Sediments of lithologic Unit IV (320.1–994.2 mbsf) exhibit volume reduction with depth that accompanies increasing overburden pressure. Within lithologic Unit IV properties of the coarse-grained turbidites (silty sandstones) and the fine-grained turbidites (clayey siltstones to claystones) differ. Downsection changes for fine-grained turbidites include decreases in porosity (48% to 31%) and water content (25% to 14%) and an increase in wet-bulk density (1.96 to 2.23 g/cm^3) (Fig. 22). Grain density of these sediments shows little change with increasing depth and averages 2.70 g/cm^3. The porosity profile of the fine-grained turbidites in lithologic Unit IV parallels the porosity profile at the nearby DSDP Site 222 (Arabian Basin), which has been used by Hamilton (1976) as a reference section for terrigenous deep-sea sediments. However, the porosity values at Site 731 are approximately 5%–8% less than the porosities at Site 222.

Index properties of the coarse-grained turbidites vary with the degree of cementation. Seven poorly cemented sandstones and four well-cemented sandstones were sampled between 428 mbsf and the base of lithologic Unit IV. Between 735.1 and 988.6 mbsf, the poorly cemented silty sandstones display downsection decreases in porosity (31% to 26%) and water content (14% to 11%) and increase in wet-bulk density (2.27 to 2.34 g/cm^3) (Tables 7 and 8). Grain density averages 2.69 g/cm^3 for these sandstones. Wet-bulk density, as determined by the 2-minute gamma ray attenuation porosity evaluator (GRAPE) technique, was the only index property measured for the well-cemented calcitic silty sandstones (Tables 7 and 8). The wet-bulk density of these sandstones averages 2.64 g/cm^3. The grain density of these sediments was not determined, but using the aver-

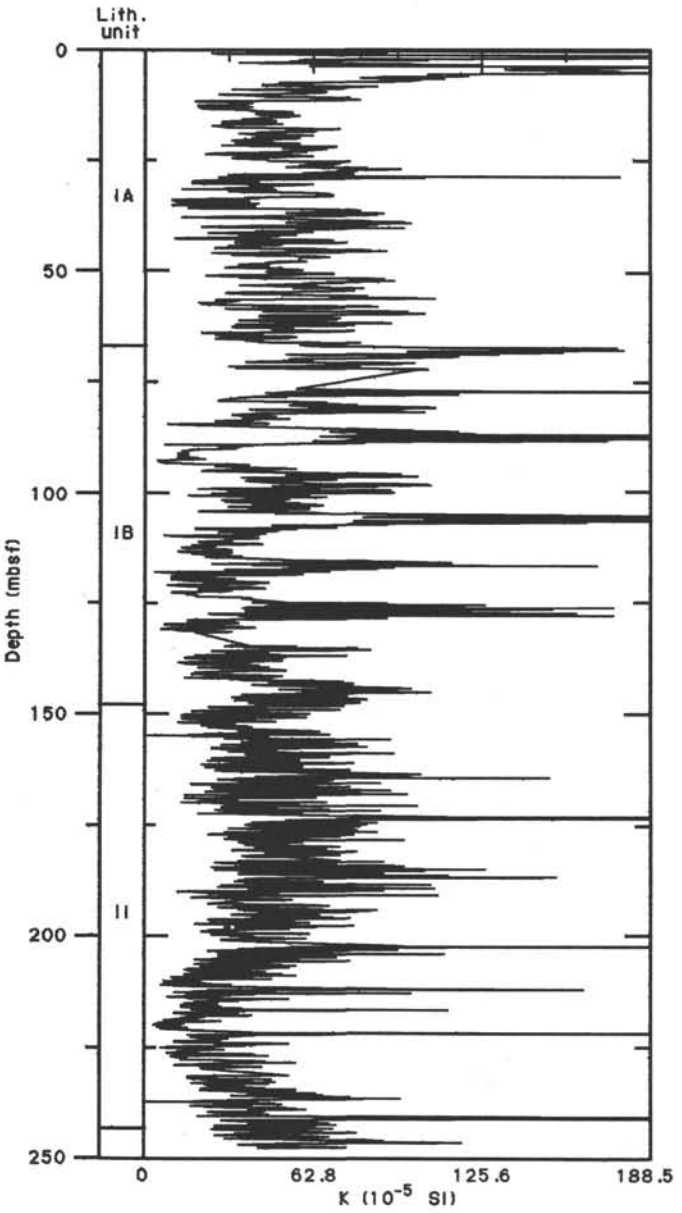

Figure 18. Volume magnetic susceptibility of Hole 731A. Measurements were made at 5-cm intervals.

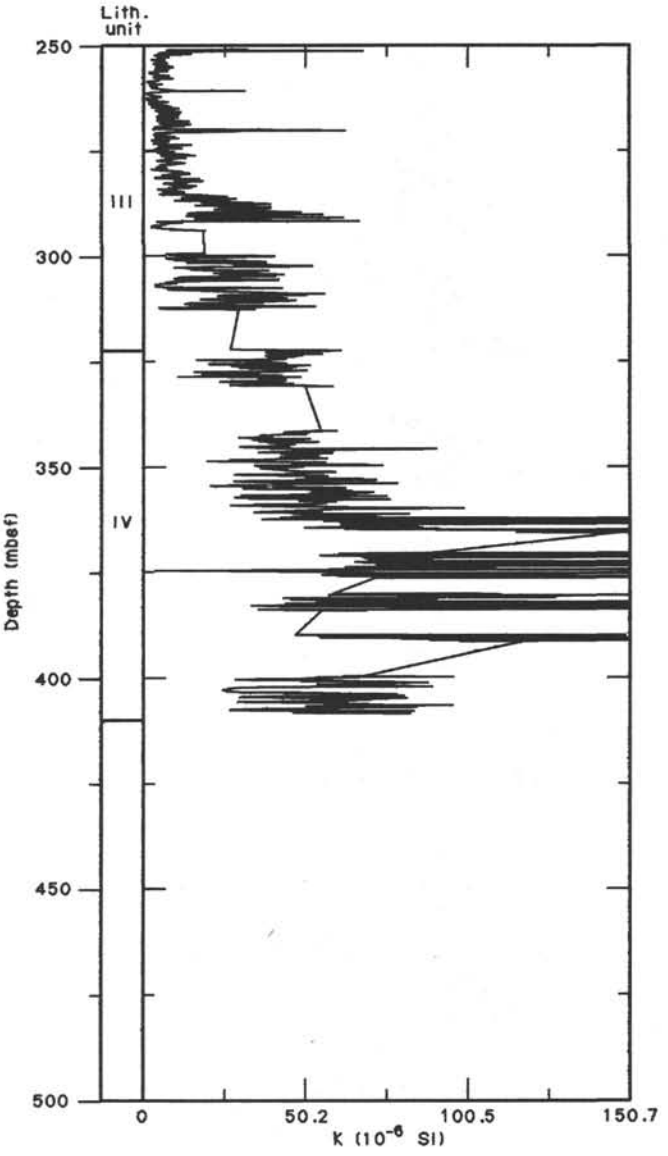

Figure 19. Volume magnetic susceptibility of Hole 731A, 250 mbsf to total depth.

Table 5. Sedimentation and accumulation rate data for Site 731.

Depth interval (mbsf)	Age range (m.y.)	$CaCO_3$ ($\bar{x}$ %)	C_{org} ($\bar{x}$ %)	Dry-bulk density ($\bar{x}$ g/cm^3)	Sed. rate ($\bar{x}$ m/m.y.)	$CaCO_3$ acc. rate (g/cm^2/k.y.)	Non-$CaCO_3$ acc. rate (g/cm^2/k.y.)	C_{org} acc. rate (mg/cm^2/k.y.)
0–6.4	0–0.19	73.7	1.37	0.741	33.7	1.84	0.657	34.2
6.4–18.9	0.19–0.49	68.2	0.26	0.984	41.7	2.80	1.30	10.7
18.9–41.7	0.49–0.82	65.4	0.50	0.934	69.1	4.22	2.23	32.3
41.7–65.2	0.82–1.45	61.6	0.42	0.982	37.3	2.26	1.41	15.4
65.2–85.1	1.45–1.9	63.6	1.01	0.996	44.2	2.80	1.60	44.5
85.1–97	1.9–2.4	68.4	0.50	1.010	23.8	1.64	0.760	24.3
115–142.5	5.75–7.15	66.1	0.35	1.029	19.6	0.683	1.33	7.06
142.5–203.1	7.15–8.85	42.8	0.65	0.882	35.6	1.80	1.34	20.4
203.1–288.3	8.85–13.1	49.3	0.65	0.937	20.0	0.950	0.924	12.2
288.3–299.8	13.1–14.4	65.0	0.08	1.474	8.85	0.457	0.848	1.04

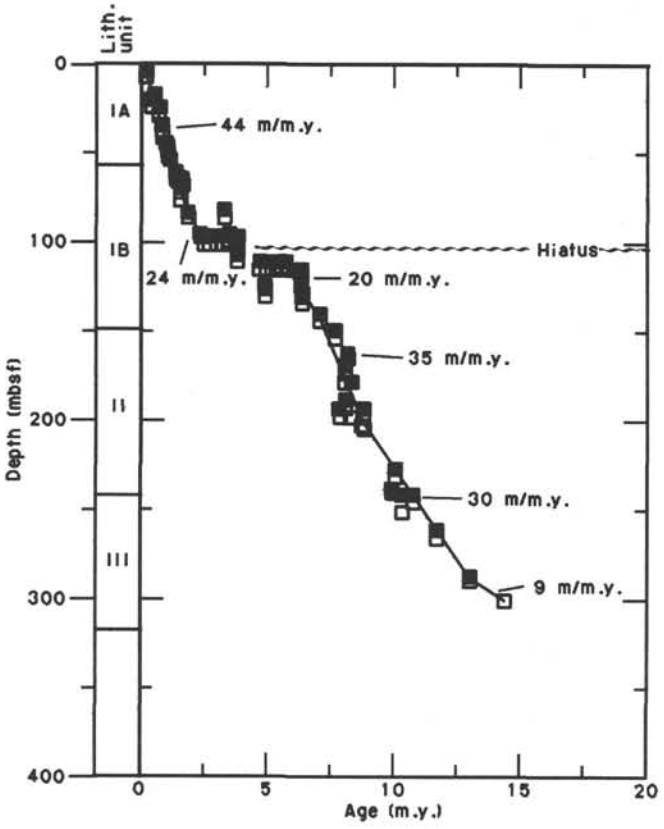

Figure 20. Age-depth plot of stratigraphic datums for Site 731 listed in Table 4. The solid and open boxes are the upper and lower depths of each datum level. Indicated sedimentation rates are based on a best fit to all stratigraphic data. Sedimentation rates calculated between reliable nannofossil datum levels in the top 85 m are listed in Table 5 and shown in Figure 21.

age grain density of the poorly cemented sandstones (2.69 g/cm^3) the porosity (ϕ) can be estimated using the equation:

$$(\phi) = [(\delta_s - \delta_{bw})/(\delta_{bw} - \delta_f)] \cdot 100$$

where δ_s = grain density, δ_{bw} = wet-bulk density, and δ_f = interstitial fluid density (assumed to be 1.025 g/cm^3). The estimated porosities range from 2% to 8% (Table 8). The porosity of Sample 117-731B-3X-1, 10–12 cm, could not be determined because its wet-bulk density (2.71 g/cm^3) is greater than the assumed grain density.

Compressional-Wave Velocity

At Site 731 compressional-wave velocities were measured perpendicular to bedding on discrete samples from cores recovered throughout Holes 731A, 731B, and 731C (Fig. 23). At depths greater than 200 mbsf, velocities were also measured parallel to bedding. The instrument-induced variation in the velocities is comparable in magnitude to that found at Sites 721 and 722. The velocity data from the nannofossil oozes/chalks and the uppermost clay-rich turbidites correlate well with wet-bulk density and display trends and gradients that are identical to those found at the other Owen Ridge sites. At this site, however, the extension of drilling to nearly 1000 mbsf has provided the opportunity to: (1) measure the velocity of the coarse-grained turbidites (silty-sandstones) recovered between 428 mbsf and total depth; (2) extend the velocity-density relationships of the turbidites to densities in excess of 2.6 g/cm^3; and (3) examine the development of velocity anisotropy in the more consolidated portions of the turbidite sequences.

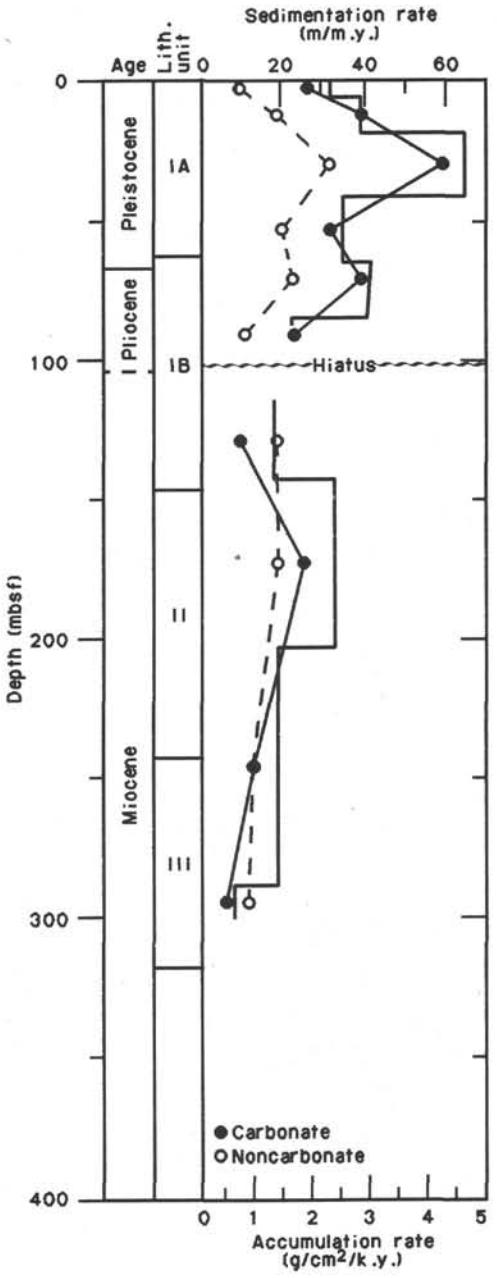

Figure 21. Sedimentation rate (m/m.y., solid line), calcium carbonate accumulation rate (g/cm^2/k.y., dots), and noncarbonate accumulation rate (g/cm^2/k.y., circles) vs. depth (mbsf) at Site 731. Accumulation rates are plotted at the midpoint of the respective depth intervals.

Within lithologic Unit I, compressional-wave velocity increases from 1510 m/s at depths just below the seafloor to 1570 m/s at 146.5 mbsf (Fig. 23). In the diatomaceous sequences of lithologic Unit II, velocity decreases slightly to a minimum value of 1540 m/s at 220 mbsf. As the biosiliceous sediment component decreases through lithologic Unit III, compressional-wave velocities increases rapidly to about 1650 m/s at 320 mbsf.

The relationships between wet-bulk density and compressional-wave velocity are well defined for both the nannofossil oozes/chalks and clay-rich turbidites for densities less than 2.0 g/cm^3 and 2.4 g/cm^3, respectively (Fig. 24). Given the limited

Table 6. Physical properties summary for Hole 731A.

Core, section, interval (cm)	Depth (mbsf)	Wet-bulk density (g/cm^3)	Porosity (%)	Water content (%)	Grain density (g/cm^3)	Dry-bulk density (g/cm^3)	Velocity (m/s)	Thermal conductivity (w/m/−k)	Vane shear strength (kPa)
117-731A-									
1H-1, 96–98	0.96	1.486	74.9	51.7	2.563	0.718			
1H-3, 80–82	3.80	1.510	72.8	49.4	2.593	0.764			7.1
1H-5, 80–82	6.80	1.590	61.9	39.9	2.609	0.956			
2H-2, 80–82	12.10	1.608	63.0	40.1	2.546	0.963		1.28	
2H-4, 80–82	15.10	1.658	66.4	41.0	2.681	0.977		1.25	12.9
2H-6, 80–82	18.10	1.692	63.9	38.7	2.625	1.038	[a]1511	1.29	
3H-2, 80–82	21.60	1.536	67.0	44.7	2.493	0.850			
3H-4, 80–82	24.60	1.480	69.2	47.9	2.550	0.770			18.5
3H-6, 80–82	27.60	1.658	63.7	39.4	2.682	1.005	[a]1507		
4H-2, 80–82	31.10	1.707	67.0	40.2	2.588	1.021		1.36	
4H-4, 80–82	34.10	1.497	72.7	49.8	2.505	0.751		1.13	36.1
4H-6, 80–82	37.10	1.667	62.1	38.2	2.574	1.030	[a]1572	1.34	
5H-2, 80–82	40.60	1.724	59.7	35.5	2.635	1.112			
5H-4, 80–82	43.60	1.655	63.3	39.2	2.621	1.007			22.3
5H-6, 80–82	46.60	1.563	68.1	44.7	2.490	0.865	[a]1529		
6H-2, 80–82	50.10	1.658	63.5	39.2	2.637	1.007		1.30	
6H-4, 80–82	53.10	1.655	60.5	37.5	2.562	1.035		1.27	
6H-6, 80–82	56.10	1.670	61.8	37.9	2.526	1.037	[a]1551	1.35	
7H-2, 80–82	59.60	1.658	55.6	34.3	2.519	1.089			
7H-4, 80–82	62.60	1.532	68.4	45.7	2.380	0.832			68.4
7H-6, 80–82	65.60	1.629	64.2	40.4	2.625	0.971	[a]1547		
8X-2, 64–66	69.14	1.694	62.1	37.6	2.664	1.057		1.35	27.6
8X-3, 80–82	70.80	1.616	64.8	41.1	2.586	0.952	[a]1545	1.33	
9X-2, 80–82	79.00	1.581	66.4	43.0	2.576	0.901			
9X-4, 80–82	82.00	1.712	60.1	36.0	2.675	1.095			37.2
9X-6, 39–41	84.59	1.635	61.7	38.7	2.498	1.002	[a]1545		
10X-2, 80–82	88.70	1.723	60.7	36.1	2.676	1.101		1.36	
10X-4, 80–82	91.70	1.623	62.6	39.5	2.505	0.982		1.10	42.0
10X-6, 82–84	94.72	1.601	63.9	40.9	2.558	0.947	[a]1534	1.15	
11X-2, 92–94	98.42	1.731	59.3	35.1	2.705	1.123			
11X-4, 92–94	101.42	1.683	59.5	36.2	2.533	1.074			49.3
11X-6, 92–94	104.42	1.684	59.5	36.2	2.539	1.075	[a]1550		
12X-2, 80–82	108.00	1.667	61.9	38.1	2.518	1.033		1.39	
12X-4, 77–79	110.97	1.659	60.7	37.5	2.532	1.038		1.14	
12X-6, 77–79	113.97	1.700	59.9	36.1	2.591	1.086	[a]1541	1.31	
13X-2, 84–86	117.74	1.657	59.7	36.9	2.489	1.046	[a]1559		
13X-4, 82–84	120.72	1.643	61.1	38.1	2.500	1.017			
13X-6, 99–101	123.89	1.665	63.4	39.0	2.499	1.015	[a]1560		
14X-3, 77–79	128.77	1.696	61.7	37.3	2.630	1.064		1.36	
14X-5, 75–77	131.75	1.650	62.3	38.7	2.556	1.012	[a]1578	1.36	
15X-4, 100–102	140.20	1.654	62.0	38.4	2.621	1.019	[a]1639		
15X-6, 62–64	142.82	1.665	60.5	37.2	2.578	1.045			
16X-2, 80–82	146.70							1.13	
16X-2, 103–105	146.93	1.669	62.9	38.6	2.679	1.025			
16X-4, 80–82	149.70							1.33	
16X-4, 100–102	149.90	1.682	63.1	38.4	2.639	1.036			
16X-6, 80–82	152.70							1.24	
17X-2, 125–127	156.75	1.489	68.7	47.3	2.367	0.785	[a]1551		
17X-4, 122–124	159.72	1.513	70.3	47.6	2.524	0.793	[a]1551		
17X-6, 113–115	162.63	1.553	66.4	43.8	2.464	0.873			
18X-2, 80–82	166.00							1.40	
18X-2, 102–104	166.22	1.584	64.4	41.7	2.482	0.924	[a]1565		
18X-4, 61–63	168.81	1.677	62.9	38.4	2.542	1.033	[a]1600		
18X-6, 80–82	172.00							0.99	
18X-6, 100–102	172.20	1.392	74.2	54.6	2.244	0.632			
19X-3, 86–88	177.26	1.624	62.5	39.4	2.529	0.984	[a]1550		
19X-6, 92–94	181.82	1.519	67.3	45.4	2.443	0.830	[a]1582		
20X-2, 80–82	185.40							1.39	
20X-4, 68–70	188.28	1.569	67.6	44.2	2.536	0.876	[a]1532		
20X-4, 80–82	188.40							1.09	
20X-6, 30–32	190.90	1.487	68.0	46.8	2.376	0.791	[a]1554		
20X-6, 80–82	191.40							1.29	
21X-2, 56–58	194.86	1.606	65.9	42.0	2.605	0.931	[a]1554		
21X-6, 48–50	200.78	1.418	72.3	52.3	2.364	0.677	[a]1571		
21X-6, 48–50	200.78						1572		
22X-2, 80–82	204.80							1.09	
22X-2, 99–101	204.99	1.409	73.2	53.2	2.332	0.659	[a]1551		
22X-2, 99–101	204.99						1555		
22X-4, 80–82	207.80							1.04	
22X-4, 98–100	207.98	1.385	76.1	56.3	2.404	0.606	[a]1558		
22X-6, 21–23	210.21	1.570	68.1	44.4	2.604	0.872	[a]1537		
22X-6, 21–23	210.21						1573		
22X-6, 80–82	210.80							0.94	
23X-2, 70–72	214.40	1.368	77.0	57.6	2.360	0.580	[a]1541		
23X-4, 70–72	217.40	1.524	69.2	46.5	2.521	0.815	[a]1538		

Table 6 (continued).

Core, section, interval (cm)	Depth (mbsf)	Wet-bulk density (g/cm^3)	Porosity (%)	Water content (%)	Grain density (g/cm^3)	Dry-bulk density (g/cm^3)	Velocity (m/s)	Thermal conductivity (w/m/−k)	Vane shear strength (kPa)
117-731A-									
23X-4, 70–72	217.40						1560		
24X-2, 108–110	224.48	1.400	72.3	52.9	2.310	0.660	[a]1549		
24X-2, 108–110	224.48						1591		
24X-4, 69–71	227.09	1.539	66.7	44.4	2.489	0.856	[a]1555		
24X-4, 69–71	227.09						1575		
24X-6, 18–20	229.58	1.389	75.9	56.0	2.339	0.611			
25X-2, 90–92	234.00	1.427	74.4	53.4	2.433	0.665	[a]1554		
25X-2, 90–92	234.00						1586		
25X-4, 94–96	237.04	1.550	66.9	44.2	2.512	0.865	[a]1558		
25X-4, 94–96	237.04						1584		
25X-6, 90–92	240.00	1.574	65.8	42.8	2.520	0.900			
26X-2, 100–102	243.80	1.625	62.7	39.5	2.551	0.983	[a]1556		
26X-2, 100–102	243.80						1562		
26X-4, 100–102	246.80	1.587	67.4	43.5	2.676	0.896	[a]1603		
26X-4, 100–102	246.80						1605		
27X-2, 79–81	253.19	1.661	60.6	37.4	2.581	1.041	[a]1591		
27X-2, 79–81	253.19						1614		
27X-4, 52–54	255.92	1.677	62.3	38.0	2.678	1.039	[a]1579		
27X-4, 52–54	255.92						1598		
27X-6, 120–122	259.60	1.687	59.3	36.0	2.604	1.080	[a]1591		
27X-6, 120–122	259.60						1610		
28X-2, 59–61	262.69	1.705	61.0	36.6	2.712	1.081	[a]1582		
28X-2, 59–61	262.69						1596		
28X-4, 63–65	265.73	1.638	64.1	40.1	2.692	0.982	[a]1602		
28X-4, 63–65	265.73						1639		
28X-6, 58–60	268.68	1.727	57.7	34.2	2.596	1.137	[a]1608		
28X-6, 58–60	268.68						1651		
29X-2, 80–82	272.50	1.753	58.0	33.9	2.662	1.159	[a]1616		
29X-2, 80–82	272.50						1629		
29X-4, 91–93	275.61	1.761	57.8	33.7	2.673	1.168	[a]1597		
29X-4, 91–93	275.61						1632		
29X-6, 92–94	278.62	1.805	54.2	30.7	2.630	1.250	[a]1616		
29X-6, 92–94	278.62						1631		
30X-2, 71–73	282.11	1.833	53.1	29.7	2.682	1.289	[a]1655		
30X-2, 71–73	282.11						1708		
30X-4, 76–78	285.16	1.821	51.1	28.8	2.664	1.297	[a]1585		
30X-4, 76–78	285.16						1614		
30X-6, 116–118	288.56	1.890	51.7	28.0	2.757	1.360	[a]1614		
30X-6, 116–118	288.56						1618		
31X-2, 51–53	291.61	1.876	48.5	26.5	2.632	1.380	[a]1640		
31X-2, 51–53	291.61						1630		
31X-CC, 18–20	294.53	2.014	42.9	21.8	2.677	1.574	[a]1704		
31X-CC, 18–20	294.53						1698		
32X-1, 28–30	299.48	2.017	42.5	21.6	2.689	1.582	[a]1835		
32X-1, 28–30	299.48						1904		
32X-5, 46–48	305.66	1.808	49.0	27.7	2.754	1.306	[a]1608		
32X-5, 46–48	305.66						1614		
33X-2, 25–27	310.65	1.965	46.9	24.5	2.705	1.485	[a]1663		
33X-2, 25–27	310.65	1691							
34X-1, 73–75	316.23	1.848	52.8	29.3	2.632	1.307	[a]1609		
34X-1, 73–75	316.23						1648		
34X-2, 69–71	317.69	1.972	45.6	23.7	2.651	1.505	[a]1606		
34X-2, 69–71	317.69						1702		
35X-1, 77–79	322.87	1.961	47.8	25.0	2.698	1.471	[a]1637		
35X-1, 77–79	322.87						1655		
35X-5, 37–39	328.47	1.951	48.8	25.6	2.704	1.451	[a]1669		
35X-5, 37–39	328.47						1675		
37X-3, 25–27	344.55	2.022	46.5	23.6	2.783	1.545	[a]1657		
37X-6, 84–86	349.64	2.075	39.5	19.5	2.589	1.671			
38X-3, 31–33	354.31	2.001	43.1	22.1	2.665	1.560	[a]1659		
38X-3, 31–33	354.31						1681		
38X-6, 66–68	359.16	1.978	47.9	24.8	2.768	1.487	[a]1619		
38X-6, 66–68	359.16						1628		
39X-1, 48–50	361.18	1.873	53.3	29.1	2.683	1.327	[a]1582		
39X-1, 48–50	361.18						1624		
39X-3, 110–112	364.80	1.847	48.8	27.1	2.733	1.348	[a]1595		
39X-3, 110–112	364.80						1587		
40X-2, 137–139	373.27	2.006	45.3	23.1	2.708	1.542	[a]1649		
40X-2, 137–139	373.27						1654		
40X-4, 91–93	375.81	2.010	44.9	22.9	2.727	1.551	[a]1665		
40X-4, 91–93	375.81						1670		
41X-2, 91–93	382.41	1.918	48.0	25.7	2.622	1.426	[a]1596		
41X-2, 91–93	382.41						1594		
42X-1, 68–70	390.38	1.916	49.0	26.2	2.728	1.414	[a]1592		
42X-1, 68–70	390.38						1629		
43X-2, 52–54	401.42	1.979	45.9	23.8	2.714	1.508	[a]1643		

Table 6 (continued).

Core, section, interval (cm)	Depth (mbsf)	Wet-bulk density (g/cm^3)	Porosity (%)	Water content (%)	Grain density (g/cm^3)	Dry-bulk density (g/cm^3)	Velocity (m/s)	Thermal conductivity (w/m/−k)	Vane shear strength (kPa)
117-731A-									
43X-2, 52–54	401.42						1707		
43X-4, 79–81	404.69	1.992	44.5	22.9	2.661	1.535	[a]1685		
43X-4, 79–81	404.69						1715		
43X-6, 92–94	407.82	1.976	46.1	23.9	2.692	1.503	[a]1668		
43X-6, 92–94	407.82						1748		

[a] Velocity measurement perpendicular to bedding; others measured parallel to bedding.

Table 7. Physical properties summary for Hole 731B.

Core, section, interval (cm)	Depth (mbsf)	Wet-bulk density (g/cm^3)	Porosity (%)	Water content (%)	Grain density (g/cm^3)	Dry-bulk density (g/cm^3)	Velocity (m/s)	Coarse-grained turbidites
117-731B-								
1X-1, 17–19	408.77	2.034	44.0	22.1	2.731	1.583	[a]1642	
1X-1, 17–19	408.77						1659	
2X-1, 34–36	418.64				2.637			ss
3X-1, 10–12	428.20	2.705					[a]4429	css
3X-1, 10–12	428.20						4638	css
3X-1, 80–82	428.90	2.021	41.3	20.9	2.658	1.599		
4X-1, 80–82	438.50				2.683			ss
4X-3, 47–49	441.17	2.176	46.1	21.7	2.752	1.704	[a]1627	
4X-3, 47–49	441.17						1653	
5X-1, 40–42	447.80	1.916	51.0	27.3	2.755	1.394	[a]1582	
5X-1, 40–42	447.80						1572	

Note: css = calcitic silty sandstone (well indurated) and ss = silty sandstone.
[a] Velocity measurement perpendicular to bedding; others measured parallel to bedding.

number of sandstone samples, the density-velocity relationship for the coarse-grained turbidites is less well-defined.

At Site 731, as at Sites 721 and 722, the variation of the velocities measured both parallel and perpendicular to bedding increases in the fine-grained turbidites of lithologic Unit IV. Four samples of poorly cemented silty sandstone recovered from depths between 900 and 1000 mbsf transmit compressional waves slightly faster than the adjacent clay-rich layers (Table 7), but are more readily distinguished by their low anisotropy (Fig. 25). In contrast, compressional-wave velocities measured perpendicular to bedding for well-indurated calcitic silty sandstone are markedly higher, ranging from 3801 to 4429 m/s.

The different lithologies recovered at Site 731 show distinctly different patterns of velocity anisotropy (Fig. 25). Within the nannofossil-rich sequences of lithologic Units I, II, and III, anisotropy varies considerably from 0.1% to 5.8% with an average value of 1.7% and little if any correlation to wet-bulk density. Anisotropy of the turbidites ranged from 0.3% to 15.1%, with considerable variation at all sub-bottom depths. On average, anisotropy of the turbidites increases with density, as a result of increased compaction and the resultant increases in preferred orientation of the platy-clay minerals. The poorly cemented silty sandstones displayed weak anisotropy. Two of the four poorly cemented sandstone samples display small negative anisotropies (velocity parallel to bedding less than that perpendicular to bedding), whereas anisotropy of the two remaining samples ranges from 1.2% to 3.3%. Velocity anisotropy of the calcitic silty sandstones is high, averaging 8.9%, but also highly variable, with values ranging from 4.6% to 18.4%.

Vane Shear Strength

Vane shear strengths were measured in Cores 117-731A-1H through -11X (0–102 mbsf). Throughout the seven APC cores, which sampled lithologic Subunit IA, shear strength increased at an average rate of 1.10 kPa/m to a maximum value of 68.4 kPa at 62.6 mbsf. In lithologic Subunit IB, beginning in Core 117-731A-8X, the shear strength dropped to 27.6 kPa and increased downsection at a rate of only 0.65 kPa/m. The low shear strengths in this unit probably reflect an increase in drilling-induced disturbance caused by the XCB coring system rather than a true decreases in shear strength associated with the change in lithology. These findings are identical to those found at Site 721 and 722 where shear strength gradients of 1.10 to 1.20 kPa/m were recorded in the intervals recovered by the APC and where markedly lower shear strengths and gradients were encountered in the XCB cores.

Thermal Conductivity

Thermal conductivity was measured on alternate cores from Hole 731A through Core 117-731A-22X (212 mbsf). Sediments recovered from greater depths were too stiff for insertion of the needle probes or too friable and brittle for accurate measurement. Through Subunits IA and IB, thermal conductivity varies from about 1.10 to 1.40 W/m·K, with a mean value for the unit of 1.30 W/m·K (Fig. 26). At depths greater than about 70 mbsf, the lowest values may result from insertion of the probe into slurry between the drilling biscuits rather than into the "undisturbed" sediment.

Within lithologic Unit II, thermal conductivity decreases downsection in tandem with the decrease in wet-bulk density. The markedly higher variability of thermal conductivity in this layer is most likely related to changes in sediment constituents, particularly the abundance of diatoms and organic matter which is responsible for the high variability of bulk density within this unit. However, given the relatively well-defined relationship between thermal conductivity and density (Fig. 27), it is likely that

Table 8. Physical properties summary for Hole 731C.

Core, section, interval (cm)	Depth (mbsf)	Wet-bulk density (g/cm^3)	Porosity (%)	Water content (%)	Grain density (g/cm^3)	Dry-bulk density (g/cm^3)	Velocity (m/s)	Coarse-grained turbidites
117-731C-								
2R-2, 76–78	504.66	2.092	38.2	18.7	2.646	1.700	[a]1724	
2R-2, 76–78	504.66						1776	
2R-3, 121–123	506.61	2.029	41.2	20.8	2.627	1.607	[a]1700	
2R-3, 121–123	506.61						1745	
4R-1, 36–38	560.56	2.120	39.9	19.3	2.755	1.711	[a]1709	
4R-1, 36–38	560.56						1803	
5W-4, 74–76	575.14	2.120	38.6	18.7	2.757	1.724	[a]1770	
5W-4, 74–76	575.14						1902	
6R-1, 94–96	619.04	2.084	39.7	19.5	2.709	1.678	[a]1748	
6R-1, 94–96	619.04						1831	
7W-1, 53–55	628.33	2.088	39.4	19.3	2.714	1.684	[a]1705	
7W-1, 53–55	628.33						1762	
8R-1, 62–64	676.52	2.082	44.4	21.9	2.779	1.627		
8R-4, 26–28	680.66	2.118	39.4	19.1	2.751	1.714	[a]1718	
8R-4, 26–28	680.66						1847	
10R-1, 22–24	733.82	2.208	36.7	17.0	2.766	1.832	[a]1815	
10R-1, 22–24	733.82						1966	
10R-2, 3–5	735.13	2.270	31.3	14.1	2.714	1.949	[a]1902	ss
10R-2, 43–45	735.53	2.216	34.3	15.9	2.760	1.865	[a]1830	
10R-2, 43–45	735.53						1899	
11W-1, 47–49	743.77	2.657	2.0				[a]3878	css
11W-1, 47–49	743.77						4691	css
11W-5, 137–139	750.67	2.204	34.8	16.2	2.761	1.847	[a]1779	
11W-5, 137–139	750.67						1854	
12R-1, 94–96	792.44	2.270	26.8	12.1	2.646	1.995	[a]2028	ss
12R-2, 137–139	794.37	2.201	33.9	15.8	2.715	1.854	[a]1832	
12R-2, 137–139	794.37						1912	
12R-3, 95–97	795.45	2.185	33.1	15.5	2.712	1.845	[a]1837	
12R-3, 95–97	795.45						1952	
14R-1, 27–29	849.67	2.566	8.0				[a]3801	css
14R-1, 27–29	849.67						4004	css
14R-1, 39–41	849.79	2.205	30.8	14.3	2.676	1.889	[a]2076	
14R-1, 39–41	849.79						2157	
16R-1, 137–139	908.67	2.222	31.0	14.3	2.636	1.904	[a]1910	
16R-1, 137–139	908.67						2143	
16R-2, 60–62	909.40	2.245	29.4	13.4	2.655	1.944	[a]1969	ss
16R-2, 60–62	909.40						1942	ss
16R-3, 6–8	910.36	2.232	30.3	13.9	2.594	1.922	[a]1938	
16R-3, 6–8	910.36						2124	
17R-2, 143–145	919.63	2.302	24.5	10.9	2.678	2.051	[a]2220	ss
17R-2, 143–145	919.63						2246	ss
17R-4, 2–4	921.22	2.227	31.0	14.2	2.699	1.910	[a]1925	
17R-4, 2–4	921.22						2085	
19R-1, 141–143	937.51	2.279	29.4	13.2	2.665	1.977	[a]1949	
19R-1, 141–143	937.51						2141	
19R-3, 8–10	939.18	2.330	29.1	12.8	2.711	2.031	[a]1980	
19R-3, 8–10	939.18						2094	
20R-1, 33–35	946.03	2.252	32.0	14.5	2.707	1.924	[a]1885	
20R-1, 33–35	946.03						2153	
20R-3, 61–63	949.31	2.260	32.2	14.6	2.710	1.930	[a]1862	
20R-3, 61–63	949.31						2166	
20R-4, 20–22	950.40	2.331	28.3	12.5	2.740	2.040	[a]1967	
20R-4, 20–22	950.40						2158	
21R-1, 17–19	955.57	2.272	33.7	15.2	2.721	1.927	[a]1853	
21R-1, 17–19	955.57						2107	
21R-2, 121–123	958.11	2.245	31.0	14.1	2.678	1.927	[a]1838	
21R-2, 121–123	958.11						2054	
21R-3, 0–2	958.40	2.629	3.7				[a]4331	css
21R-3, 0–2	958.40						4667	css
22R-1, 90–92	966.00	2.286	28.2	12.6	2.670	1.997	[a]2001	ss
22R-2, 82–84	967.42	2.265	29.6	13.4	2.689	1.962	[a]1975	
22R-2, 82–84	967.42						2243	
22R-4, 15–17	969.75	2.250	28.3	12.9	2.665	1.960	[a]1983	
22R-4, 15–17	969.75						2207	
23R-1, 68–70	975.48	2.320	30.2	13.4	2.711	2.010	[a]1951	
23R-1, 68–70	975.48						2196	
23R-2, 83–85	977.13	2.434	27.2	11.4	2.737	2.156	[a]2346	ss
23R-2, 83–85	977.13						2426	ss
23R-4, 13–15	979.43	2.237	29.2	13.4	2.759	1.938	[a]1959	
23R-4, 13–15	979.43						2289	
24R-1, 54–56	985.04	2.249	29.9	13.6	2.639	1.943	[a]1942	
24R-1, 54–56	985.04						2175	
24R-2, 136–138	987.36	2.226	30.5	14.1	2.675	1.913	[a]1875	
24R-2, 136–138	987.36						2067	
24R-3, 110–112	988.60	2.336	26.3	11.5	2.722	2.066	[a]2247	ss
24R-3, 110–112	988.60						2241	ss

Note: css = calcitic silty sandstone (well indurated) and ss = silty sandstone.
[a] Velocity measurement perpendicular to bedding; others measured parallel to bedding.

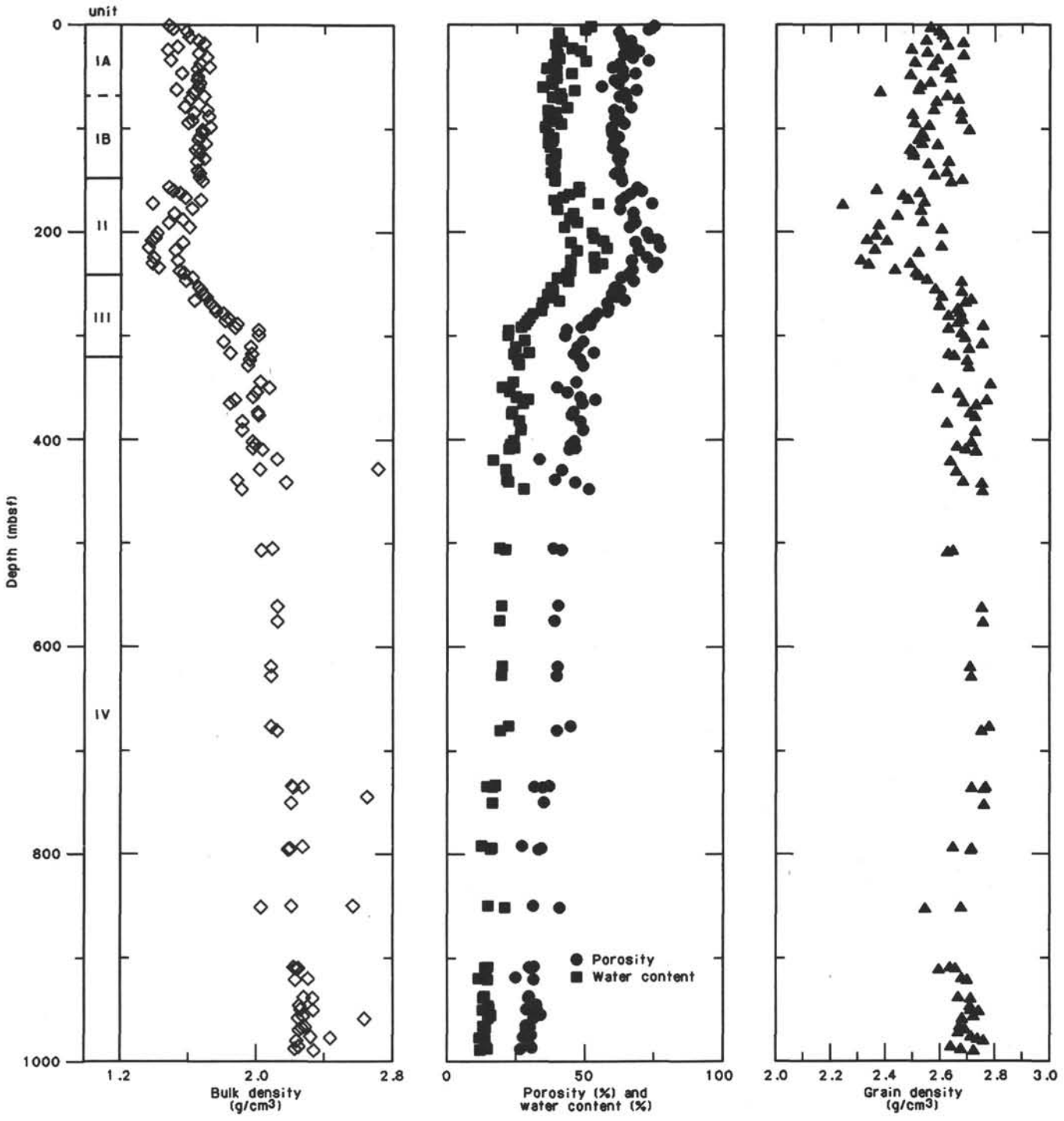

Figure 22. Index properties (wet-bulk density, porosity, water content, and grain density) measured on discrete samples for Holes 731A, 731B, and 731C.

some of the scatter also results from the increased drilling disturbance of this low density layer and inherent difficulties in positioning the probes into undisturbed sediment in the whole-round core sections.

GRAPE and P-Wave Logs

GRAPE and *P*-wave logger records of very good quality were obtained for the entire interval cored in Hole 731A (Figs. 28 and 29). The measurements of both logging systems correspond well to measurements made on discrete samples. The cyclic variation on the scale of 1–2 m in lithologic Unit I, which is present in the GRAPE and *P*-wave logs from Sites 721 and 722, is also present in the records from Site 731. Although the character of the logs from all of the Owen Ridge sites is similar, the correlation of features of the logs from Site 731 with features of the logs from Sites 721 and 722 is not readily apparent.

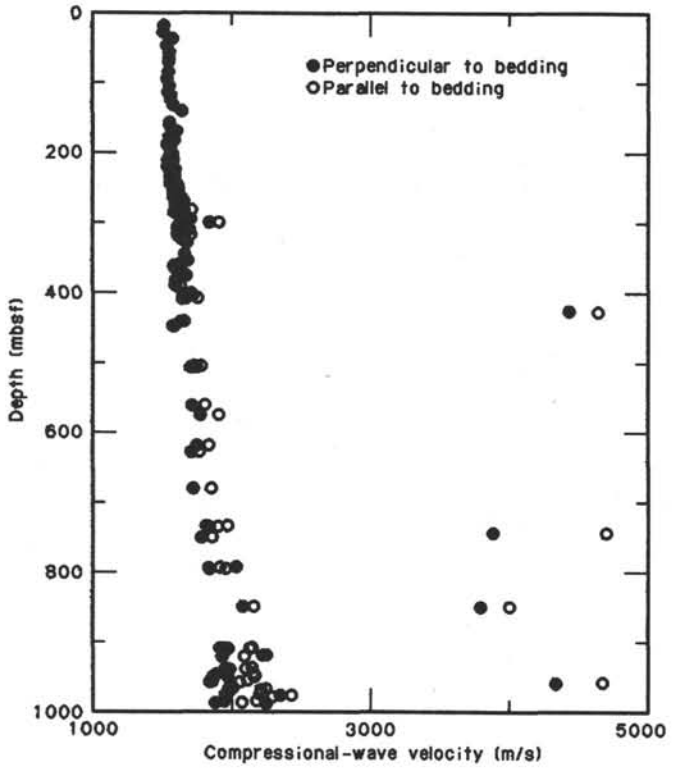

Figure 23. Compressional-wave velocity as measured on discrete samples in the Hamilton Frame Velocimeter for Holes 731A, 731B, and 731C.

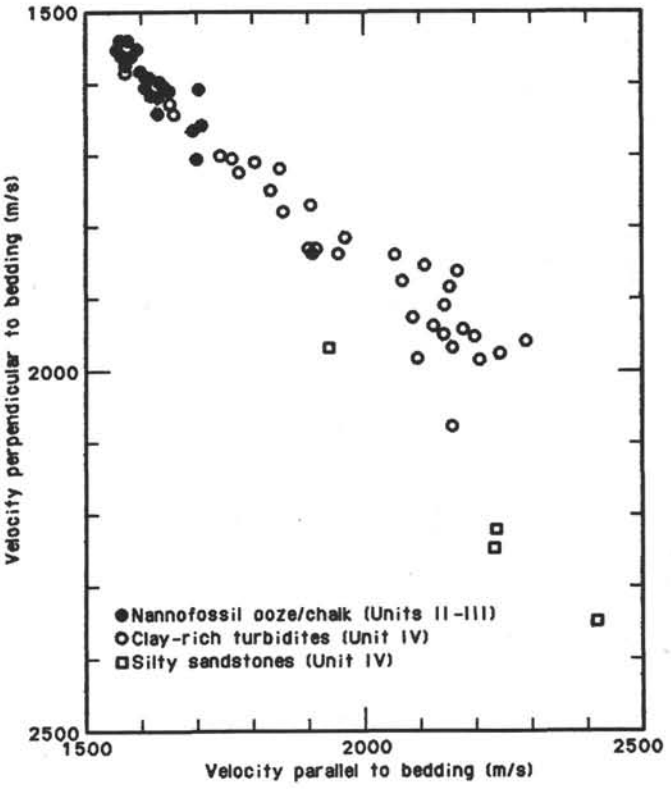

Figure 25. Crossplot of compressional-wave velocity measured perpendicular and parallel to bedding on discrete samples for Holes 731A, 731B, and 731C.

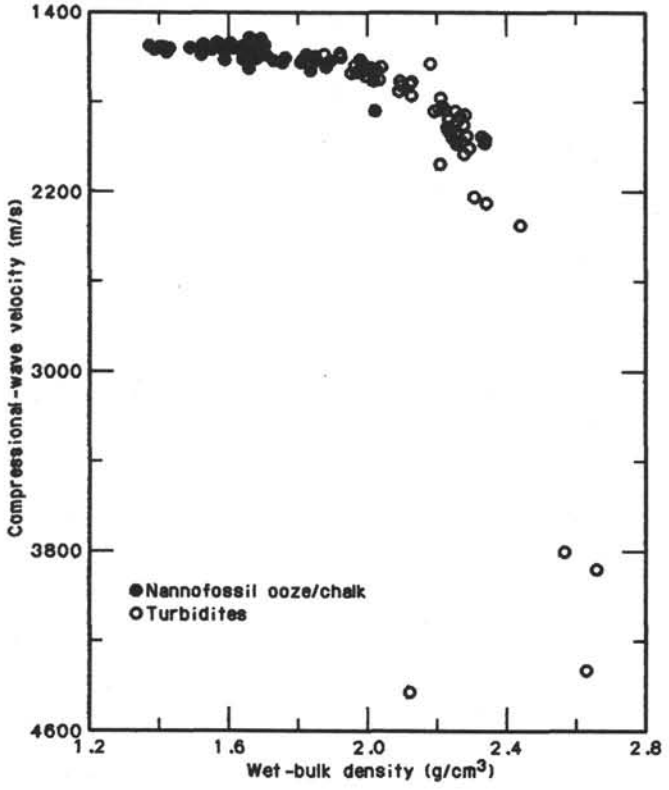

Figure 24. Wet-bulk density vs. compressional-wave velocity measured on discrete samples for Holes 731A, 731B, and 731C.

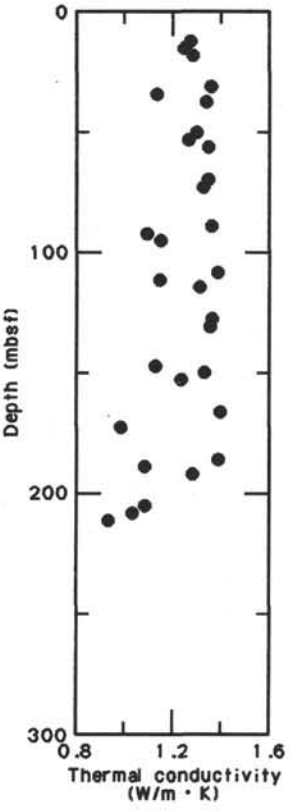

Figure 26. Thermal conductivity in Hole 731A.

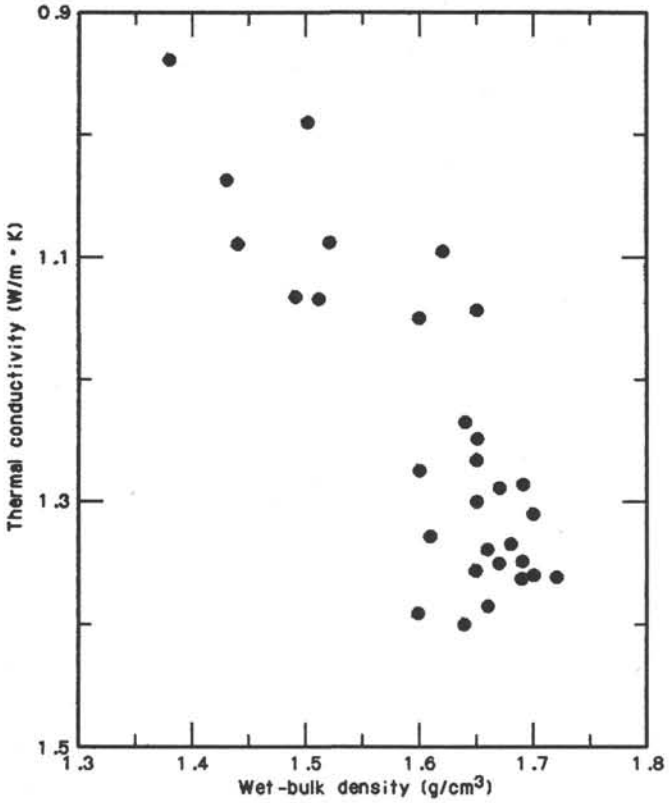

Figure 27. Thermal conductivity vs. wet-bulk density for Hole 731A. GRAPE densities were used to estimate wet-bulk density for intervals of conductivity which lack corresponding discrete-sample wet-bulk density determinations.

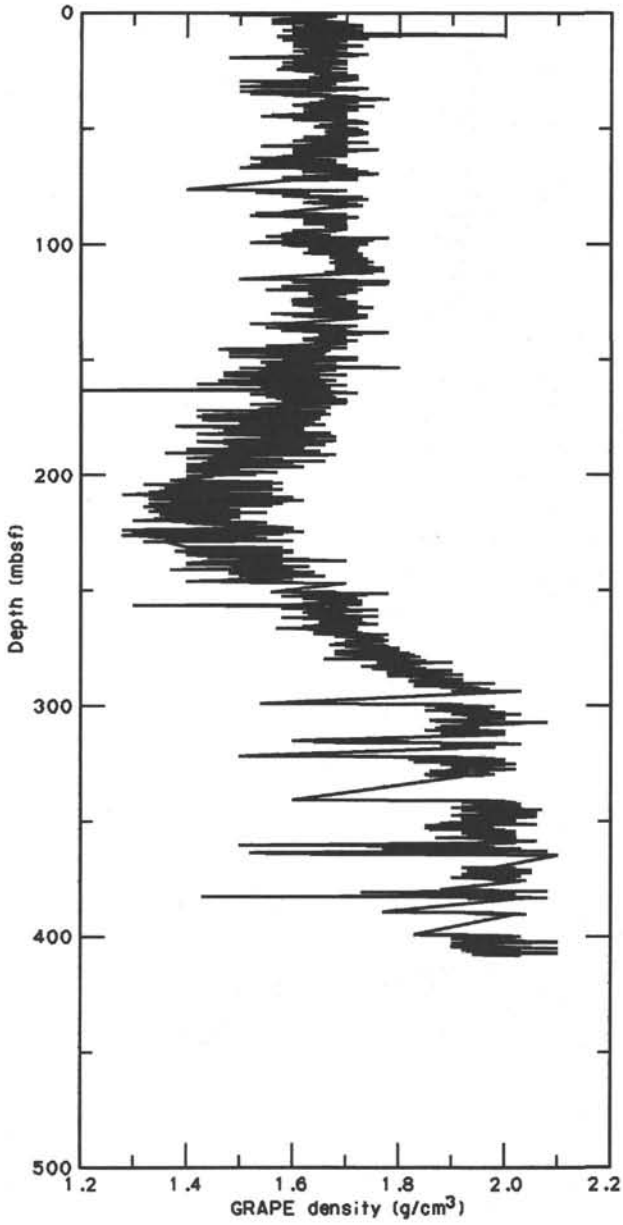

Figure 28. GRAPE wet-bulk density for Hole 731A. The profile is based on 10-cm-block averages of the data.

INORGANIC GEOCHEMISTRY

Introduction

Twenty-five interstitial water samples were collected by squeezing from Holes 731A (16 samples), 731B (1 sample), and 731C (8 samples). A single *in-situ* sample was collected from Hole 731A with the *in-situ* water sampler. All analytical data are listed in Table 9 and displayed as composite plots in Figure 30. The deepest sample, collected at 989 mbsf, appears to contain a significant proportion of seawater as indicated by calcium and chloride concentrations which are lower than expected and salinity, sulfate, and magnesium levels which are apparently too high. The *in-situ* sample also appears to have been contaminated by the addition of some seawater.

In general, the pore-water profiles at this site are very similar to the results from the two previous Owen Ridge sites (721 and 722). The one significant difference is that Site 731 was drilled to a much greater depth; the interstitial water data span nearly 1 km of section, which permits a better definition of the diagenetic reaction paths on the ridge.

Salinity, Chloride, and pH

The decrease in salinity over the top ~150 m (Fig. 30) reflects sulfate reduction and magnesium depletion in the pore waters, a phenomenon which was almost universally encountered during Leg 117. In contrast, the chloride content increases with depth, from about 560 mmol/L near the top of Hole 731A (equivalent to a bottom water salinity of ~35‰) to ~580 mmol/L near the bottom of Hole 731C (Table 9). The higher concentrations occur in the turbidite unit (lithologic Unit IV) only, and it appears that Cl^- is currently diffusing upward from the turbidites into the overlying nannofossil chalks (Fig. 30). A similar increase in the chloride concentration with depth was noted at both sites drilled previously on the Owen Ridge. This distribution can potentially be explained by either or both of two processes. First, the high chloride levels at depth could simply represent burial of more saline bottom water during the late Oligocene to early Miocene. Rapid accumulation of the turbidites would obviate the subsequent loss of salt via diffusion from the deeper part of the sequence. The second possibility is that the formation of authigenic clay minerals during the alteration of both volcanic ash and detrital silicates in the turbidites could increase the salinity by incorporating water into interlayer sites in the clays. However, given the limited volume of smectites observed in the turbidites (see "Inorganic Geochemistry" section, "Site 721" chapter, this volume), we believe that this mechanism is unlikely to account for the observed increase in the chloride content. Bottom water would have had to have been about

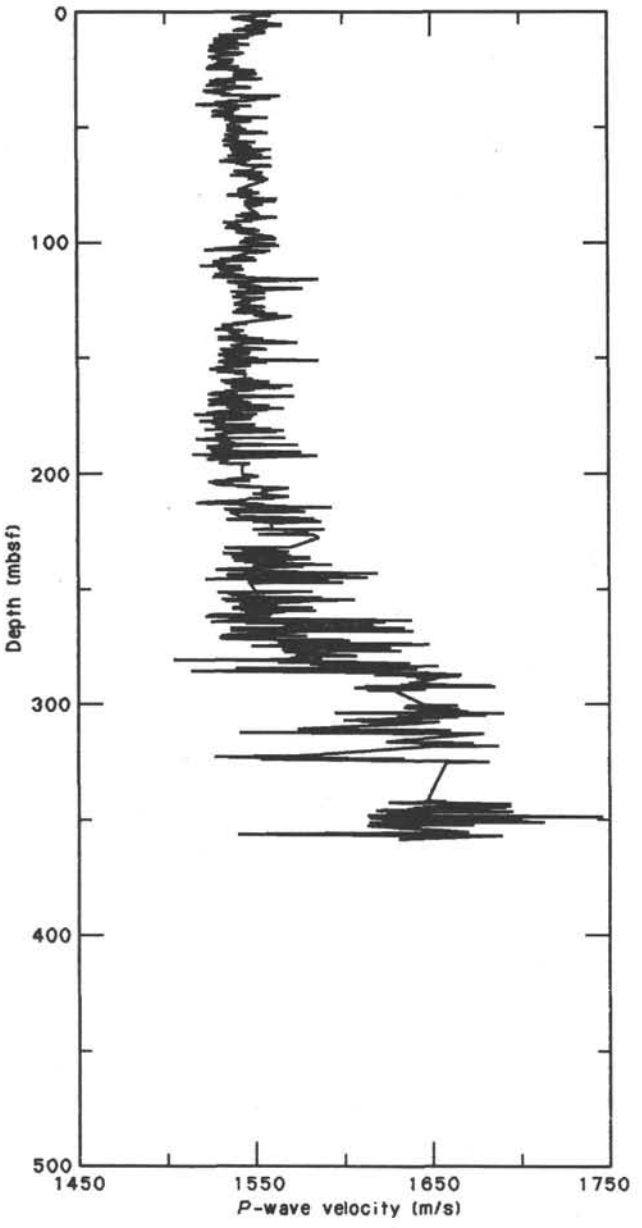

Figure 29. Compressional-wave velocity as measured by the *P*-wave logger for Hole 731A. The profile is based on 10-cm-block averages of the data.

1 g/kg saltier during the early Miocene in order to produce a 20 mmol/L increase in the chloride concentration; we consider this to be a reasonable possibility and prefer it to the alteration hypothesis.

It is interesting to note that the topmost pore-water sample at Site 731 contained 559 mmol/L Cl^-, similar to that at Site 721 (556 mmol/L). The chloride content measured in the shallowest sample at Site 722 (549 mmol/L) is somewhat lower which may be the result of an analytical error. Several sites on the Oman margin had significantly higher concentrations of chloride, ranging up to 570 mmol/L, in near-surface interstitial waters. Such high levels probably indicate the influence of inflow at intermediate depths of high-salinity water from the Red Sea and the Persian Gulf.

The pH profile (Fig. 30) shows little variation with depth. Measured values are ~0.5 pH units less than "normal" seawater pH, which can probably be explained by the production of H_2S during sulfate reduction.

Alkalinity and Sulfate

The alkalinity profile (Fig. 30) is very similar to the distributions seen at Sites 721 and 722 on the northern Owen Ridge. A maximum of ~9 mmol/L at 90 mbsf results from a balance between production and consumption of HCO_3^-. Above 90 mbsf, the rate of production of HCO_3^- ion during sulfate reduction exceeds the rate of consumption as authigenic carbonates are precipitated. The opposite is probably true in the nannofossil oozes and chalks below the maximum. As noted by Gieskes (1981, and references therein), chemical alteration of volcanic ash in the turbidites (see below) may be consuming alkalinity at greater depths.

Sulfate depletion is nearly complete at depths below about 250 m but minor concentrations appear to persist to the bottom of the hole. The greatest rate of reduction occurs in the top 60 m, as evidenced by the slope of the upper portion of the profile in Figure 30. The persistence of sulfate to considerable depths at this site differs from the distribution observed at Site 721, where no sulfate was detectable between 100 and 380 mbsf (see "Inorganic Geochemistry" section, "Site 721" chapter, this volume), but bears some similarity to the profile measured at Site 722. It was thought (see "Inorganic Geochemistry" section, "Site 722" chapter, this volume) that the trapping of seawater during the rapid emplacement of the turbidite facies, coupled with a relatively low input of labile organic matter, might account for the presence of the residual interstitial sulfate at depth at Site 722; a similar phenomenon might account for the distribution seen at Site 731. Presumably, the absence of sulfate in the 100–380 mbsf interval in Hole 721A resulted from a slightly higher oxidant demand compared to Sites 722 and 731. This may in part reflect the shallower water column at the former site, which would encourage the deposition of slightly less oxidized organic matter at the sediment-water interface.

Note that sulfate is depleted at many of the Oman margin sites at depths very similar to that seen at Site 731. We find this to be very surprising given that the sediments at the margin sites are deposited within the oxygen minimum, contain generally higher organic carbon contents, and accumulate at a faster rate. All three of these factors should result in complete depletion of sulfate at considerably shallower depths on the margin than on Owen Ridge, but no such contrast is observed. We are unable to explain this seeming enigma at present, but it has important implications for any hypothesis which attempts to account for the accumulation of organic matter under the oxygen minimum on the Oman margin. The major question which such a hypothesis will need to embrace is: why isn't there a profound difference in the distribution of dissolved sulfate between the ridge and the margin?

Calcium and Magnesium

Calcium and magnesium distributions at Site 731 (Fig. 30) are very similar to those observed at Sites 721 and 722. The depletion of magnesium with depth is attributed to precipitation of dolomite or dolomitization of pre-existing calcite, and to the alteration of volcanic ash in the turbidites (to magnesian smectite or sepiolite?). Smear slide observations indicate that ash is a common constituent, ranging up to 10% by volume (see "Lithostratigraphy" section, this chapter). The calcium minimum appears to reflect two controls: first, precipitation of calcite at relatively shallow depths (which leads to an increase in the Mg/Ca ratio; see Fig. 30); and second, release of Ca^{2+} during alteration of feldspars (and ash?) in the turbidites. Smear slide observations indicate that alteration of feldspars is a common phenomenon in the turbidite facies (S. Clemens, pers. comm.). Calcium

Table 9. Summary of interstitial water geochemical data, Site 731.

Hole, core, section, interval (cm)	Depth (mbsf)	Vol. (mL)	pH	Alk. (mmol/L)	Sal. (g/kg)	Mg (mmol/L)	Ca (mmol/L)	Cl (mmol/L)	SO_4 (mmol/L)	PO_4 (μmol/L)	NH_4 (mmol/L)	SiO_2 (μmol/L)	Mg/Ca	DOC (a.u.)
731A-1H-4, 145–150	5.95	52	7.65	5.60	34.2	51.15	8.06	559	22.2	9.8	0.16	722	6.34	0.243
731A-3H-4, 145–150	25.25	45	7.41	7.83	34.2	49.55	6.96	562	16.1	11.9	0.96	815	7.12	0.623
731A-6H-4, 145–150	53.75	50	7.60	8.77	33.2	41.50	6.51	563	9.3	12.0	1.61	982	6.37	0.885
731A-7I-6, 145–150	64.80	13	7.65	6.80	33.9	44.37	7.21	565	12.1	1.4	1.28	788	6.15	0.429
731A-9X-4, 145–150	82.65	35	7.64	9.06	32.5	37.99	6.68	560	6.0	8.7	1.79	918	5.69	0.908
731A-12X-4, 145–150	111.65	33	7.58	7.68	32.3	34.92	7.84	559	4.2	5.8	1.84	957	4.45	0.605
731A-15X-4, 145–150	140.65	34	7.44	6.33	32.2	33.23	8.66	561	3.9	4.7	1.66	963	3.84	0.453
731A-18X-4, 145–150	169.65	42	7.45	5.33	32.2	31.45	9.09	562	3.5	4.2	1.63	1114	3.46	0.378
731A-21X-4, 145–150	198.75	51	7.56	3.41	32.2	30.27	9.71	559	3.2	3.2	1.46	1223	3.12	0.300
731A-24X-4, 145–150	227.85	41	7.30	4.52	32.1	29.19	10.47	559	2.0	1.9	1.38	1126	2.79	0.256
731A-27X-4, 145–150	256.85	48	7.45	3.44	32.0	28.26	10.69	557	2.0	0.7	1.25	1219	2.64	0.172
731A-30X-4, 145–150	285.85	28	7.58	2.39	32.1	27.71	10.84	555	1.7	0.2	1.18	698	2.56	0.120
731A-33X-2, 145–150	311.85	18	7.63	1.67	32.1	27.31	12.11	560	0.5	0.1	1.01	417	2.25	0.186
731A-37X-1, 140–150	347.20	25	7.67	2.24	32.0	27.22	12.28	561	0.0	0.2	0.50	310	2.22	0.121
731A-40X-2, 140–150	374.80	14	7.84	2.25	32.3	28.66	13.86	564	2.0	0.1	0.17	317	2.07	0.179
731A-43X-4, 140–150	405.30	27	7.87	2.16	32.1	27.22	14.03	565	0.2	0.1	0.35	230	1.94	0.143
731B-3X-1, 140–150	429.50	35	7.84	2.10	33.0	27.65	14.24	577	4.4	0.5	0.68	168	1.94	0.106
731C-2R-2, 140–150	505.30	26	7.79	1.79	31.3	25.58	16.22	560	1.1	0.4	0.41	174	1.58	0.133
731C-10R-1, 140–150	735.00	15	8.27	0.83	32.2	19.89	20.07	580	1.1	0.6	0.79	90	0.99	0.183
731C-12R-1, 140–150	792.90	12	8.10	1.14	32.2	20.04	21.84	579	2.1	0.1	0.61	100	0.92	0.166
731C-14R-1, 140–150	850.80	16	8.18	1.28	32.1	19.08	24.44	580	0.7	1.0	0.82	110	0.78	0.140
731C-16R-2, 140–150	910.20	10	7.73	0.71	32.3	22.05	24.55	580	2.4	0.3	0.56	96	0.90	0.193
731C-19R-2, 140–150	939.00	5	—	—	32.8	21.36	25.64	579	2.4	0.5	0.59	110	0.83	0.224
731C-22R-3, 140–150	969.50	14	8.26	1.20	32.5	20.89	25.47	582	1.1	0.5	0.82	78	0.82	0.160
731C-24R-3, 140–150	988.90	7	—	1.04	33.6	24.93	24.55	575	5.1	0.1	0.69	86	1.02	0.160

may also diffuse upward into the drilled section from an unknown source at greater depths. The approximately vertical form of the profile between 900 and 1000 mbsf suggests, however, that such a contribution is at best minor.

Ammonia, Phosphate, Silica, and Dissolved Organic Carbon

Ammonia, phosphate and dissolved silica distributions at Site 731 (Fig. 30) are almost identical in form to those observed at Sites 721 and 722. Ammonia concentrations are relatively low compared to levels which would be expected if organic matter with a composition equivalent to Redfield stoichiometry was being degraded. The deficiency implies that the buried organic material at the site has a higher C:N ratio than does the organic substrate in buried sediments on the Oman margin, where the concentration of ammonia produced per mole of sulfate reduced is significantly higher. It is possible that the uptake of NH_4^+ by clay minerals may also contribute to the relative ammonia deficiency in pore waters at Site 731, but we are unable to assess this.

Phosphate concentrations generally decrease with depth to values below ~250 mbsf which are near the analytical detection limit (Table 9). The profile is attributed to the precipitation of authigenic apatite in lithologic Units I–IV (nannofossil oozes and chalks) and to very limited diagenetic activity in the turbidites at depth.

The dissolved silica distribution clearly outlines the change from opal-bearing nannofossil ooze and chalk to opal-poor terrigenous turbidites at the boundary between lithologic Units III and IV (at about 320 mbsf; see "Lithostratigraphy" section, this chapter). Silica must be diffusing downward into lithologic Unit IV where it is presumably precipitated as quartz overgrowths. Indeed, the dissolved silica concentrations measured in the lower 200 m of lithologic Unit IV are very near the solubility limit for quartz, which is ~100 μmol/L at 20°C (Blatt et al., 1980).

The dissolved organic carbon (DOC) profile measured at Site 731 (Fig. 30) broadly reflects the distribution of organic carbon in the drilled section. The highest DOC levels occur between 50 and 90 mbsf, approximately coincident with a local maximum of the organic carbon concentration at about 75 mbsf (see "Organic Geochemistry" section, this chapter). Other pronounced sedimentary organic carbon maxima at ~150 and ~225 mbsf do not reflect such a direct association with DOC. This may be the result of smearing of the DOC profile by diffusion or a lower level of reactivity of the organic matter buried in the deeper horizons. The DOC maximum occurs within the zone of rapid sulfate reduction and coincides with the peak in the alkalinity profile. These three sets of data indicate clearly that diagenetic activity at this site is most pronounced in the upper 100 m. Organic matter in the carbon-rich bands at greater depths is apparently not subject to significant continuing degradation.

ORGANIC GEOCHEMISTRY

Forty-two physical property samples of Hole 731A, covering all four lithologic units, were analyzed for their organic carbon content (Fig. 31) and pyrolysis characteristics (Table 10). Sediments of lithologic Units I (0–146.5 mbsf) and II (146.5–240.9 mbsf) have an average organic carbon content of 0.71%. These values are more or less comparable with those measured in samples from other sites on the Owen Ridge (721, 722), although in these latter sites organic carbon values as high as 3.68% have been measured (see "Organic Geochemistry" sections, "Site 721" and "Site 722" chapters, this volume). Sediments of lithologic Units III and IV are characterized by very low organic carbon concentrations (average 0.12%). As the organic carbon values of lithologic Unit IV are within the limit of detection, no further organic carbon measurements were made on sediments of this lithologic unit recovered in Holes 731B and 731C. The results of the Rock-Eval pyrolysis are given in Table 10. The hydrogen indices are comparable with the results from the other Owen Ridge sites, but are generally lower than values measured in samples from the Oman margin sites.

DOWNHOLE MEASUREMENTS

Logging

Operations

Logging operations at Hole 731C began at 0415 hr on 8 October, with a hole conditioning program similar to that used at Site 720. The seismic stratigraphic combination was rigged up at 1610 hr. At this site the seismic stratigraphic combination consisted of borehole compensated sonic (BHC), dual induction resistivity (DIT), and gamma ray (GR) tools. This tool string was run from 1655 to 2155. Downgoing logs were obtained from the

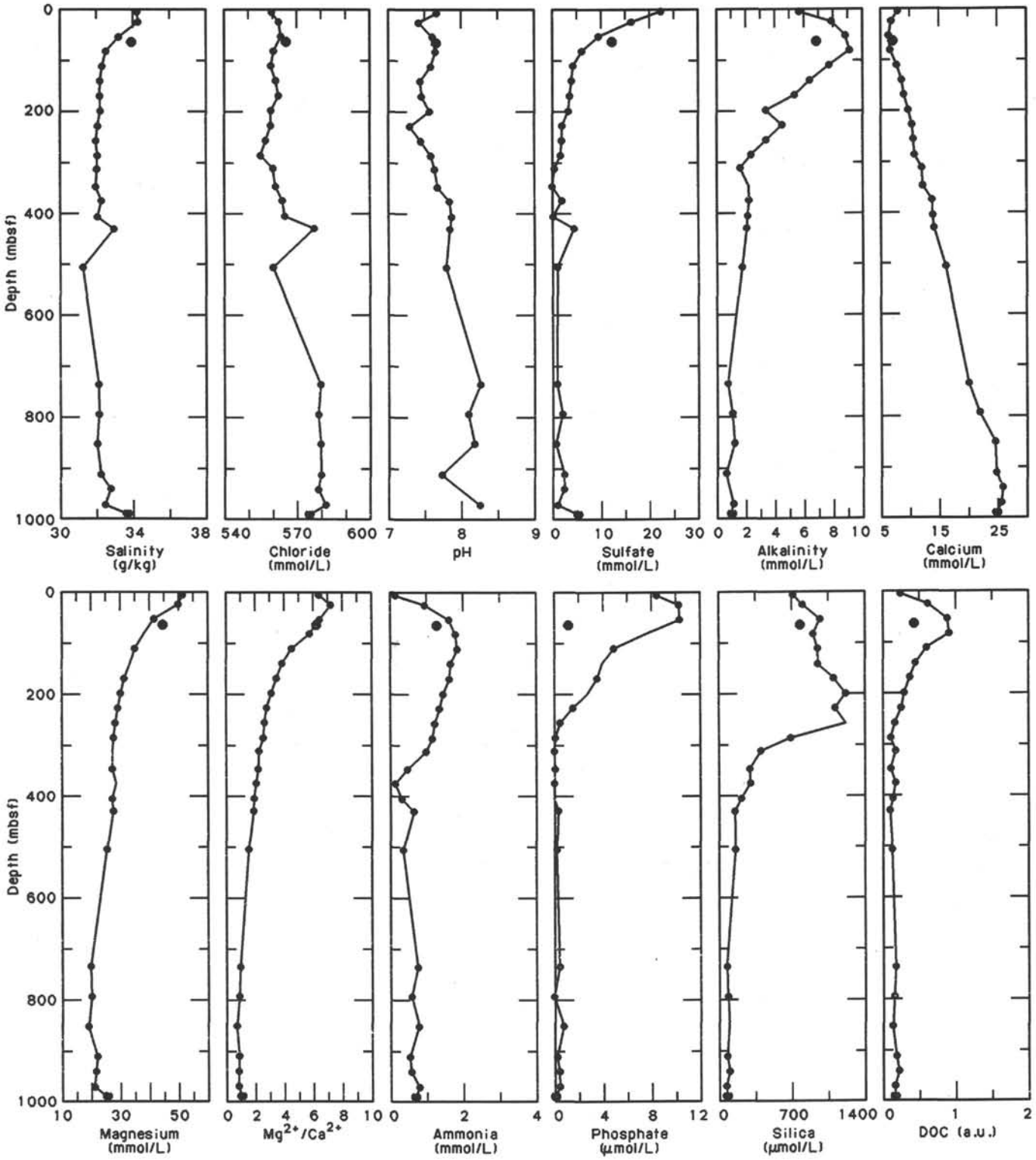

Figure 30. Concentrations vs. depth for Site 731. Compiled by stacking data from Holes 731A, 731B, and 731C. The large dot represents the *in-situ* sample. Parentheses enclose the lowermost point, which is believed to be partly contaminated with seawater. It is not clear why anomalously high sulfate concentrations were measured at 375 and 430 mbsf. The data shown in other profiles indicate that the presence of sulfate in these two samples cannot simply be attributed to contamination with drilling fluid. Dissolved organic carbon measured in absorbance units.

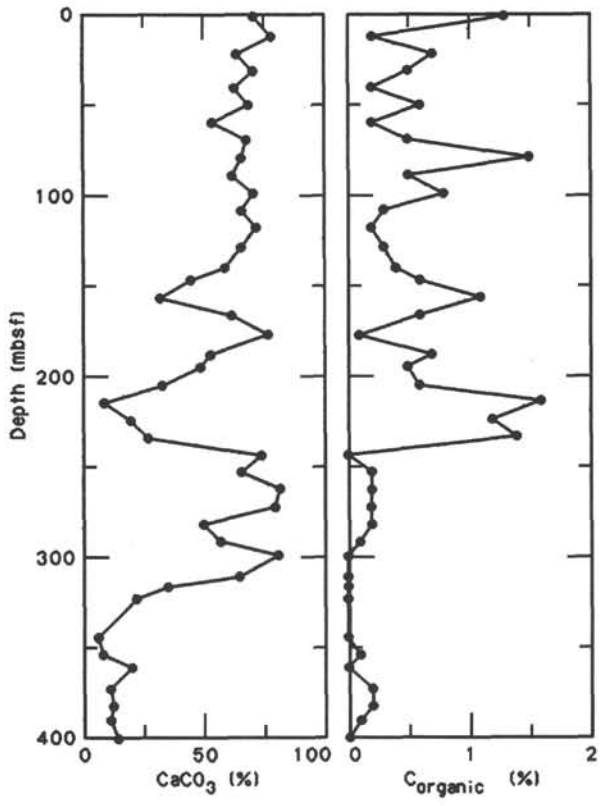

Figure 31. Downhole plot of $CaCO_3$ and organic carbon for samples of Hole 731A.

Table 10. Results of Rock-Eval pyrolysis of samples from Hole 731A.

Core, section, interval (cm)	Depth	T_{max} (°C)	S_1	S_2	S_3	S_2/S_3	TOC	HI	OI
117-731A-									
1H-1, 96-98	0.96	429	0.44	2.52	2.67	0.94	1.37	184	195
2H-2, 80-82	12.10	424	0.10	0.33	1.57	0.21	0.26	127	604
3H-2, 80-82	21.60	430	0.24	1.63	2.00	0.81	0.79	206	253
4H-2, 80-82	31.10	421	0.15	0.55	1.72	0.31	0.51	108	337
6H-2, 80-82	50.10	428	0.12	0.48	1.80	0.26	0.60	80	300
8X-2, 64-66	69.14	427	0.08	0.47	1.50	0.31	0.50	94	300
9X-2, 80-82	79.00	429	0.46	4.17	2.39	1.74	1.52	274	157
10X-2, 80-82	88.70	422	0.15	0.78	1.74	0.44	0.50	156	348
11X-2, 92-94	98.42	429	0.09	0.71	1.39	0.51	0.88	81	158
12X-2, 80-82	108.00	422	0.14	0.66	1.62	0.40	0.38	174	426
13X-2, 84-86	117.74	421	0.07	0.40	1.33	0.30	0.28	143	475
14X-3, 77-79	128.77	420	0.08	0.44	1.31	0.33	0.33	133	397
15X-4, 100-101	140.20	414	0.11	0.34	1.42	0.23	0.43	79	330
16X-2, 103-105	146.93	417	0.16	0.70	1.62	0.43	0.65	108	249
17X-2, 125-127	156.75	425	0.38	2.22	2.15	1.03	1.15	193	187
18X-2, 101-103	166.21	426	0.21	1.19	1.49	0.79	0.62	192	240
20X-4, 67-69	188.27	421	0.21	1.38	1.65	0.83	0.87	159	190
21X-2, 56-58	194.86	414	0.19	0.61	1.53	0.39	0.51	120	300
22X-2, 99-101	204.99	424	0.20	1.56	1.68	0.92	0.67	233	251
23X-2, 70-72	214.40	423	0.57	3.76	1.68	2.23	1.61	233	104
24X-2, 108-110	224.48	424	0.42	2.92	1.69	1.72	1.29	226	131
25X-2, 90-92	234.00	427	0.36	3.34	1.90	1.75	1.44	232	132

Note: HI = hydrogen index and OI = oxygen index. Results of samples from Units III and IV have been omitted because of the very low organic carbon values.

base of pipe (85 mbsf) to 973 mbsf. Upcoming logs were obtained from 979 mbsf to the base of pipe (65 mbsf after raising pipe during logging).

The geochemical combination was run between 2319 hr on 8 October and 1100 hr on 9 October. At this site the geochemical combination consisted of spectral gamma ray (NGT), neutron porosity (CNT-G), gamma spectroscopy (GST), and accelerometer (GPIT) tools. Downgoing logs were obtained from the seafloor to 966 mbsf. The gamma spectroscopy tool was not activated during this run, because the downgoing logging speed is too fast for this tool and because its irradiation effect on the formation degrades the quality of the spectral gamma ray tool. With the gamma spectroscopy tool activated, upcoming logs were obtained from 968 mbsf to the seafloor. A short repeat section (129–78 mbsf) was also logged.

Rigdown from logging was completed at 1140 hr on 9 October. In all, 12 hr was used for hole conditioning and 19.5 hr was used for logging. No significant problems or delays were encountered, and the total time for logging operations was almost identical to the 32 hr scheduled. No bridges were encountered, so the sidewall entry sub was not needed. The wireline heave compensator was not used either, because seas were flat.

Log Quality and Editing

Most logs were of good quality and required no editing. Replicability of results was generally very good, as indicated by agreement of downgoing and upcoming logs. Subsequently, only upcoming logs are discussed. Geochemical logs obtained through pipe will require gain correction for pipe attenuation, but this correction has not been undertaken yet. Logs from four tools warranted some reprocessing: sonic, gamma spectroscopy, resistivity, and spectral gamma ray.

The upcoming sonic log was generally of high quality. No cycle skipping was detected. However, of the two source-receiver spacings in the BHC sonic tool, the short (0.9 m) spacing records the direct water waves before formation refracted waves in sediments with very slow velocities (high porosities). Consequently, no formation traveltimes were obtained from the short source-receiver spacing in the intervals 68.4–245.8 mbsf, 319.3–378.4 mbsf, and several other shorter low-velocity intervals. This problem rarely occurs even with the longer (1.5 m) source-receiver spacing. Revised short-spaced traveltimes were estimated for these intervals from the long-spaced traveltimes, based on a regression equation (R = 0.921) between short- and long-spaced traveltimes for the interval 585.7–616.1 mbsf, in which both spacings were reliable. Sonic velocities were then recalculated, using an algorithm described in Arthur et al. (in press). This reprocessed velocity log (Fig. 32) is likely to be quite accurate in general, but it may slightly overestimate the lowest velocities.

The resistivity logs at Site 731 exhibited the same low quality of calibration in the chalks that occurred in this unit at Site 722 (see "Downhole Measurements" section, "Site 722" chapter, this volume). Unlike at Site 722, the spherically focused log was consistent with medium and deep resistivity logs in the chalks, but all three logs have rare spurious spikes in the chalks (e.g., Fig. 32). No editing of these spikes has been undertaken yet. The gamma spectroscopy and spectral gamma log data were reprocessed post-cruise as described in the "Explanatory Notes" chapter (this volume). Data from both tools appeared to be of good quality, based on internal calibration tests.

Hole Deviation

Deviation from vertical of the borehole was measured with the GPIT accelerometer tool during both downgoing and upcoming runs of the geochemical combination (Fig. 33). Because this tool string is neither centralized nor padded against the borehole wall, tool wobble causes local deviation errors of as much as 0.5° in the top half of the hole and as much as 1.5° in the deepest part of the hole. Nevertheless, the pattern of hole deviation is easily seen.

From 80 to 320 mbsf, the hole is deviated by about 0.5° to the southeast. In the upper turbidites (320–460 mbsf), the hole deviation changes to near-vertical, with associated loss of accuracy of measurements of deviation azimuth. With continued

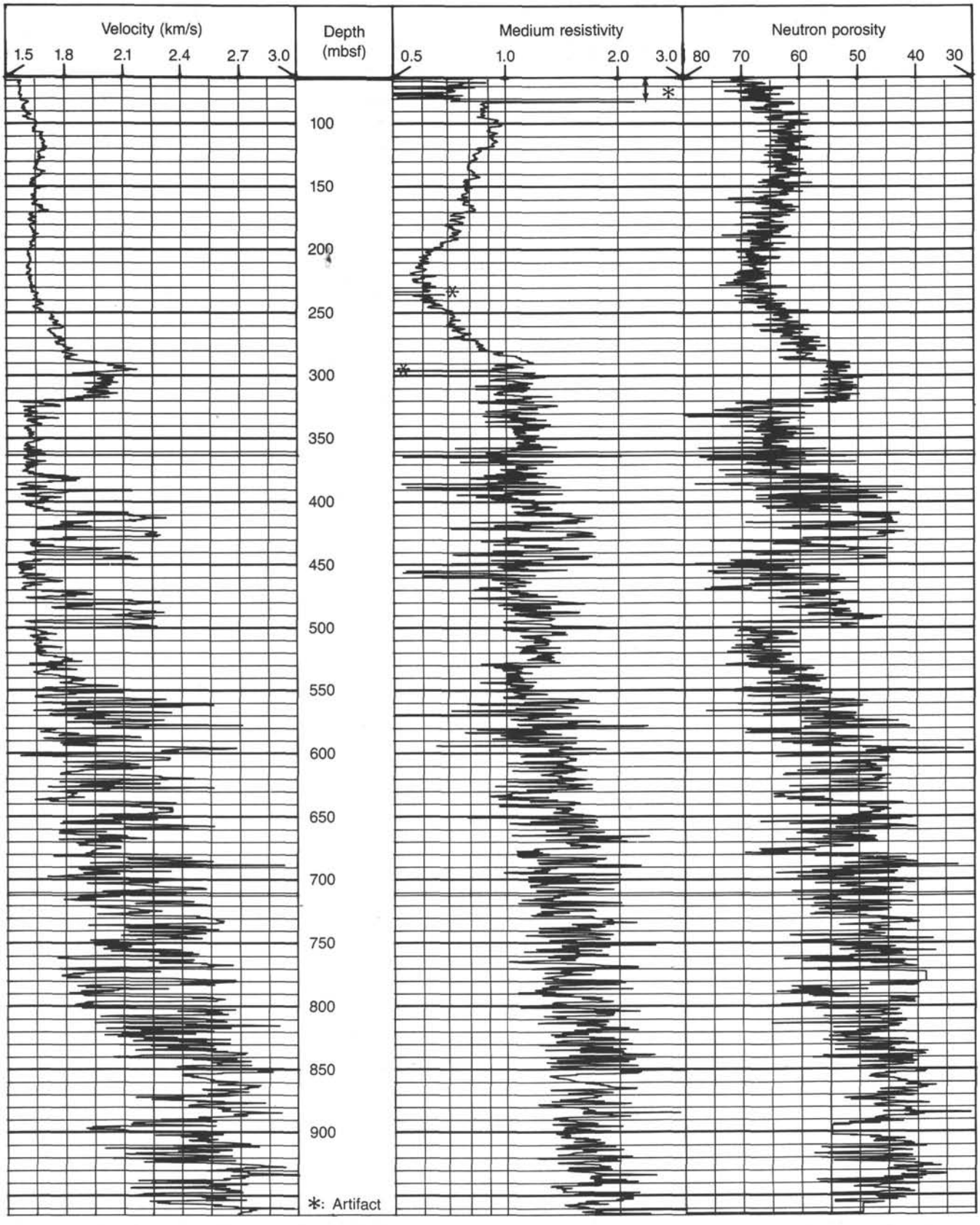

Figure 32. Sound velocity, resistivity, and neutron porosity logs for Site 731.

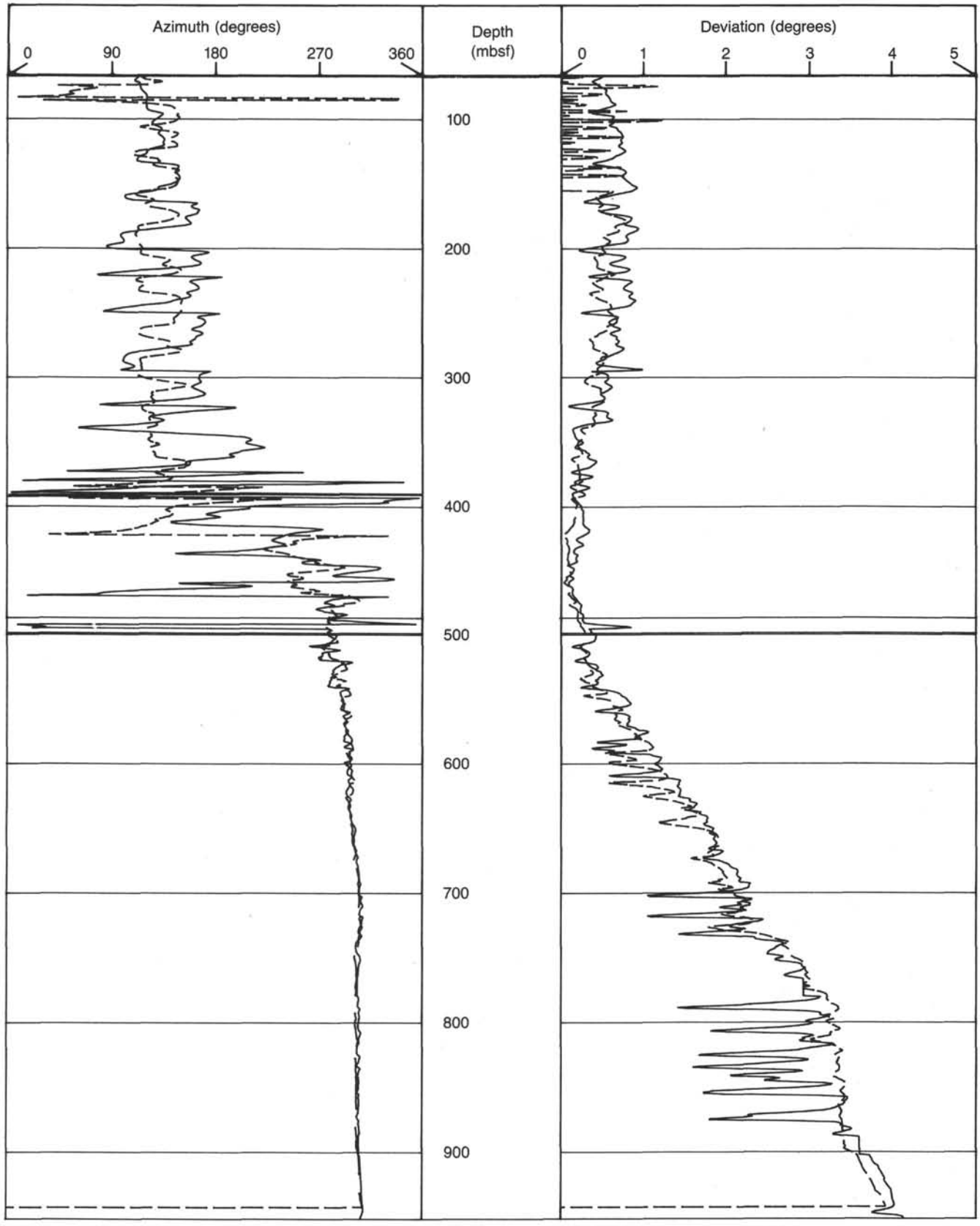

Figure 33. Logs of hole deviation and of azimuth of the deviation for Site 731. Replicate logs were obtained from downgoing (dashed line) and upcoming (solid line) passes of the same tool string.

penetration of the turbidites, this deviation increases gradually to a maximum of 4° toward the northwest.

This magnitude of hole deviation is sufficient to have a slight effect on magnetic inclinations in cores and to be detectable as inclined bedding in cores. Core orientation using the inclined bedding is possible. Such orientation would have an accuracy of 30°–45° in azimuth, sufficient to assist in polarity determination for the low-inclination paleomagnetic results from the lower turbidites (see "Paleomagnetism" section, this chapter).

Log Responses of Lithologic Units

Lithologic Unit I (0–146.5 mbsf) consists of nannofossil ooze and marly nannofossil ooze, with rare biogenic silica in the upper 66 m (see "Lithostratigraphy" section, this chapter). Openhole logging of this unit began at 65 mbsf. Calcium values are high throughout the interval 65-146.5 mbsf, and potassium and thorium values are low (Figs. 34 and 35), consistent with smear slide identification of this unit as a nannofossil ooze with low clay content. Velocity and resistivity increase downhole and neutron porosities decrease. These changes partially reflect some increase of compaction with depth but also result from a gradual decrease in clay content and increase in calcite, as indicated by the potassium and calcium logs (Figs. 34 and 35). The unconformity at about 115 mbsf is not obvious on any log though a significant increase in titanium occurs at 117 mbsf (Fig. 35).

Lithologic Unit II (146.5–240.9 mbsf) is similar to Unit I, except that clay content is higher and diatoms sometimes constitute 20% or more of the sediment volume. This high diatom content affects both porosity-sensitive and geochemical logs. Even minor diatom content substantially increases porosity; resistivity and velocity are decreased accordingly. Porosity fluctuations at Site 731 are similar in character to those for comparable ages at Site 722 (see "Site 722" chapter, this volume): a slow cyclic increase in porosity downhole from 118 to 192 mbsf, rapid porosity increase between 192 and 200 mbsf, highest porosities between 200 and 246 mbsf, then rapid porosity decrease down to 286 mbsf (Fig. 32). Of these porosity changes only the increase between 118 and 170 mbsf may arise partly or entirely from clay mineral increase (Figs. 34 and 35). Based on porosity alone, maximum diatom abundance occurs between 200 and 246 mbsf.

A silicon abundance log shows maximum silicon between 145 and 242 mbsf (Fig. 34), a depth range that closely corresponds to the boundaries of Unit II. Within this interval, the highest silicon log yields are between 202 and 242 mbsf, very similar to the 200–246 mbsf interval of maximum porosity. Silica in either diatoms or clay minerals could account for these two correlations. However, the very high porosities, the lack of a correlation between potassium and silicon, and the actual reduction of potassium in the highest silicon zone 202–242 mbsf (Fig. 34) all indicate that diatoms, not clay minerals, are the dominant silicon component in lithologic Unit II.

Organic carbon is highest at about 200–240 mbsf (see "Organic Geochemistry" section, this chapter), corresponding with the interval of highest porosities. However, organic carbon levels are too low to dominate the character of the uranium log, as occurred at Site 728 (see "Downhole Measurements" section, "Site 728" chapter, this volume). Instead, the broad trends in the uranium log in the upper few hundred meters of both Site 731 and 722 parallel those of potassium (Figs. 34 and 35) and "Downhole Measurements" section, "Site 722" chapter, this volume), and suggest that much of the uranium is in clays.

Smear slides indicate that clay mineral abundance is somewhat higher in lithologic Unit II than in Unit I (see "Lithostratigraphy" section, this chapter). Increased iron, potassium, and thorium beneath 140–142 mbsf (Figs. 34 and 35) are consistent with this observation. Calcium abundance is significantly lower in Unit II than in Units I and III (Fig. 34), but with gradational boundaries rather than sudden changes at the unit boundaries. The calcium lowering is caused primarily by diatom dilution but is augmented near the lithologic Unit I/Unit II boundary by clay dilution.

Lithologic Unit III (240.9–320.1 mbsf) is composed of about 75% nannofossils and 15%–20% clay, with no diatoms. Accordingly, relative calcium abundance reaches some of the highest values at Site 731, and porosities are rather low (Figs. 32 and 34). Based on log responses alone, the unit is divided into two subunits. The upper subunit is a continuation of the gradual downward decrease in porosity and increase in velocity that began in lithologic Unit II. These changes probably reflect a gradual downward increase in the ratio of biogenic calcite to opal. The lithostratigraphic basis for the Unit II/III boundary is the lowest occurrence of biogenic opal in smear slides (see "Lithostratigraphy" section, this chapter). However, the lowest occurrence indicated by biostratigraphic studies of core-catcher samples is in Core 117-731C-29X, only 6 m shallower than the base of the log-determined subunit at 286 mbsf.

The second subunit of lithologic Unit III, as indicated by logs, is in the interval 286–315 mbsf. The subunit has a gradational base from 315 to 322 mbsf, characterized by a major decrease in calcium and increases in potassium, thorium, and iron. The base is close to the sedimentologically determined base of lithologic Unit III at 320.1 mbsf. Calcium is very high in this subunit, and silicon, iron, potassium, thorium, and uranium are quite low (Figs. 34 and 35). Porosities are low, as indicated by the velocity, resistivity, and neutron porosity logs (Fig. 32). This unit is more distinctive on the velocity and neutron porosity logs than on the resistivity log, because the latter reveals only the lower porosity of this subunit, while the former respond to both its lower porosity and its lower clay content. All of the log responses suggest a relatively pure chalk with low porosity.

In contrast to lithologic Units I–III, Unit IV (320–994 mbsf) is almost entirely detrital (see "Lithostratigraphy" section, this chapter). The interval 320–360 mbsf is thought to represent a transition zone from strong dominance of biogenic calcite above to even stronger dominance of terrigenous turbidites below. Biogenic calcite is very rare below the transition zone (see "Lithostratigraphy" and "Biostratigraphy" sections, this chapter), but detrital calcite is present to varying degrees and averages about 10%. The low but variable response of the calcium log in the turbidites (Fig. 34) probably reflects variations in detrital calcite content, though some contribution from plagioclase is possible.

Based on log responses, the majority of the transition is accomplished in the rather short interval 315–322 mbsf. Calcite (Ca log) decreases markedly, and clay abundance increases substantially (K, Th, and Fe logs; Figs. 34 and 35). The more gradual transition deduced from cores is also evident in nearly all of the geochemical logs, with a poorly defined base at about 355–380 mbsf.

The turbidites of lithologic Unit IV have a complex mineralogy, as indicated by both smear slides and log responses. The dominant minerals are clay (probably mainly illite and chlorite) and quartz, but mica and detrital calcite are abundant and feldspar and hornblende are common (see "Lithostratigraphy" section, this chapter). Changes in the relative abundances of these minerals cause few consistent patterns to be obvious in the logs. For example, potassium and thorium are positively correlated with porosity logs over some intervals (indicating that the potassium and thorium are dominantly in the clay minerals), but negatively correlated with porosity over other intervals (indicating that mica and/or potassium feldspar in the silts contribute more potassium and thorium than do the clays). These complexities can be handled by post-cruise mineralogical inversion of the logs.

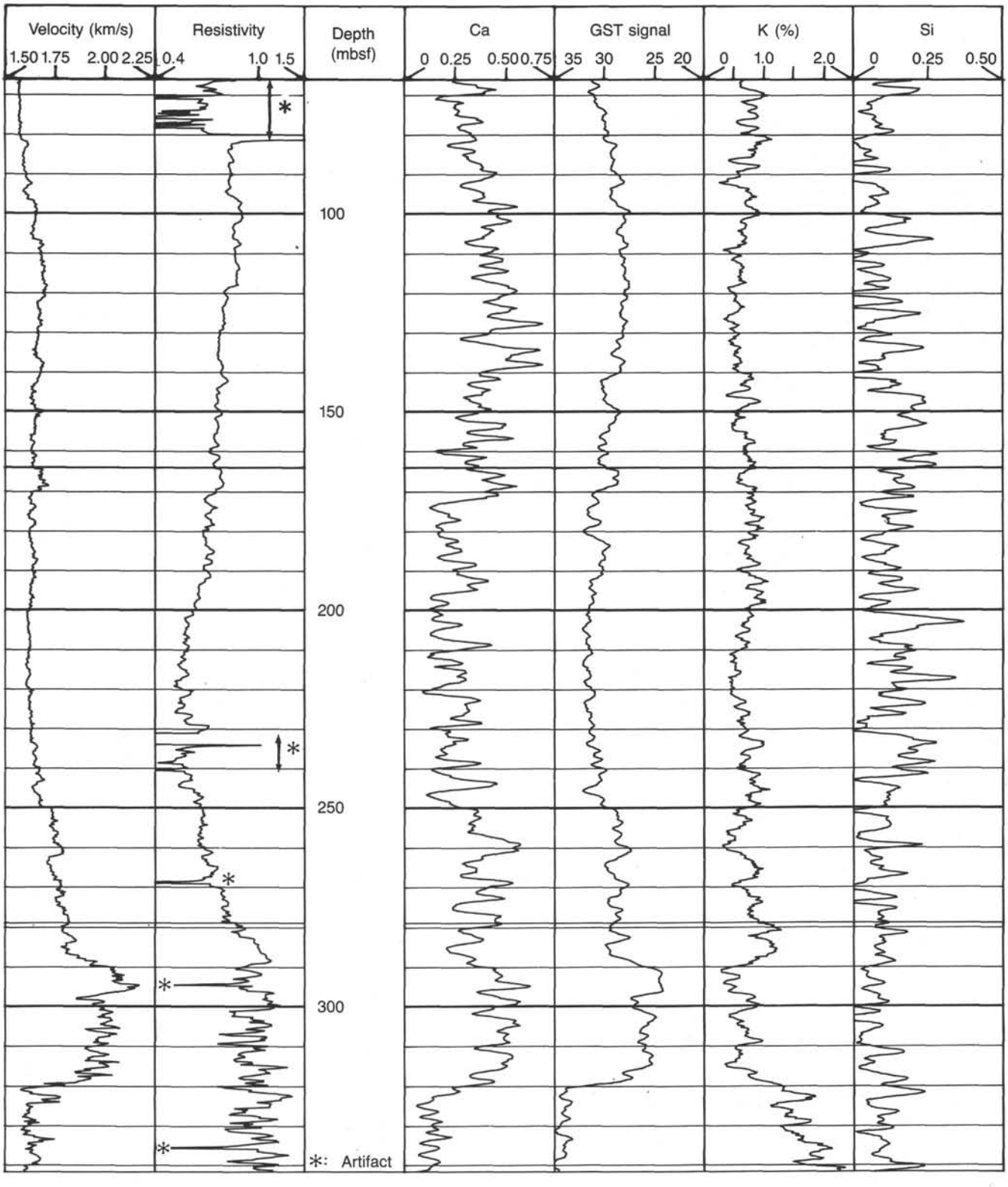

Figure 34. Comparison of velocity and resistivity logs with geochemical logs of potassium volume percent, calcium and silicon relative yields, and total formation signal from the GST tool.

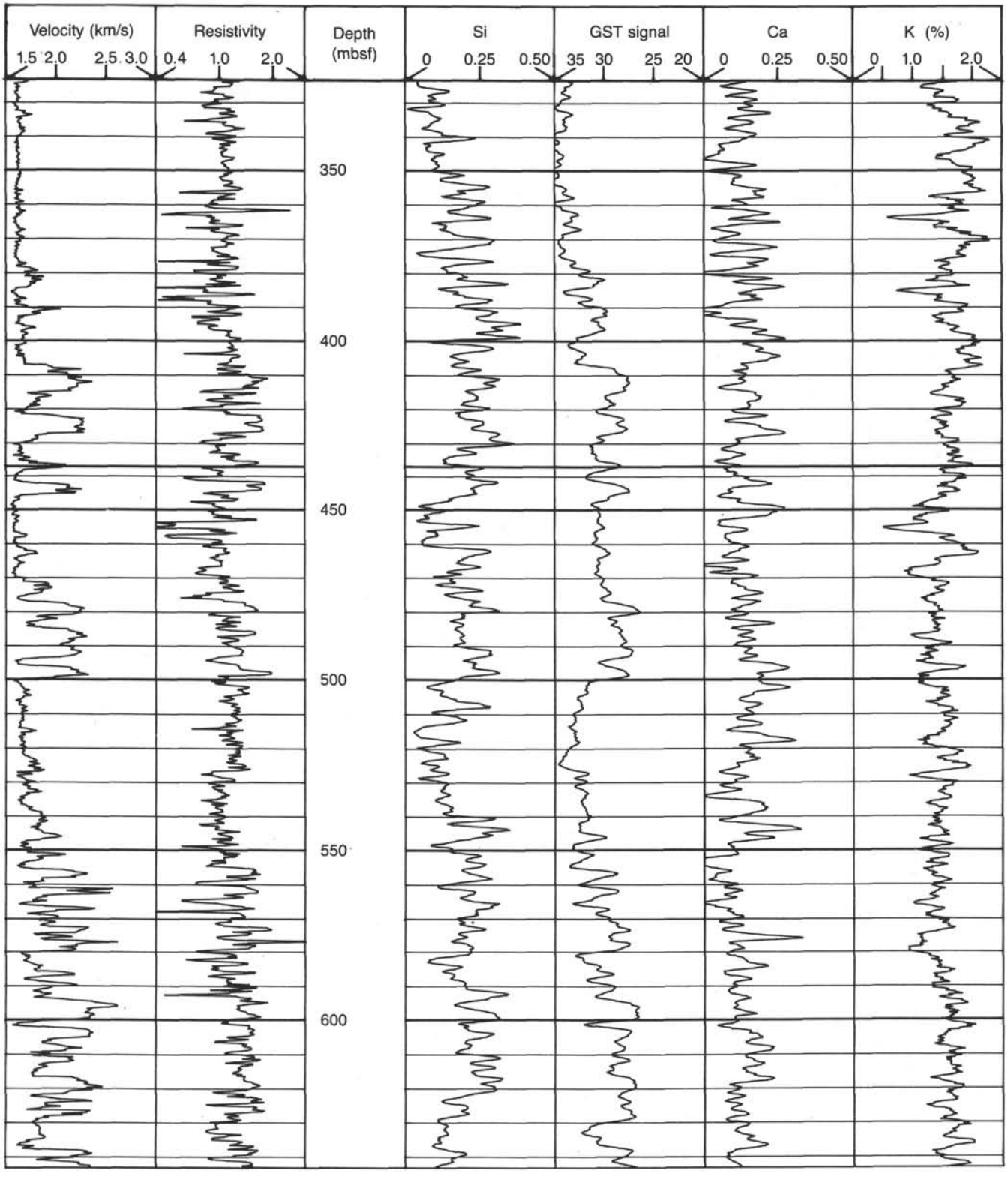

Figure 34 (continued).

Clay-rich and silt-rich units are best defined on the velocity log (Fig. 32). Superimposed on the overall compaction trend of the velocity log is a bimodal character, alternating between low-velocity clays and higher-velocity silts and sands. Neither is a complete end point in the clay/quartz continuum, but the two relative end points are well developed. In the interval 317–530 mbsf, clay-rich beds dominate, with most of the sands occurring in clusters in the two short intervals 404–443 and 470–500 mbsf. From 530 to 840 mbsf, clay-rich and sand-rich beds are present in about equal proportions. Below 840 mbsf, sand-rich

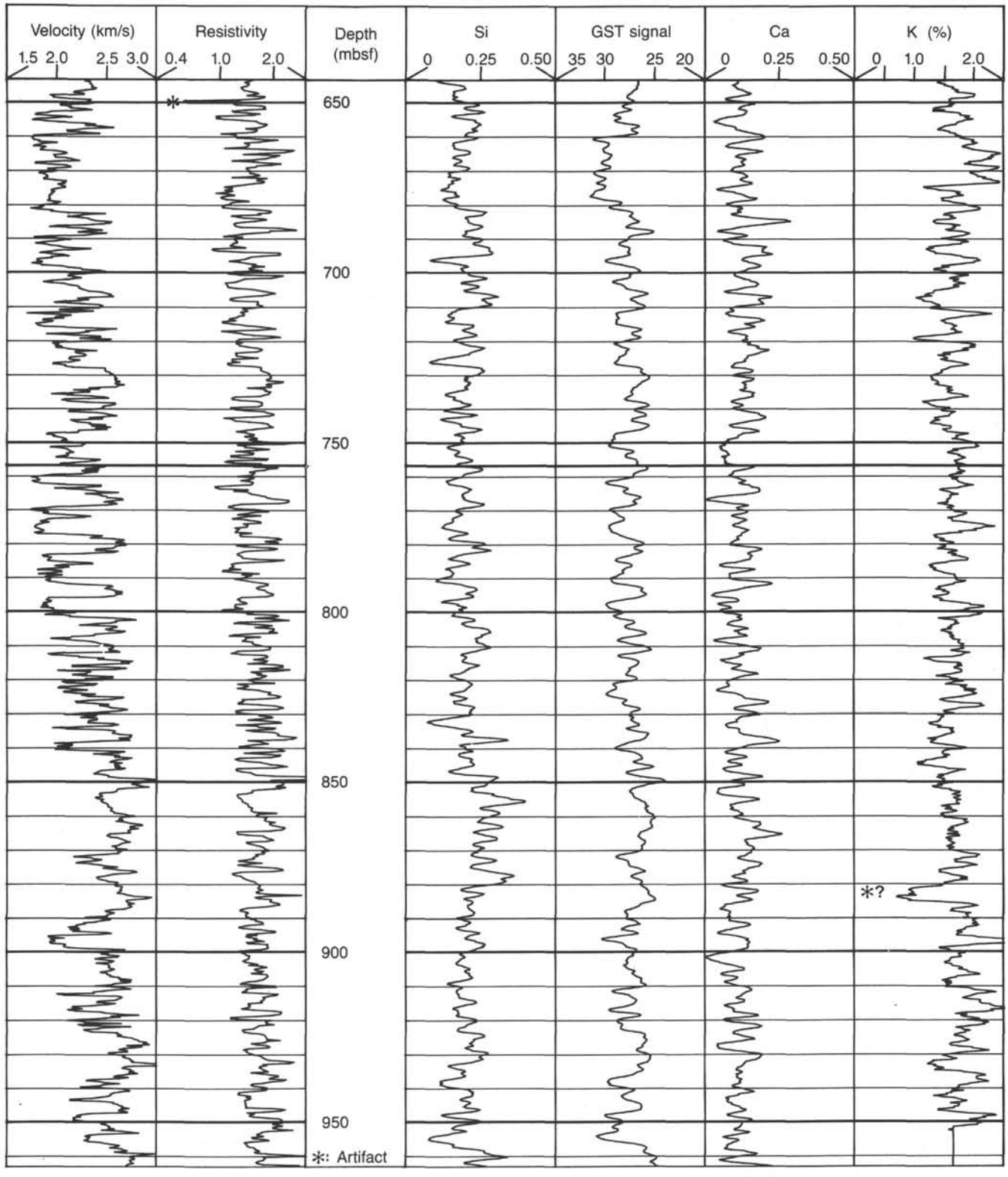

Figure 34 (continued).

beds slightly predominate. Throughout the turbidites, there is very little evidence of fining-upward or coarsening-upward sequences, as indicated by either porosity or clay indicator logs. Most individual turbidites have thicknesses of less than a meter (see "Lithostratigraphy" section, this chapter). The vertical resolution of the logs is not sufficient for detection of fining-upward patterns on this scale.

The velocity increase as a function of depth is greater in the turbidites of Site 731 than in most other regions. The empirical curve of velocity vs. depth of Hamilton (1979), based on 20

areas of terrigenous sediments, predicts a velocity of 1.9 km/s at the top of the turbidites and 2.3 km/s at the bottom of Site 731. In contrast, average velocities at Site 731 increase from about 1.65 km/s in the upper 50 m of the turbidites to about 2.6 km/s in the lowest 100 m of sediments penetrated (Fig. 32). Similarly low velocities were found in the upper turbidites at Site 722 (see "Downhole Measurements" section, "Site 722" chapter, this volume). Nearly all of this difference between turbidite velocities of Owen Ridge and other regions can be attributed to the downhole change from clay dominance to silt dominance. The clay base line compaction trend increases from 1.6 to 2.0 km/s downhole, and the silt and sand base line increases from 2.1 to 2.8 km/s. The 1.9 km/s prediction is less than 0.1 km/s higher than the average of clay and silt baselines near the top of the turbidites. Near the bottom of the hole, the 2.3 km/s predicted average is only about 0.1 km/s higher than the average of clay and silt base lines.

INTERHOLE CORRELATIONS

Layer-by-layer Correlation at Site 731

The three holes drilled at Site 731 are located in 2366 m water depth on the west of the Owen Ridge flank, 23 km west-southwest of Site 721 and 14 km west-southwest of Site 722. Hole 731A was drilled to 67.0 mbsf with the APC and to 409.0 mbsf with the XCB. Recovery with the APC was almost perfect, but the top of Hole 731A did not obtain the mud line. Holes 731B and 731B were drilled from 408.7 and 502.4 mbsf to 457.1 and 994.2 mbsf with the XCB and RCB, respectively. The age of the sedimentary sequence ranges from the late Oligocene(?) to Pleistocene.

We attempt detailed correlations in the upper 300 m of the covered sediments in Hole 731A. The upper interval has an age range from 0 to 14 Ma, and is characterized by cyclic changes in the nature of sediments that can be identified by visual observation and by variations of magnetic susceptibility and $CaCO_3$ content. Correlation of the sedimentary coherence and similarity among the sites of the Owen Ridge provides valuable information on the relative rate of sedimentation, which is necessary information for study of depositional environments and sedimentation.

Site-to-site correlations were made on the basis of visual identification of distinctive layers, as well as on physical and magnetic properties. The magnetic susceptibility was measured continuously and at 10-cm intervals before splitting the sections. Photographs were taken of the split cores.

The visual correlation of the cores relied primarily on the core photographs. Twenty-six distinct and traceable marker horizons have been determined in the correlatable sedimentary sequence at Sites 721 and 722, and have been notated as OR-a_0, ..., y_1, and y_2, based on the correlation between the holes at Sites 721 and 722 (see "Interhole Correlations" sections, "Site 721" and "Site 722" chapters, this volume). The letter code (i.e., a, b, c, ...) refers to the sequence of cores, and the number code indicates the number of marker horizons in each core. For example, the notation "a_2" corresponds to the second marker horizon defined in Core 117-721A-1H, and "b_1" denotes the first marker layer in Core 117-721A-2H. The criterion to define a marker horizon is that the horizon is distinct enough to trace it in the sedimentary sequence of the other holes and that the character does not change. The useful criteria for recognizing the marker are color boundaries, distinctly colored layers, shape of bioturbations, and sequence of color change in surrounding sediments. These marker horizons have been traced between Sites 721 and 722. At Site 731, forty-two marker horizons are traced. Below y_2 horizon, six marker horizons, z_1 to z_6, were newly identified and traced between Sites 731 and 722. Table 11 (OR = Owen Ridge; notation is omitted in table) lists the depth of the traced marker horizons in the Owen Ridge Sites 721, 722,and 731.

The pattern of the magnetic susceptibility and the positions of marker layers match very well between Sites 722 and 731 (Fig. 17). The stratigraphy of the magnetic susceptibility data and the visually identified layers are extremely consistent in that a particular visually characteristic layer always coincides in depth with a distinct feature in the magnetic susceptibility curve.

Because Site 731 has not double-cored the sedimentary sequences, we can not calculate true stratigraphic thickness after the correction for core-boundary disturbance. The intersite correlation of the marker horizons, a_0 to a_4, indicates that the top 2 m of the surface sediments was missing in Core 117-731A-1H (Fig. 36). The layer-by-layer correlation allows us to determine the existence and time interval of hiatuses. The disconformable contact was observed at the horizon 75 cm below the marker horizon h_1, and the marker horizon n_1 was identified at 480 cm below the contact. The thickness between h_1 and n_1 is 49.75 m at Site 721, while the thickness at Site 731 is 5.55 m. The hiatus above the marker n_1 was also found at Site 722. The coincidence of the horizon of hiatus at Site 731 and 722 indicates that the horizon above the marker n_1 may have a character similar to a basal plane of a submarine slide.

Another sharp contact is observed 19.75 m below the previous hiatus, and marker x_1 was identified 2.10 m below the contact. The thickness for the missing interval at Site 731 is calculated as 80.80 m based on occurrence of the markers at Site 721 and 74.90 m at Site 722.

SUMMARY AND CONCLUSIONS

Site 731 is located in the western Arabian Sea on the Owen Ridge. The Owen Ridge is an asymmetric, northeast-trending ridge 300 km offshore Oman that dips steeply to the east and gently to the west.

The main scientific objectives for drilling at Site 731 were to recover a continuous Neogene sequence of pelagic sediments from the crest of the Owen Ridge. The second objective was to penetrate and possibly recover a thick sequence of turbiditic sediments in order to reconstruct the tectonic history of Owen Ridge and adjacent Owen Basin. The sedimentary sequence recovered here, along with those at Site 721 and 722, was expected to yield records of long-term and short-term variations in the biotic, sedimentologic, and chemical response of the depositional system to initiation of and changes in the monsoonal circulation system, and of tectonic control on facies evolution.

The most significant findings at Site 731 are (Fig. 37):

1. The thick turbidite sequence from 320 to 994 mbsf, which is characteristic of deep-sea fan deposition;
2. The gradual transition from clastic turbiditic depositional mode to pelagic sedimentation in the lower middle Miocene, which marks the uplift over the reach of turbidites and above the lysocline;
3. The onset of opaline sedimentation in the upper Miocene concomitant with the onset of cyclic variations in sedimentary properties;
4. The excellent correlation of magnetic susceptibility records between all three sites on the Owen Ridge (721, 722, and 723).

Site 731 penetrated to 994.2 mbsf and recovered sediments that range from possibly Oligocene (NP25) to late Pleistocene in age. The section has been divided into four major lithologic units:

Unit I (0–146.5 mbsf) consists of alternating light and dark layers of foraminifer-nannofossil ooze, marly nannofossil ooze, and nannofossil ooze with biosiliceous intervals of late Pleisto-

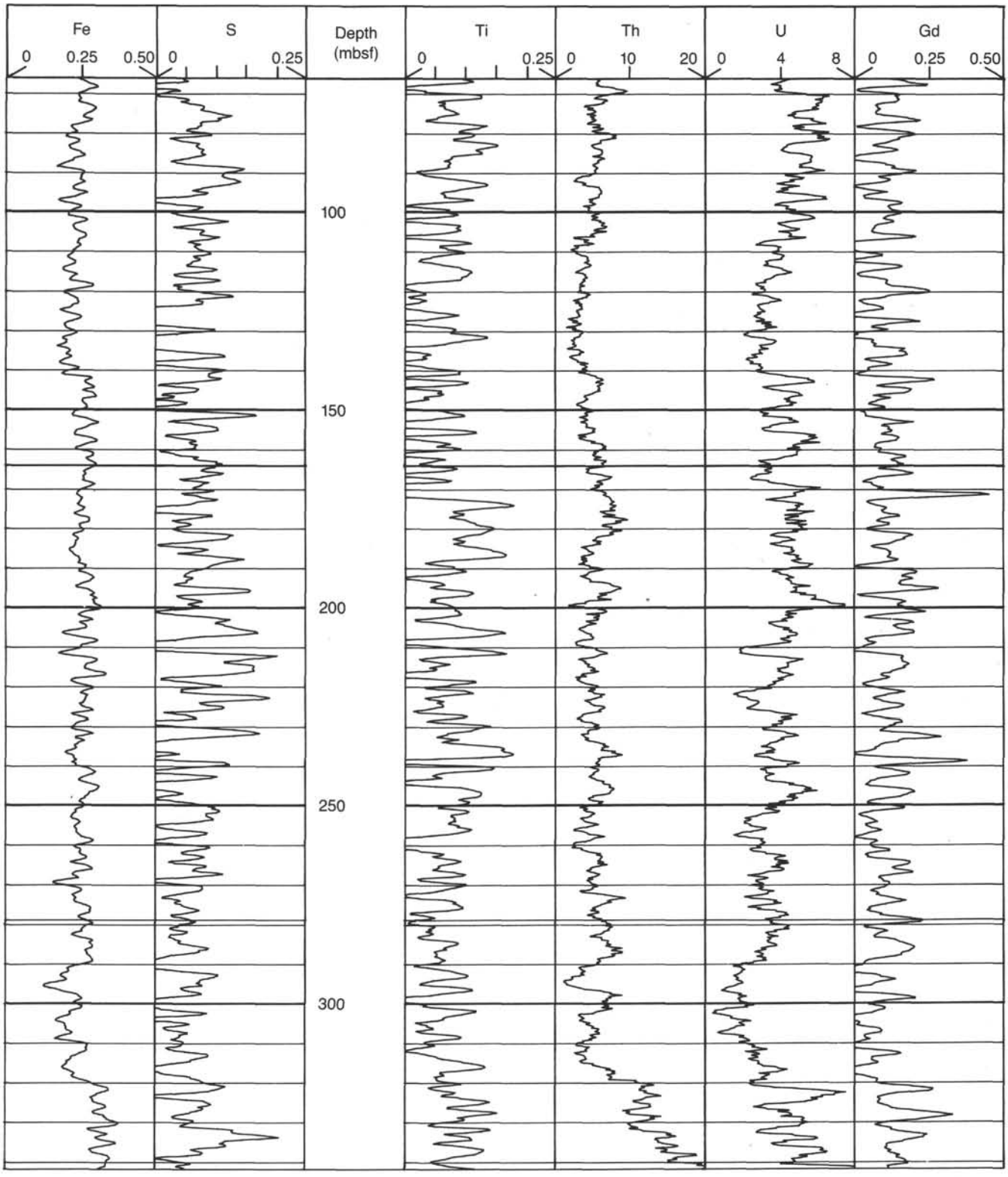

Figure 35. Geochemical logs of iron, sulfur, titanium, and gadolinium yields, and of thorium and uranium abundance by volume.

cene to late Miocene age. The uppper part of Unit I (0–66.3 mbsf) contains variable amounts (as much as 20%) of opaline material, which decreases in the remainder of lithologic Unit I. The amount of opal found in Unit I at Site 731 appears to exceed the opal content found in coeval sediments of Sites 721 and 722 on the Owen Ridge. As at Sites 721 and 722, the sediments here reveal strong cyclicity indicated by changes in colors, bulk densities, carbonate content, and particularly well by magnetic susceptibility on whole-round cores. Two hiatus horizons were recognized at 97 mbsf and 117 mbsf, which correspond to the late Pliocene and early Pliocene to middle late Miocene ages, respectively.

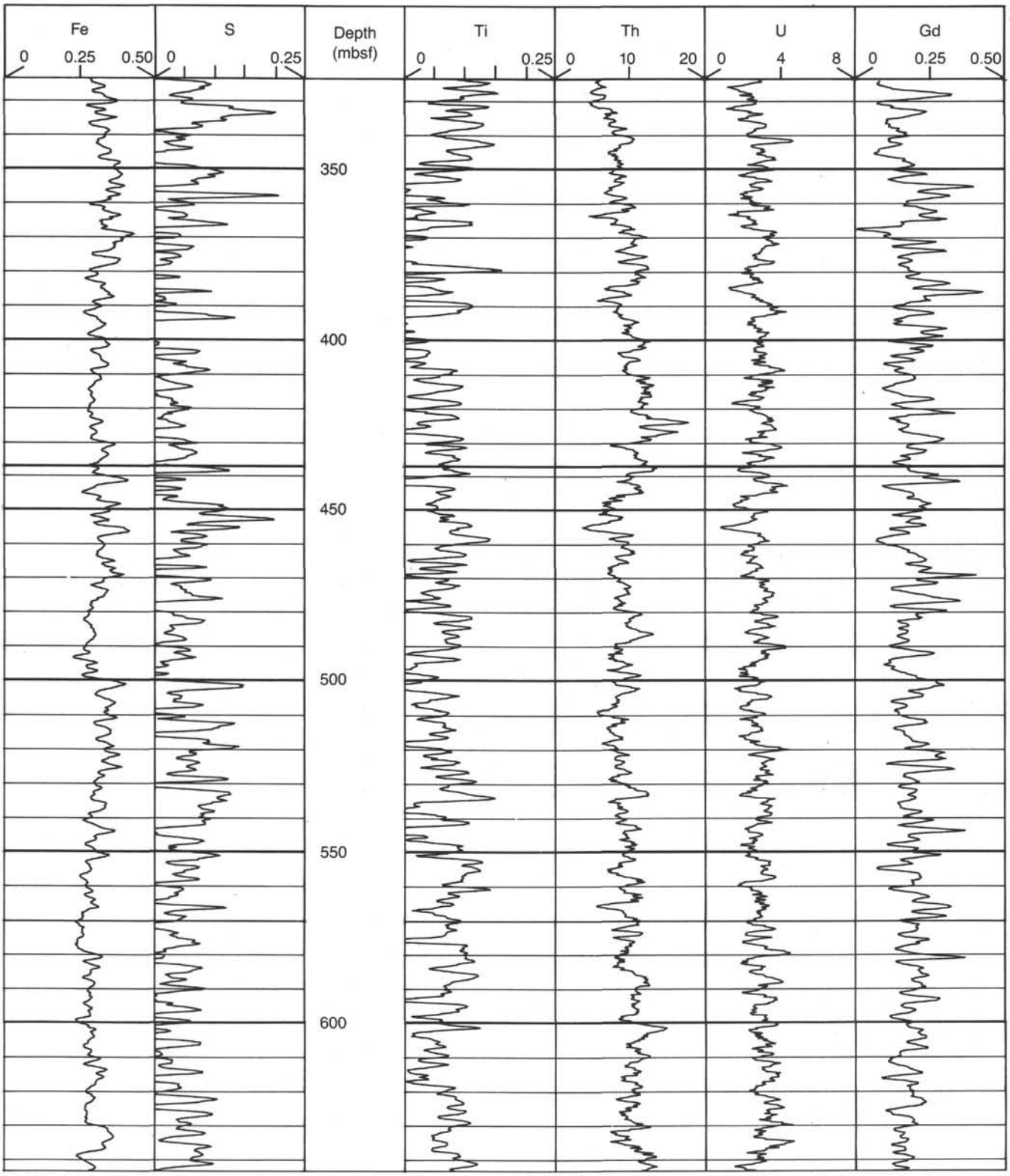

Figure 35 (continued).

Lithologic Unit II (146.5–240.9 mbsf) is composed of nannofossil oozes, diatomaceous marly nannofossil oozes, minor nannofossil-rich siliceous muds, and alternations of nannofossil chalks and diatomaceous muds of late Miocene age. Biogenic opal is an abundant component and its influence on the physical properties of the sediment is clearly observed in the density, porosity, and velocity measured onbord ship and by downhole logging. The abundance of opal (as much as 35% from smear slides) is the major difference between lithologic Units I and II.

Lithologic Unit III (240.9–320.1 mbsf) consists of cyclic bedding of nannofossil chalks and marly nannofossil chalks. This lithology is observed in the physical properties by a steady in-

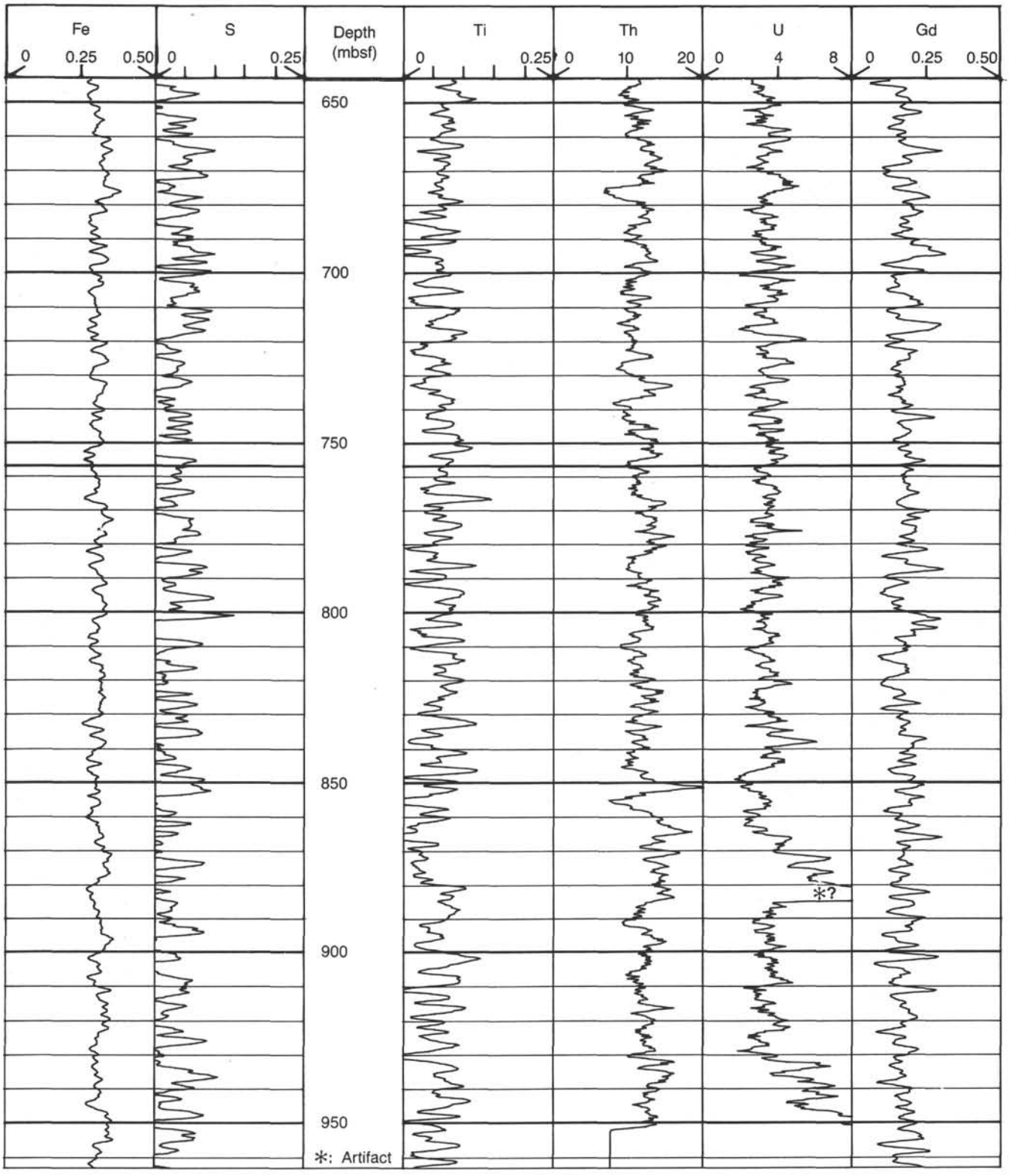

Figure 35 (continued).

crease in bulk density (Fig. 37) and velocity values, and low porosity.

Lithologic Unit IV (320.1–994.2 mbsf) is primarily composed of turbidites of silty clays grading upward to nannofossil chalks on the scale of beds and coarsening downsection to almost barren silty clays with coarse bases of early Miocene to Oligocene(?) age. Mud turbidites of 5–10 cm thickness are frequent and are stacked into beds of 2–3 m thickness. A transition zone between Units IV and III is found between 320.1 and 359.5 mbsf, which may designate the time when the ridge was uplifted above the influence of turbidites and above the lysocline. This latter boundary is indicated by improved preservation of planktonic calcare-

Table 11. List of the stratigraphic depth of the marker horizons at Sites 721 and 722, and ODP depth (based on core logs) of the marker horizons in Site 731.

	Hole 721B		Hole 722B		Hole 731A	
	Core, section, interval (cm)	Corrected depth (mbsf)	Core, section, interval (cm)	Corrected depth (mbsf)	Core, section, interval (cm)	ODP depth (mbsf)
a_0	1H-2, 105	2.95	1H-2, 85	2.35	1H-1, 75	0.75
a_1	1H-3, 90	3.90	1H-3, 50	3.50	1H-2, 75	2.25
a_2	1H-5, 45	6.45	2H-1, 25	6.05	1H-4, 15	4.65
a_3	1H-6, 32	7.82	2H-2, 20	7.50	1H-5, 45	6.45
a_4	2H-2, 85	11.25	2H-4, 65	10.95	2H-1, 60	10.40
b_1	2H-4, 85	14.25	2A-3, 20	14.20	2H-4, 55	14.85
b_2	2H-6, 115	17.55	3H-2, 105	17.95	2H-6, 120	18.50
b_3	2H-7, 40	18.30	3H-3, 45	18.85	2H-7, 45	19.25
b_4	3H-1, 140	20.50	3H-5, 10	21.50	3H-2, 85	21.65
c_1	3H-3, 130	23.40	3H-7, 15	24.55	3H-6, 35	27.15
c_2	3H-4, 130	24.90	4H-1, 85	26.35		
c_3	3H-5, 105	26.15	4H-2, 60	27.60	4H-2, 150	31.80
c_4	3H-6, 110	27.70	4H-3, 85	29.35	4H-4, 120	34.50
c_5	3H-7, 50	28.60	4H-4, 40	30.40	4H-5, 80	35.60
c_6	4H-1, 75	29.75	4H-5, 5	31.55	4H-6, 80	37.10
c_7	4H-2, 20	30.70	4H-5, 100	32.50		
d_1,	4H-3, 70	32.70	4H-6, 140	34.40	5H-1, 45	38.75
d_1	4H-4, 0	33.50	4A-4, 5	35.45	5H-2, 5	39.85
d_2,	4H-4, 70	34.20	5H-1, 70	36.00	5H-2, 100	40.80
d_2	4H-4, 145	34.95	5H-2, 10	36.90	5H-3, 75	42.05
d_3,	4H-6, 85	37.35	5H-3, 100	39.30	5H-5, 75	45.05
d_3	4H-7, 30	38.30	5H-4, 30	40.10	5H-6, 70	46.50
d_4	5H-1, 125	41.05	5H-5, 20	41.50	6H-2, 30	49.60
e_1	5H-6, 75	48.05	6H-3, 130	49.30		
e_2	6H-1, 35	50.25	6H-5, 60	51.60	7H-2, 30	59.10
e_3	6H-2, 95	52.35	6H-6, 130	53.80	7H-4, 135	63.15
f_1	6H-4, 115	55.55	7H-1, 45	56.05	8X-1, 95	67.95
f_2	6H-5, 60	56.50	7H-1, 140	57.00	8X-2, 120	69.70
f_3	6H-7, 15	59.05	7H-3, 85	59.45	8X-4, 100	72.50
f_4	7H-3, 45	62.95	7H-5, 100	62.60	9X-2, 80	79.00
f_5	7H-4, 65	64.65	7H-6, 120	64.40	9X-3, 90	80.60
g_1	7H-5, 45	65.95	7A-4, 40	65.70	9X-4, 85	82.05
g_2	8H-1, 85	70.35	8H-3, 75	69.25	10X-1, 5	86.45
g_3	8H-2, 50	71.50	8H-4, 120	71.20	10X-2, 20	88.10
g_4	8H-3, 70	73.20	8H-5, 140	72.90	10X-3, 15	89.55
h_1	8H-7, 50	79.00	9H-3, 50	79.00	11X-1, 5	96.05
h_2	9H-1, 35	79.45	9H-3, 110	79.60		
h_3	9H-2, 60	81.20	9H-4, 110	81.10		
h_4	9H-4, 40	84.00	9H-6, 60	83.60		
i_1	9H-5, 45	85.35	9H-7, 50	85.00		
i_2	9H-7, 40	88.50	10X-2, 60	86.40		
i_*	10X-2, 50	90.40	10X-3, 75	88.05		
i_3	10X-4, 25	93.15	10X-5, 40	90.70		
i_4	10X-4, 120	94.10	10X-5, 135	91.65		
i_5	10X-6, 75	96.65	10A-3, 25	93.95		
j_1	11X-1, 120	98.90	11X-2, 5	95.65		
j_2	11X-2, 130	100.50	11X-3, 35	97.45		
j_3	11X-3, 70	101.40	11X-3, 80	97.90		
j_4	11X-4, 65	102.85	11X-4, 50	99.10		
j_5	11X-5, 90	104.60	11A-2, 95	101.05		
k_1	12X-1, 55	108.65	11A-3, 100	102.60		
k_2			12X-3, 45	107.05		
l_1	13X-1, 60	115.40	12A-1, 45	108.75		
l_2	13X-2, 60	116.90	12A-2, 45	110.25		
l_3	13X-4, 40	119.70	13X-1, 65	112.95		
l_4	13X-6, 30	122.30	13X-3, 45	115.75		
m_1	14X-2, 115	127.05	13A-1, 50	119.00		
m_2	14X-3, 120	128.60	13A-2, 90	120.90		
m_3	14X-4, 70	129.60	13A-3, 35	121.85		
n_1	15X-1, 75	134.85	14X-3, 90	126.90	11X-4, 110	101.60
n_2	15X-2, 135	136.95	14X-4, 65	128.15	11X-5, 130	103.30
n_3	15X-3, 130	138.40	14X-5, 20	129.20	11X-6, 90	104.40
n_4	15X-6, 15	141.75	15X-1, 95	133.55	12X-2, 55	107.75
o_1	16X-2, 70	146.00	14A-4, 100	134.60	12X-4, 70	110.90
o_2	16X-3, 30	147.10	14A-5, 15	135.75	12X-5, 10	111.80
p_1	17X-1, 95	154.40	15A-2, 120	140.50		
p_2	17X-2, 45	155.45	15A-3, 65	141.45		
p_3	17X-3, 90	157.40	15A-4, 45	142.75		
p_4	17X-4, 70	158.70	16X-2, 35	144.15		
p_5	17X-5, 100	160.50	16X-3, 75	146.05		
p_6	17X-6, 90	161.90	16X-4, 15	146.95		
q_1	18X-1, 120	164.40	16X-5, 35	148.65		
q_2	18X-2, 90	165.60	16X-5, 130	149.60		
q_3	18X-3, 45	166.65	16X-6, 60	150.40		
q_4	18X-4, 100	168.70	16A-3, 100	151.90		
q_5	18X-5, 70	169.90	16A-4, 30	152.70		
q_6	18X-6, 90	171.60	17X-2, 5	154.05		
r_1	19X-1, 110	174.00	17X-4, 145	158.45		
r_2	19X-2, 55	174.95	17X-5, 75	159.25		
r_3	19X-4, 70	178.10	17X-C, 20	161.90		
r_4	19X-5, 100	179.90	18X-1, 125	163.45		

Table 11 (continued).

	Hole 721B		Hole 722B		Hole 731A	
	Core, section, interval (cm)	Corrected depth (mbsf)	Core, section, interval (cm)	Corrected depth (mbsf)	Core, section, interval (cm)	ODP depth (mbsf)
s_1	20X-2, 105	185.15	18X-4, 130	168.00		
s_2	20X-3, 100	186.60	18X-6, 50	170.20		
s_3	20X-4, 65	187.75	18X-7, 5	171.25		
s_4	20X-4, 140	188.5	19X-1, 90	176.80		
t_1	21X-1, 20	192.50	19X-5, 90	182.80		
t_2	21X-2, 110	194.90	20X-1, 110	184.80		
u_1	22X-3, 30	205.30	20A-2, 90	188.15		
u_2	22X-4, 65	207.15	20A-3, 75	189.75		
v_1	23X-2, 45	213.65	21X-2, 40	195.20		
v_2	23X-3, 120	215.90	21X-3, 90	197.20		
w_1	24X-2, 60	223.40	22X-6, 50	211.00		
w_2	24X-3, 100	225.30	22A-4, 120	213.40		
x_1	25X-3, 125	234.75	23X-3, 130	217.00	13X-3, 25	118.65
x_2	25X-5, 65	237.15	23X-5, 45	219.15	13X-4, 110	121.00
y_1	26X-3, 50	243.60	24X-3, 45	224.45	14X-3, 80	128.80
y_2	26X-4, 90	245.50	24X-4, 75	226.25	14X-4, 120	130.70
z_1			27X-2, 120	249.2	15X-5, 90	141.60
z_2			29X-1, 110	267.00	18X-6, 75	171.95
z_3			31X-2, 120	288.00	19X-6, 120	182.10
z_4			35X-4, 55	329.05	25X-4, 80	236.90
z_5			37X-3, 40	346.80	27X-4, 60	256.00
z_6			38X-4, 65	358.25	28X-4, 75	265.85

Note: Corrected depth = corrected depth for stratigraphic thickness. Depths are based on ODP CORELOG data. Core number + A = the marker layer was not identified in Hole B, but was identified in Hole A, and the core number listed is from Hole 731A.

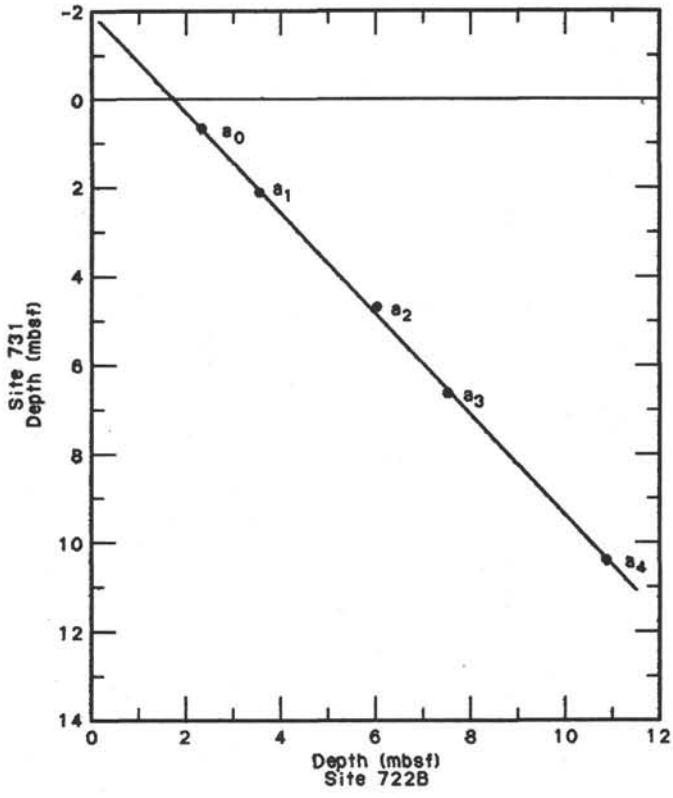

Figure 36. Correlation of the corrected sub-bottom depths at Hole 722B and depth at Site 731 for the marker horizons a_0–a_4. This graph shows that the top 2 m of surface sediments are missing in the cored sedimentary sequence at Site 731.

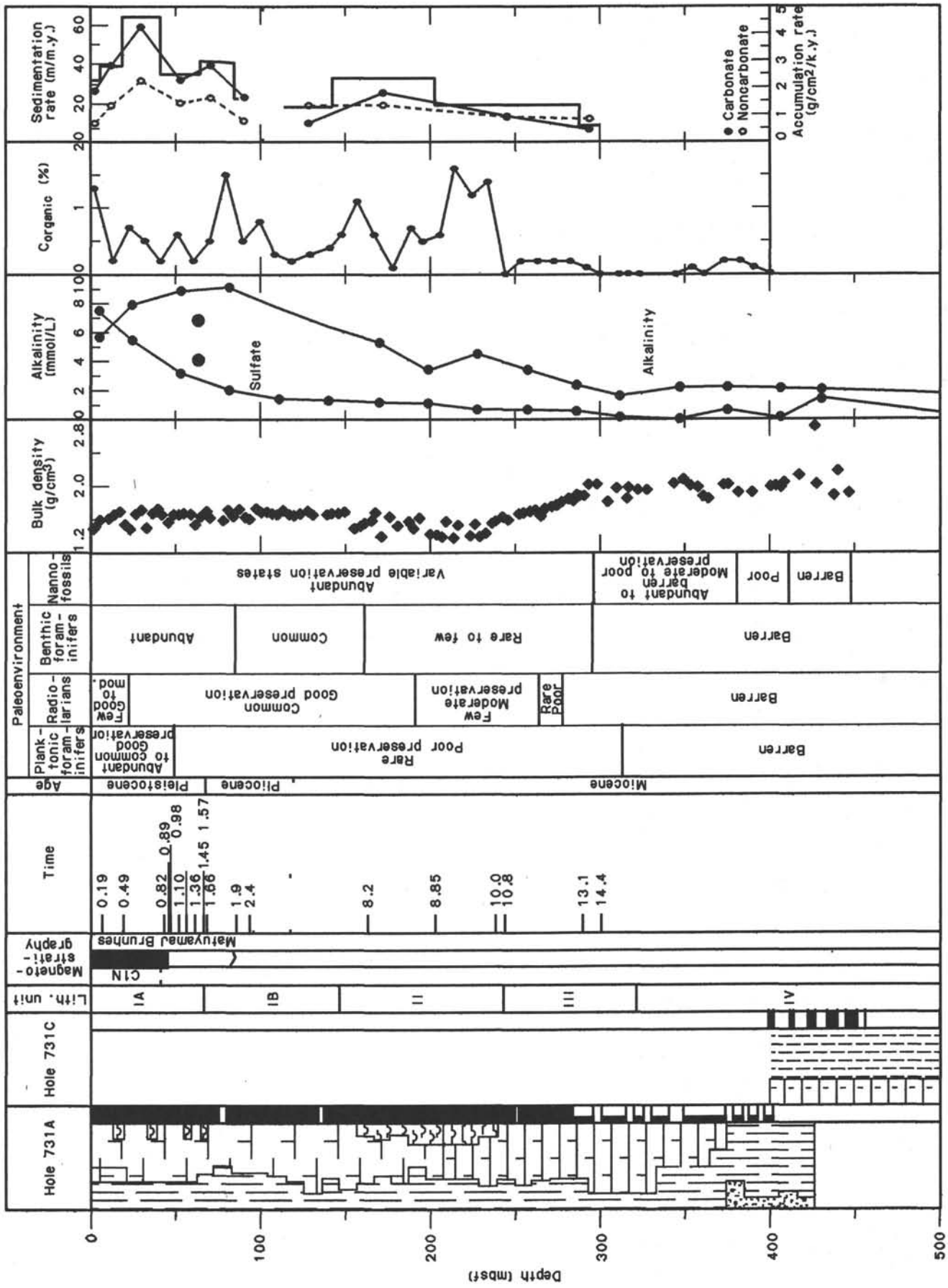
Sedimentation rate (m/m.y.)
Carbonate
Noncarbonate
Accumulation rate (g/cm2/k.y.)
Corganic (%)
Alkalinity (mmol/L)
Sulfate
Alkalinity
Bulk density (g/cm3)
Paleoenvironment
Nanno-fossils
Benthic foram-inifers
Radio-larians
Plank-tonic foram-inifers
Abundant
Variable preservation states
Abundant to barren
Moderate to poor preservation
Poor
Barren
Common
Rare to few
Good preservation
Few
Moderate preservation
Rare
Poor
Age
Pleistocene
Pliocene
Miocene
Time
0.19
0.49
0.82
0.89
0.98
1.10
1.36
1.45
1.57
1.66
1.9
2.4
8.2
8.85
10.0
10.8
13.1
14.4
Magneto-stratig-raphy
Matuyama& Brunhes
C1N
Lith. unit
IA
IB
II
III
IV
Hole 731C
Hole 731A
Depth (mbsf)
0
100
200
300
400
500

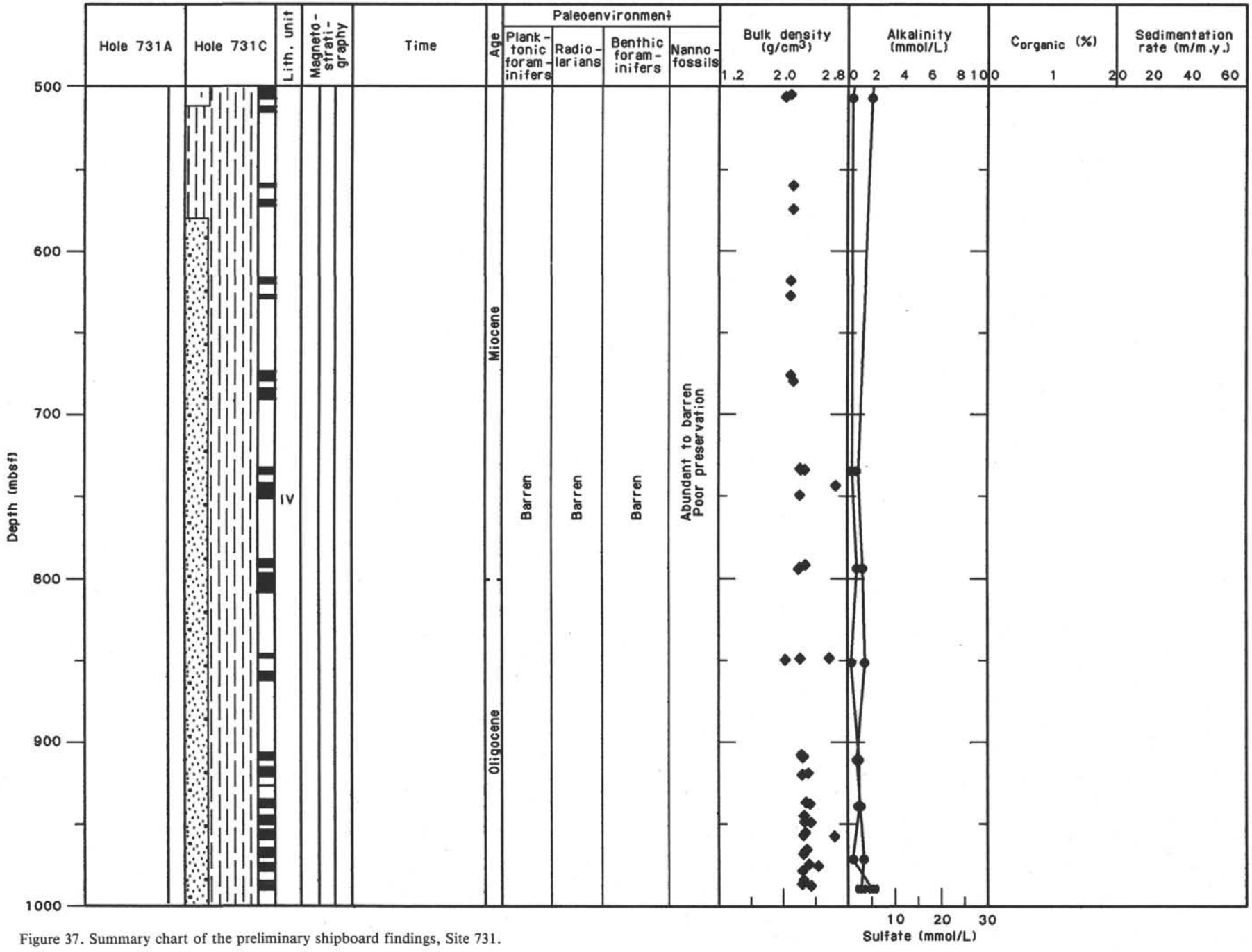

Figure 37. Summary chart of the preliminary shipboard findings, Site 731.

ous tests toward younger sediments, and the increased abundance of benthic foraminifers in lithologic Unit III. The trend from turbiditic to increasingly pelagic deposition is related to the uplift of the Owen Ridge.

Hole 731C was logged under good conditions with two tool combinations over 968 m of the 994-m-deep hole. Log quality is excellent and will provide insight into lithologic changes in the thick and sparsely recovered turbiditic Unit IV.

Site 731 and nearby Sites 721 and 722 provide an excellent record of the onset and evolution of monsoonal upwelling from the late middle Miocene to the Pliocene-Pleistocene. This sequence should provide insights into the relationship of orbital changes and the uplift of the Himalaya to the history of monsoon-related upwelling and eolian sedimentation on the Owen Ridge, as well as on tectonic uplift of Owen Ridge and the evolution of Owen Basin.

REFERENCES

Arthur, M. A., Srivastrava, S. P., Jarrard, R., and Aksu, A. E., in press. Seismic and log correlation ... *In* Arthur, M. A., Srirastrava, S. P., et al., *Proc. ODP, Sci. Results*, 105: College Station, TX (Ocean Drilling Program).

Berggren, W. A., Kent, D. V., and Van Couvering, J. A., 1985. The Neogene: Part 2, Neogene geochronology and chronostratigraphy. *In* Snelling, N. J. (Ed.), *The Chronology of the Geological Record*: Geol. Soc. Mem. (London), 10:211–259.

Blatt, H., Middleton, G. V., and Murray, R., 1980. *Origin of Sedimentary Rocks*: New Jersey (Prentice-Hall).

Gieskes, J. M., 1981. Deep sea drilling interstitial water studies: implications for chemical alteration of the ocean crust, Layers I and II. *In* Warme, J. E., Douglas, R. C., and Winterer, E. L. (Eds.), *The Deep Sea Drilling Project: A Decade of Progress*, Soc. Econ. Paleontol. Mineral. Spec. Publ., 32:149–168.

Hamilton, E. L., 1976. Variations of density and porosity with depth in deep-sea sediments. *J. Sediment. Petrol.*, 46:280–300.

_____, 1979. Sound velocity gradients in marine sediments. *J. Acoust. Soc. Am.*, 65:909–922.

Johnson, D. A., Nigrini, C. A., Caulet, J. P., Schneider, D., and Kent, D., in press. Pliocene-Pleistocene radiolarian events and magnetostratigraphic calibrations for the tropical Indian Ocean. *Mar. Micropaleontol.*

Johnson, D. A., and Nigrini, C. A., 1985. Synchronous and time-transgressive Neogene radiolarian datum levels in the equatorial Indian and Pacific Oceans. *Mar. Micropaleontol.*, 9:489–523.

Kolla, V., Kostecki, J. A., Robinson, F., and Biscaye, P. E., 1981. Distribution and origins of clay minerals and quartz in surface sediments of the Arabian Sea. *J. Sediment. Petrol.*, 51:563–569.

Martini, E., 1970. Standard Palaeogene calcareous nannoplankton zonation. *Nature*, 226:560–561.

McIntyre, A., and Bé, A.W.H., 1967. Modern Coccolithophoridae of the Atlantic Ocean—I: placoliths and cyrtoliths. *Deep-Sea Res.*, 14: 561–597.

Mountain, G., and Prell, W. L., 1987. Leg 117 ODP site survey: a revised history of Owen Basin. *Eos, Trans. Am. Geophys. Union*, 68: 424.

Prell, W. L., 1984. Monsoonal climate of the Arabian Sea during the late Quaternary: a response to changing solar radiation. *In* Berger, A., and Imbrie, J. (Eds.), *Milankovitch and Climate*: Dordrecht (D. Reidel), 349–366.

Roth, P. H., 1974. Calcareous nannofossils from the northwestern Indian Ocean, Leg 24, Deep Sea Drilling Project. *In* Fisher, R. L., Bunce, E. T., et al., *Init. Repts. DSDP*, 24: Washington (U.S. Govt. Printing Office), 969–994.

Sato, T., Takayama, T., Kato, M., Kudo, T., and Kameo, K., in press. Calcareous microfossil biostratigraphy of the uppermost Cenozoic formations distributed in the coast of the Japan Sea. Part. 4: Conclusion. *Sekiyu Gijutsu Kyokaishi.*

Takayama, T., and Sato, T., 1987. Coccolith biostratigraphy of the North Atlantic Ocean, Deep Sea Drilling Project Leg 94. *In* Ruddiman, W. F., Kidd, R. B., Thomas, E., et al., *Init. Repts. DSDP*, 94, Pt. 2: Washington (U.S. Govt Printing Office), 651–702.

Whitmarsh, R. B., 1974. Summary of general features of Arabian Sea and Red Sea Cenozoic history based on Leg 23 cores. *In* Whitmarsh, R. B., Weser, O. E., Ross, D. A., et al., *Init. Repts. DSDP*, 23: Washington (U.S. Govt. Printing Office), 1115–1123.

_____, 1979. The Owen Basin off the southeast margin of Arabia and the evolution of the Owen Fracture Zone. *Geophys. J. R. Astron. Soc.*, 58:441–470.

Whitmarsh, R. B., Weser, O. E., Ross, D. A., et al., 1974. *Init. Repts. DSDP*, 23: Washington (U.S. Govt. Printing Office).

Ms 117A-108

Summary Log for Hole 731C (continued)

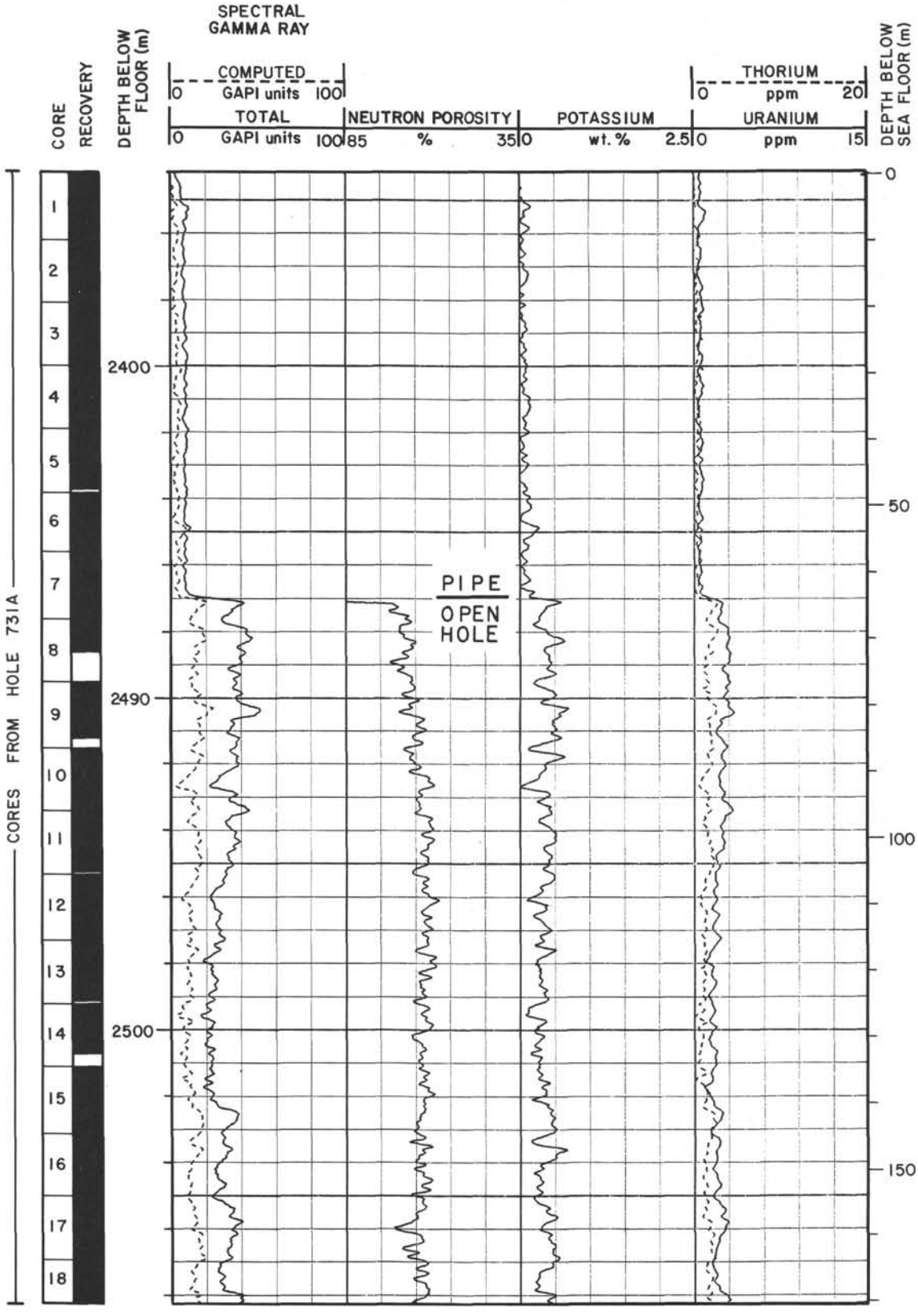

Summary Log for Hole 731C (continued)

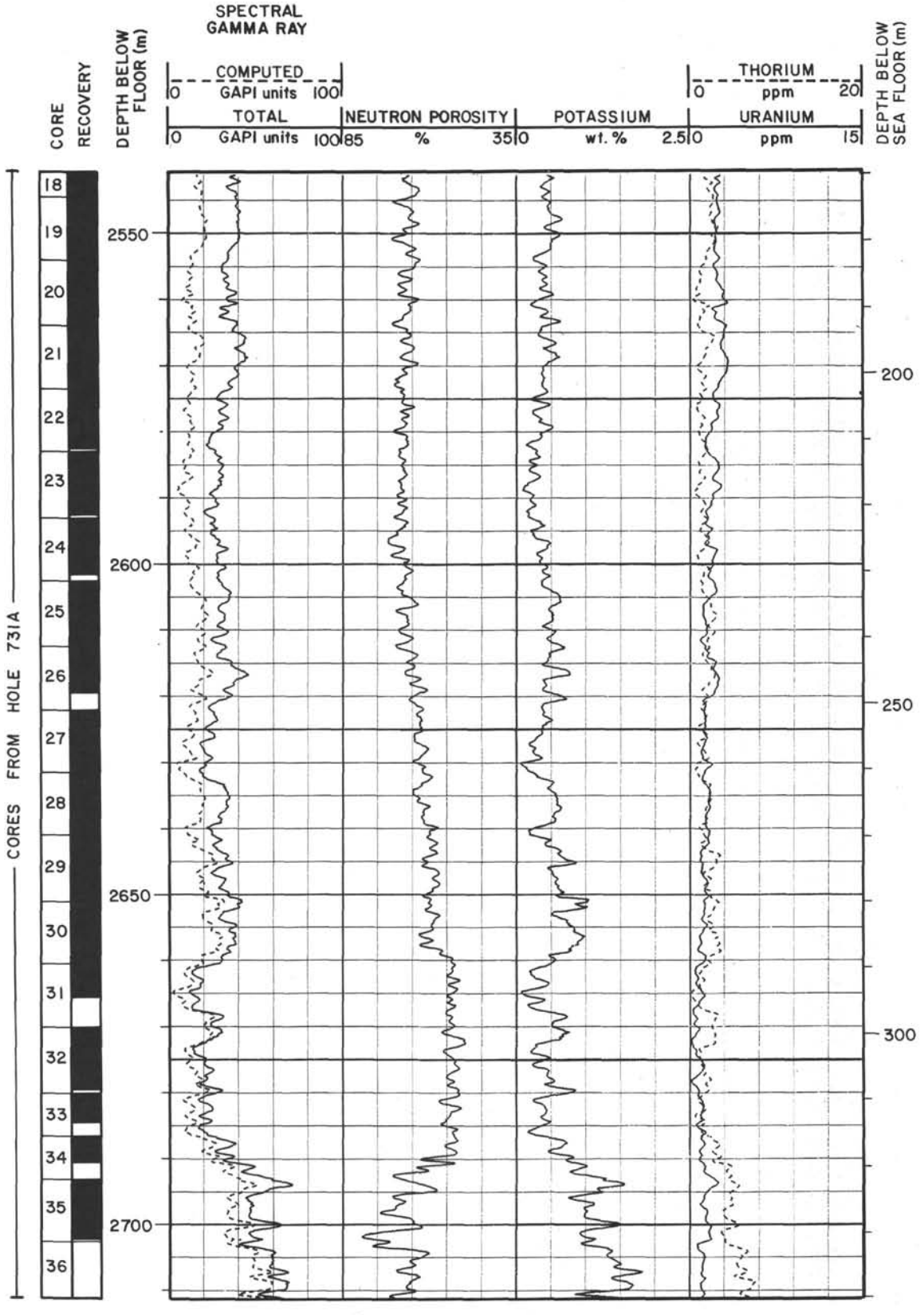

Summary Log for Hole 731C (continued)

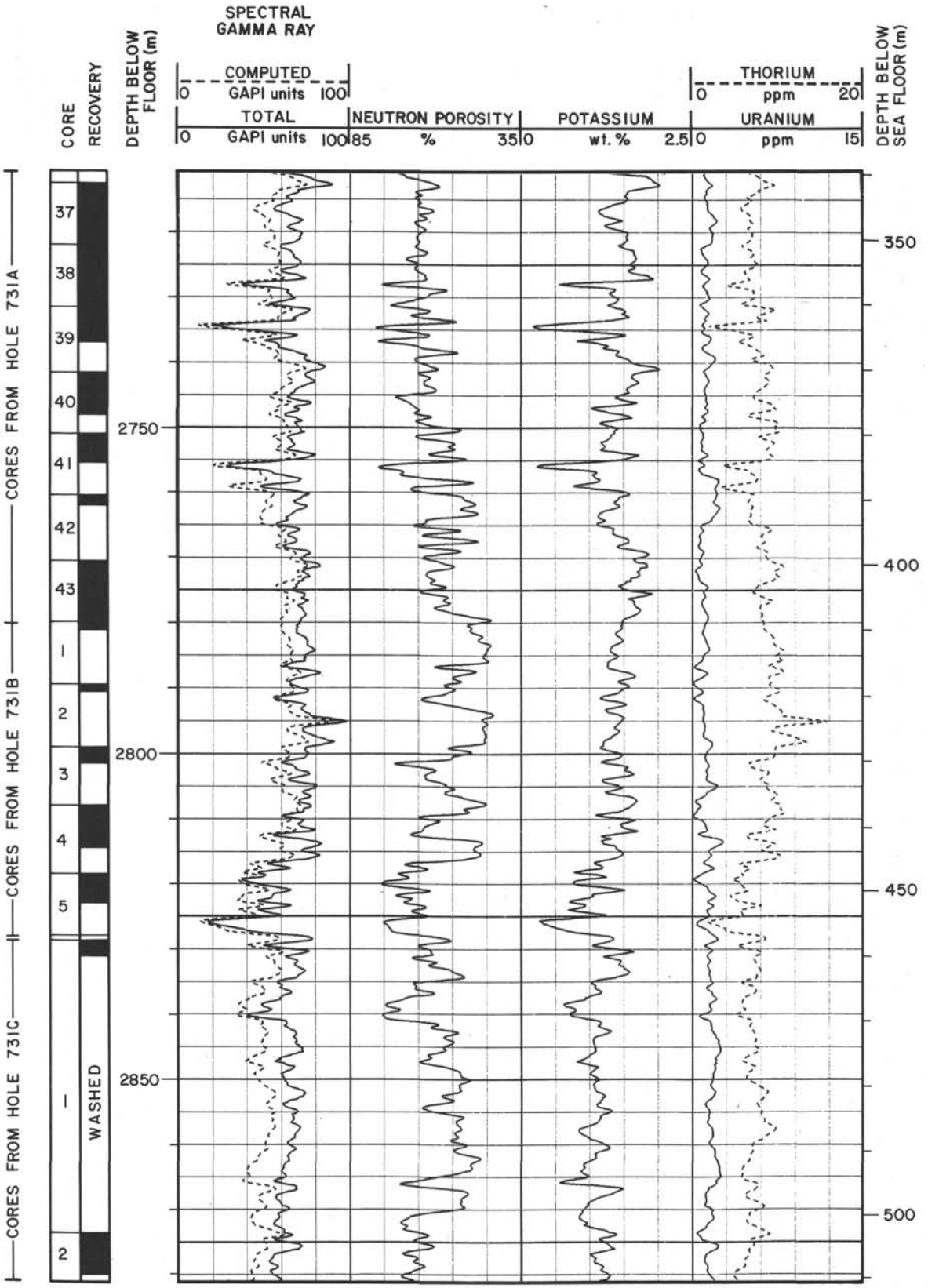

Summary Log for Hole 731C (continued)

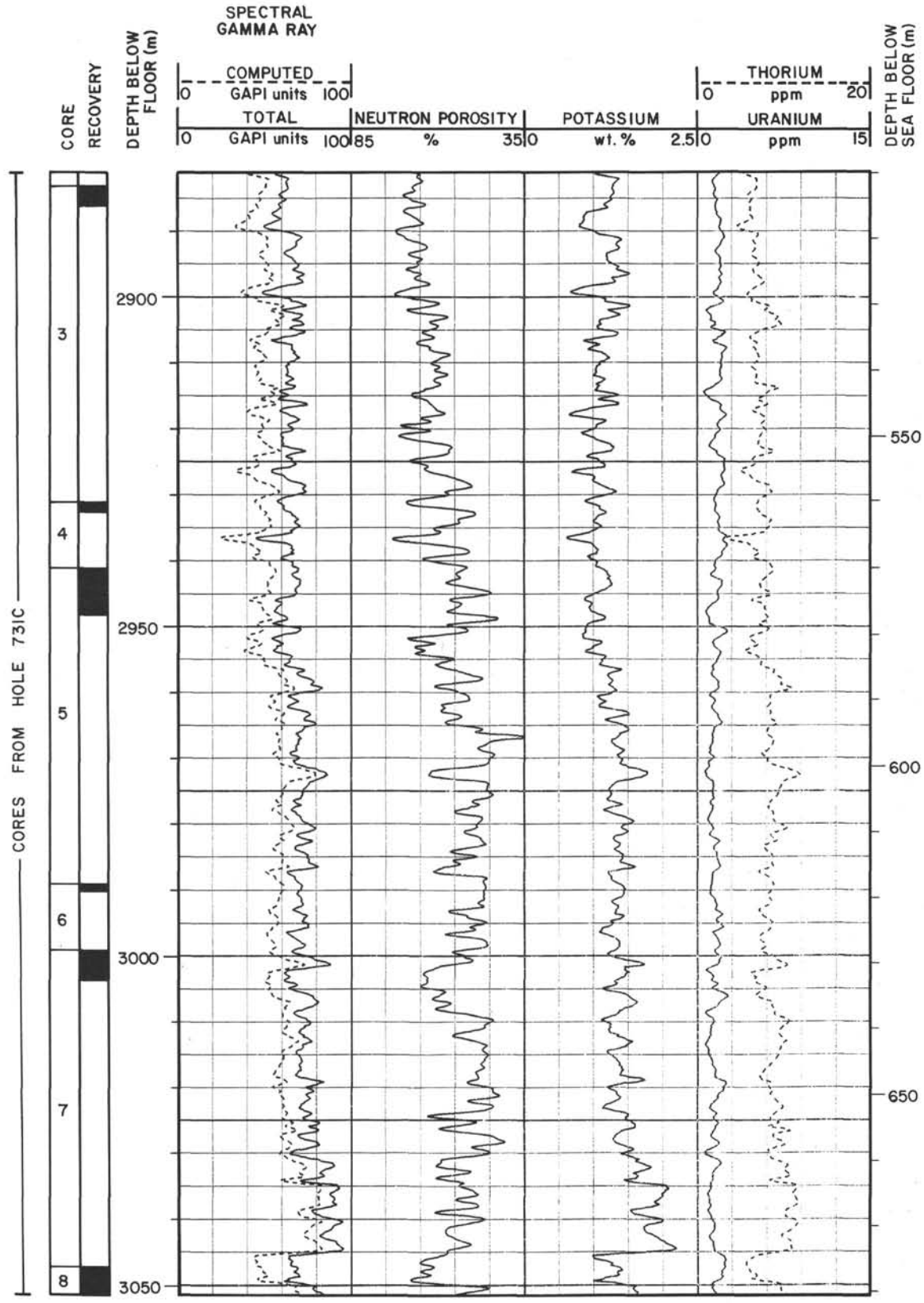

Summary Log for Hole 731C (continued)

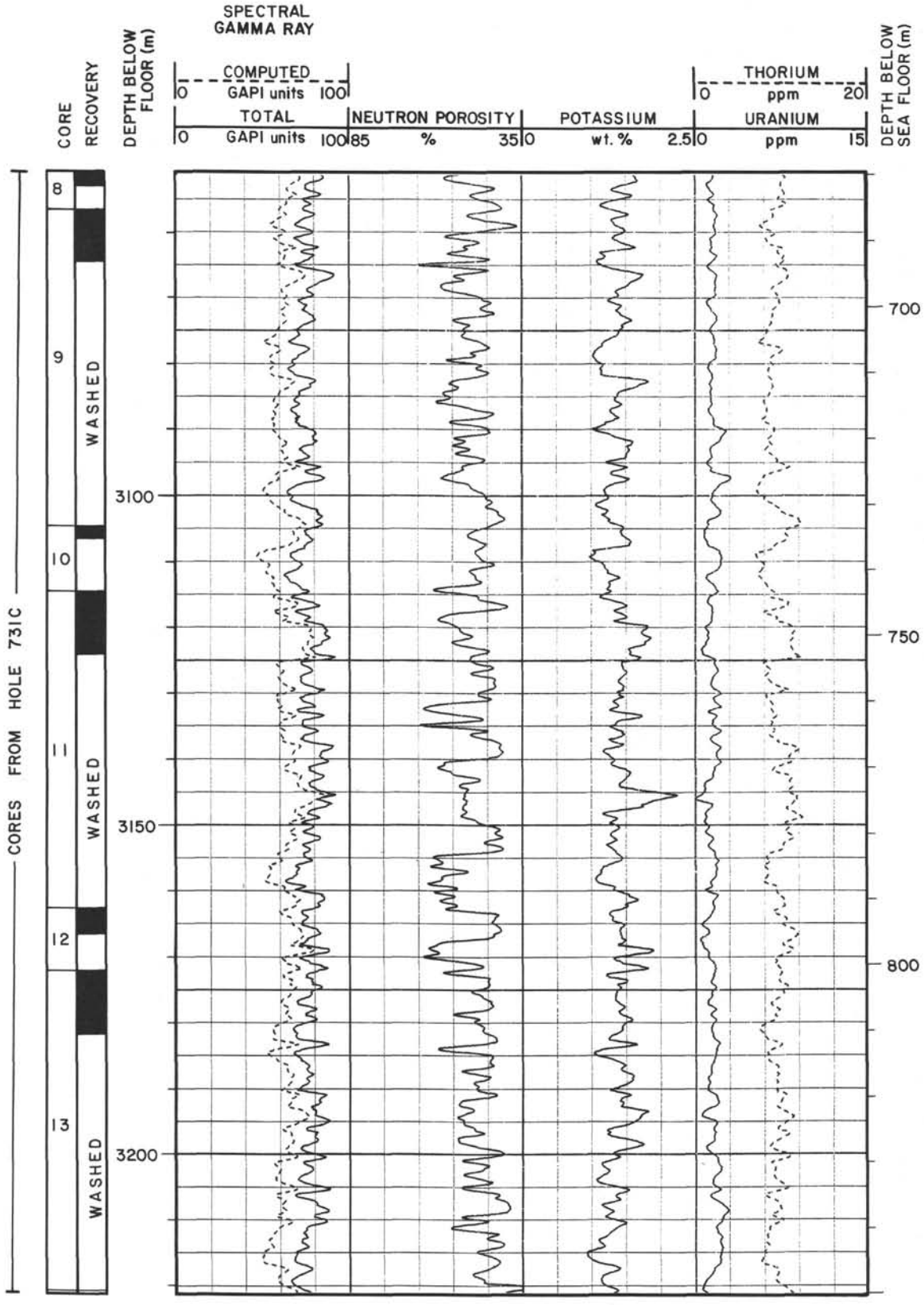

Summary Log for Hole 731C (continued)

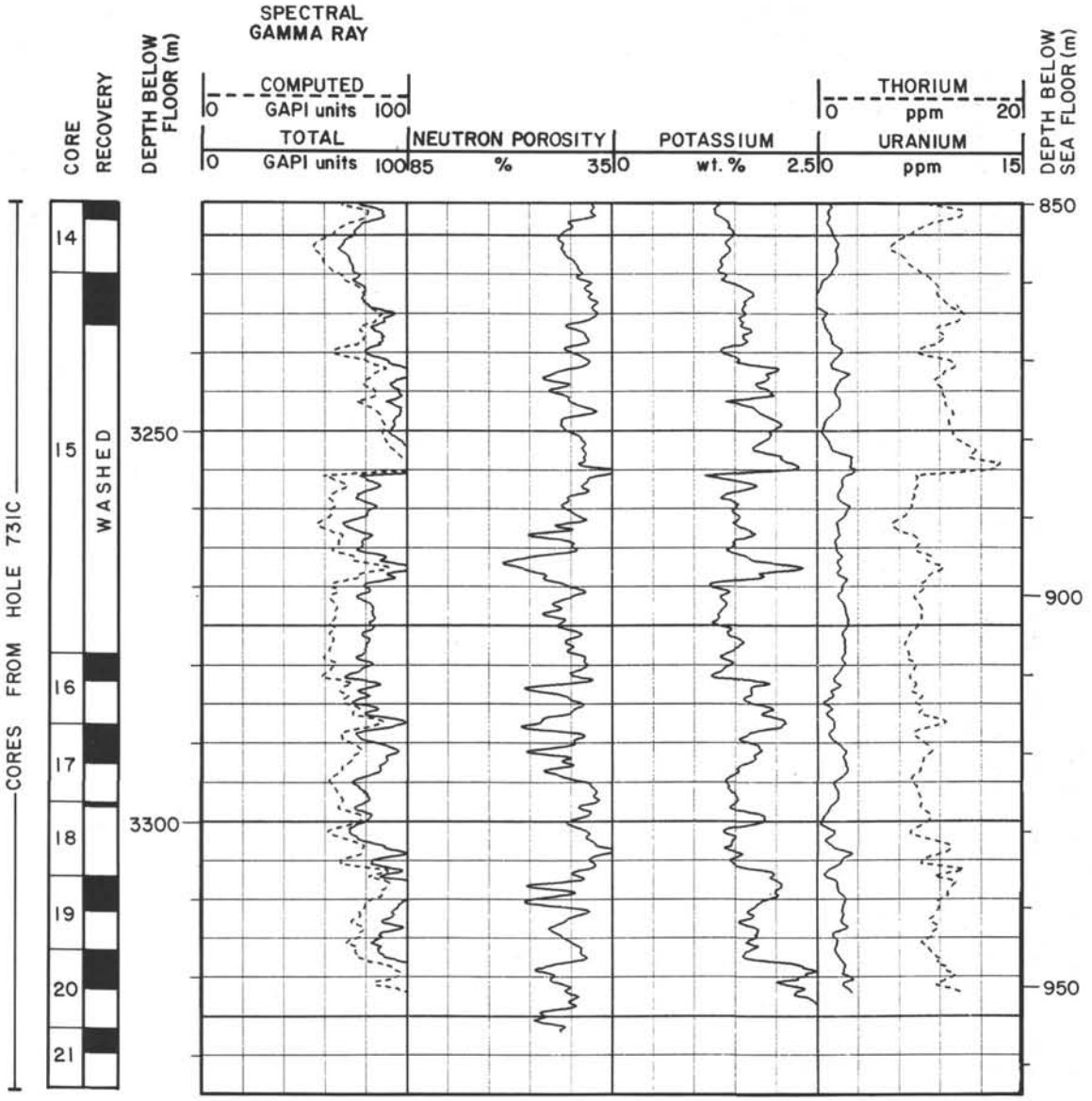

Summary Log for Hole 731C (continued)

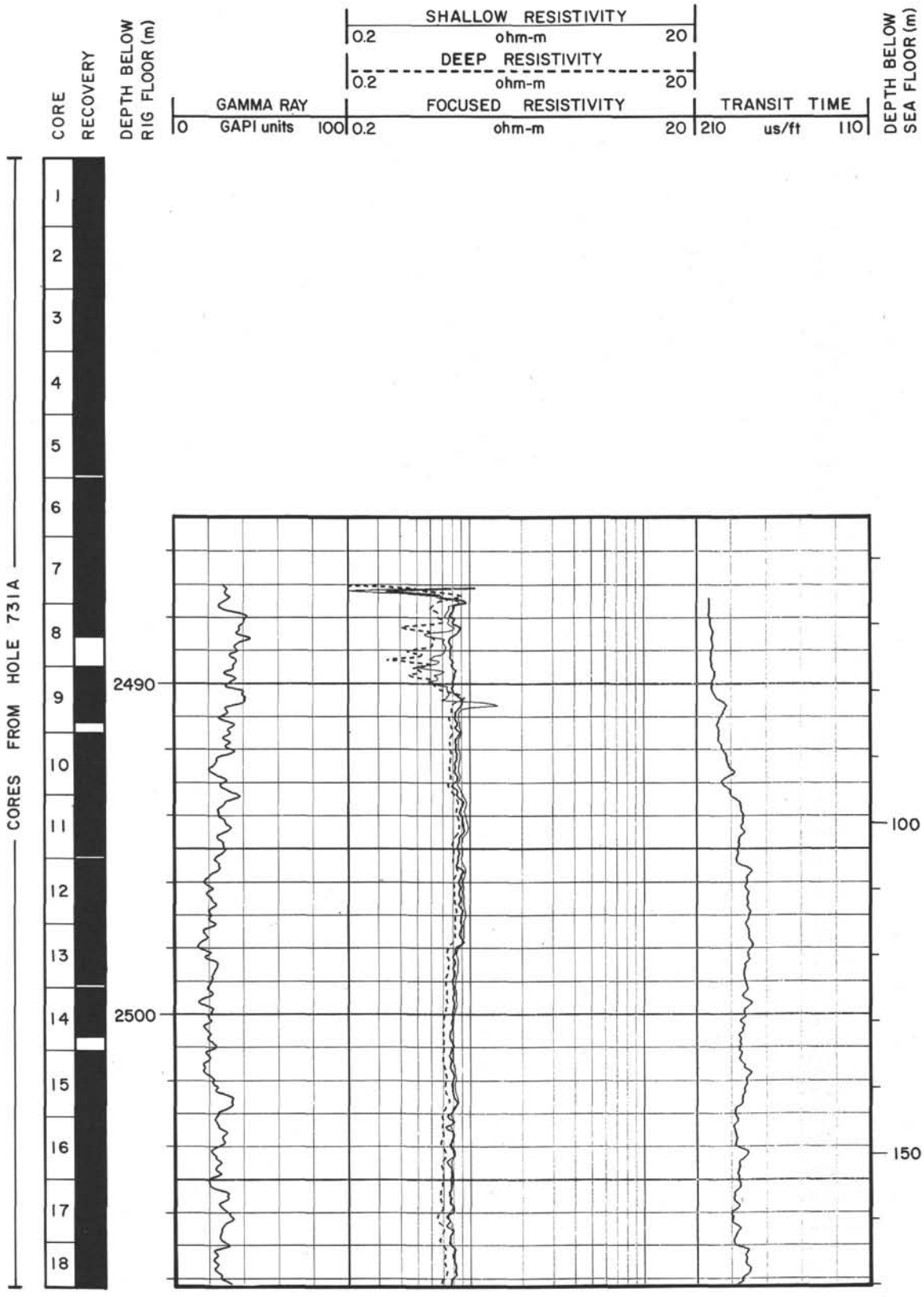

Summary Log for Hole 731C (continued)

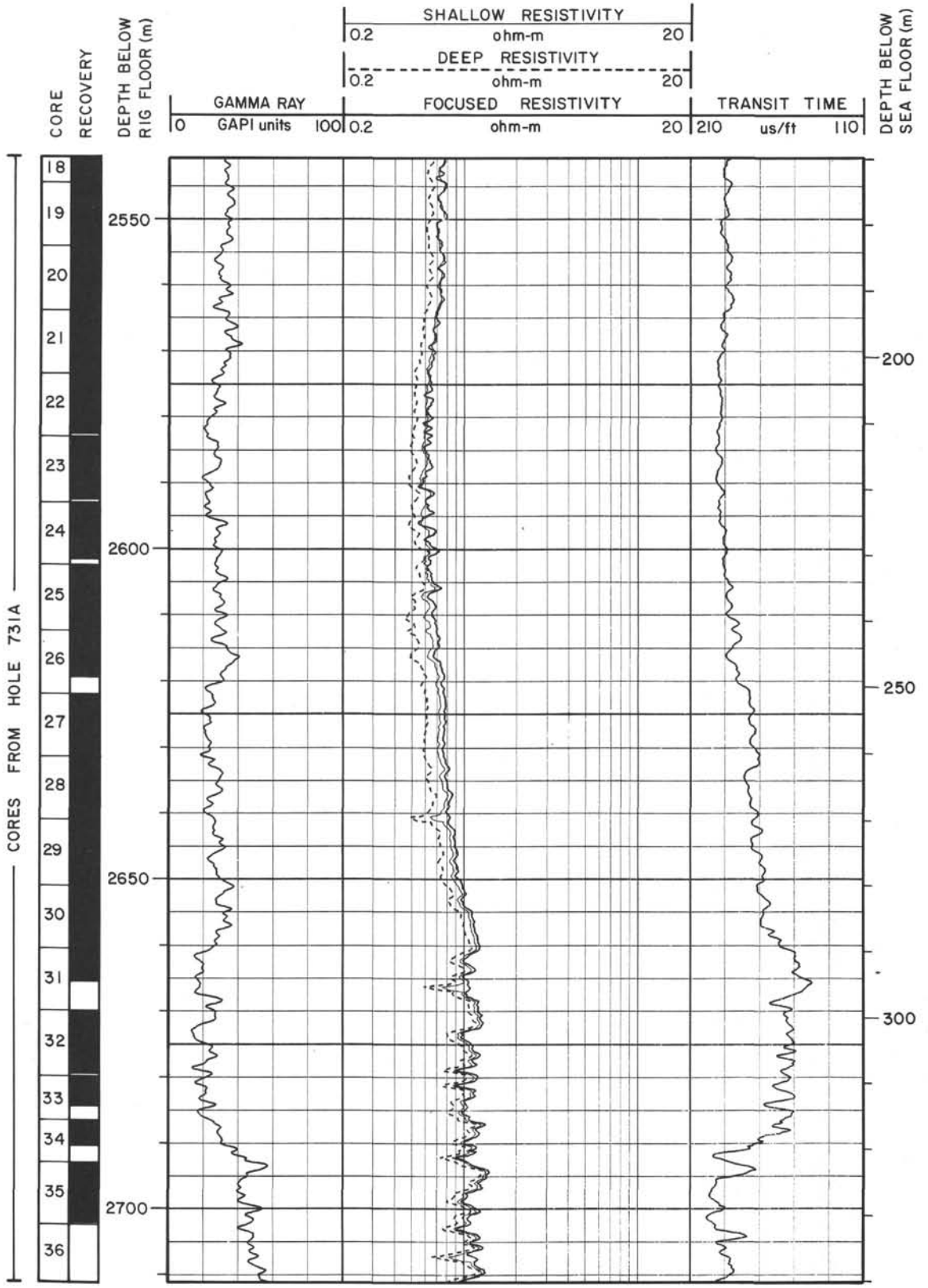

Summary Log for Hole 731C (continued)

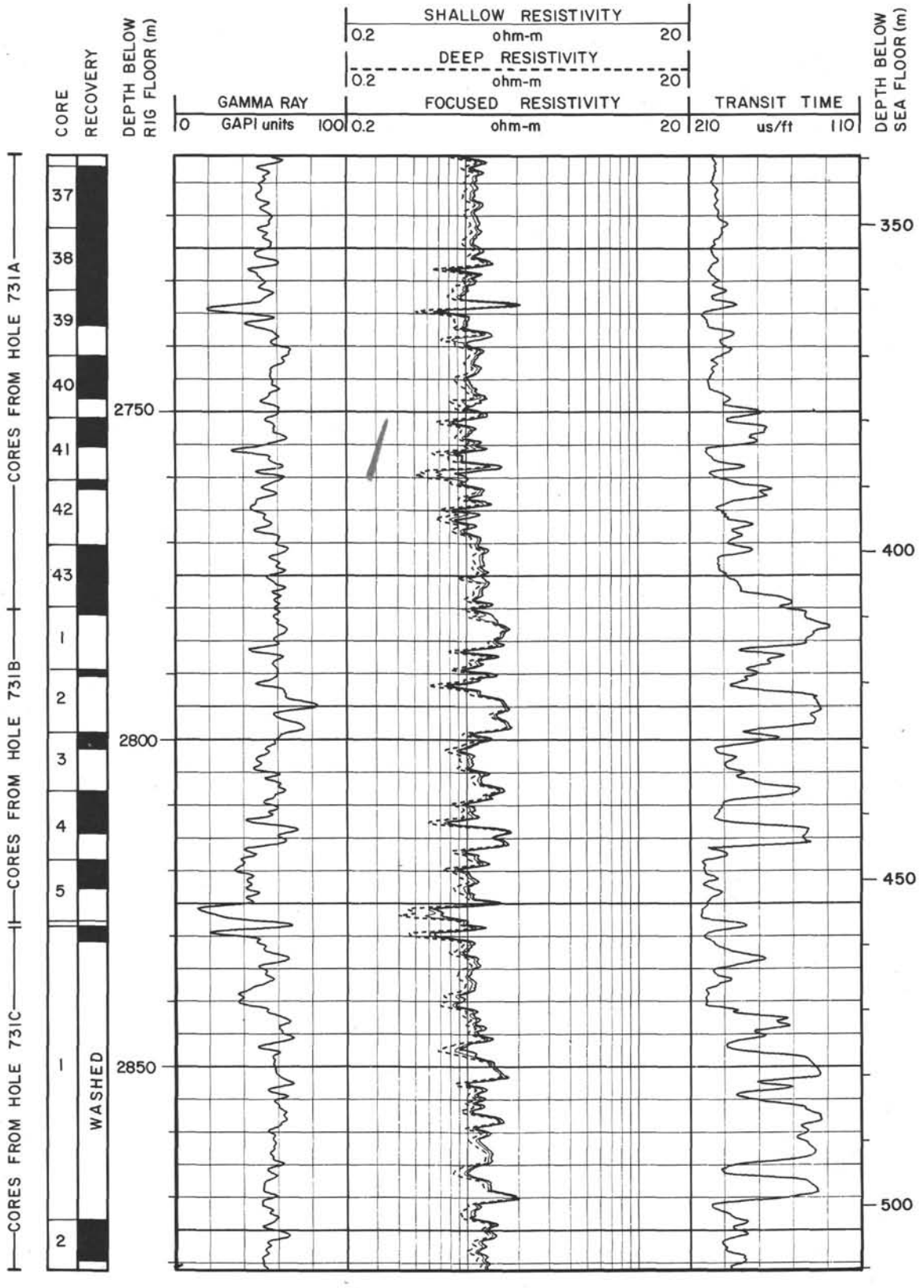

Summary Log for Hole 731C (continued)

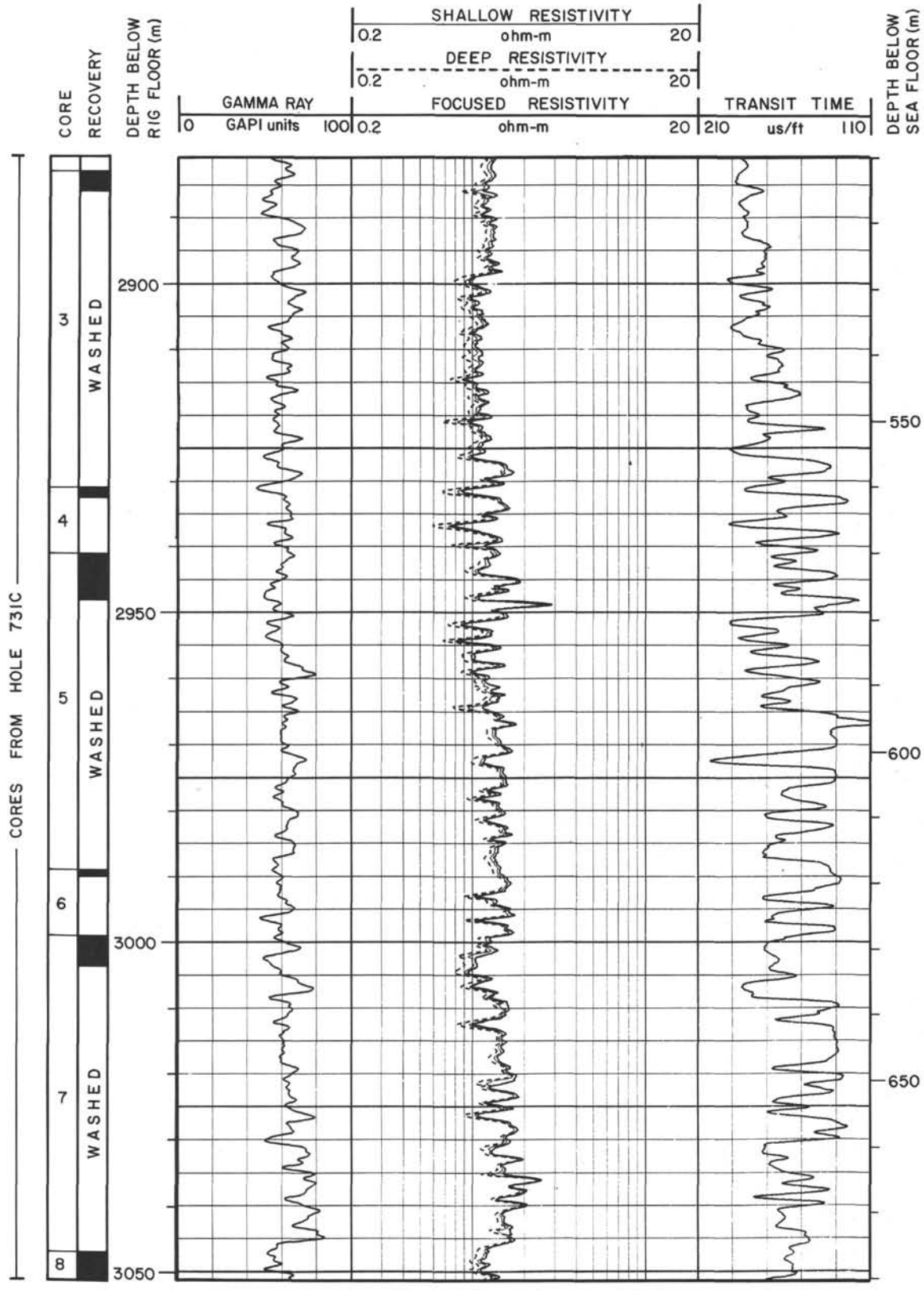

Summary Log for Hole 731C (continued)

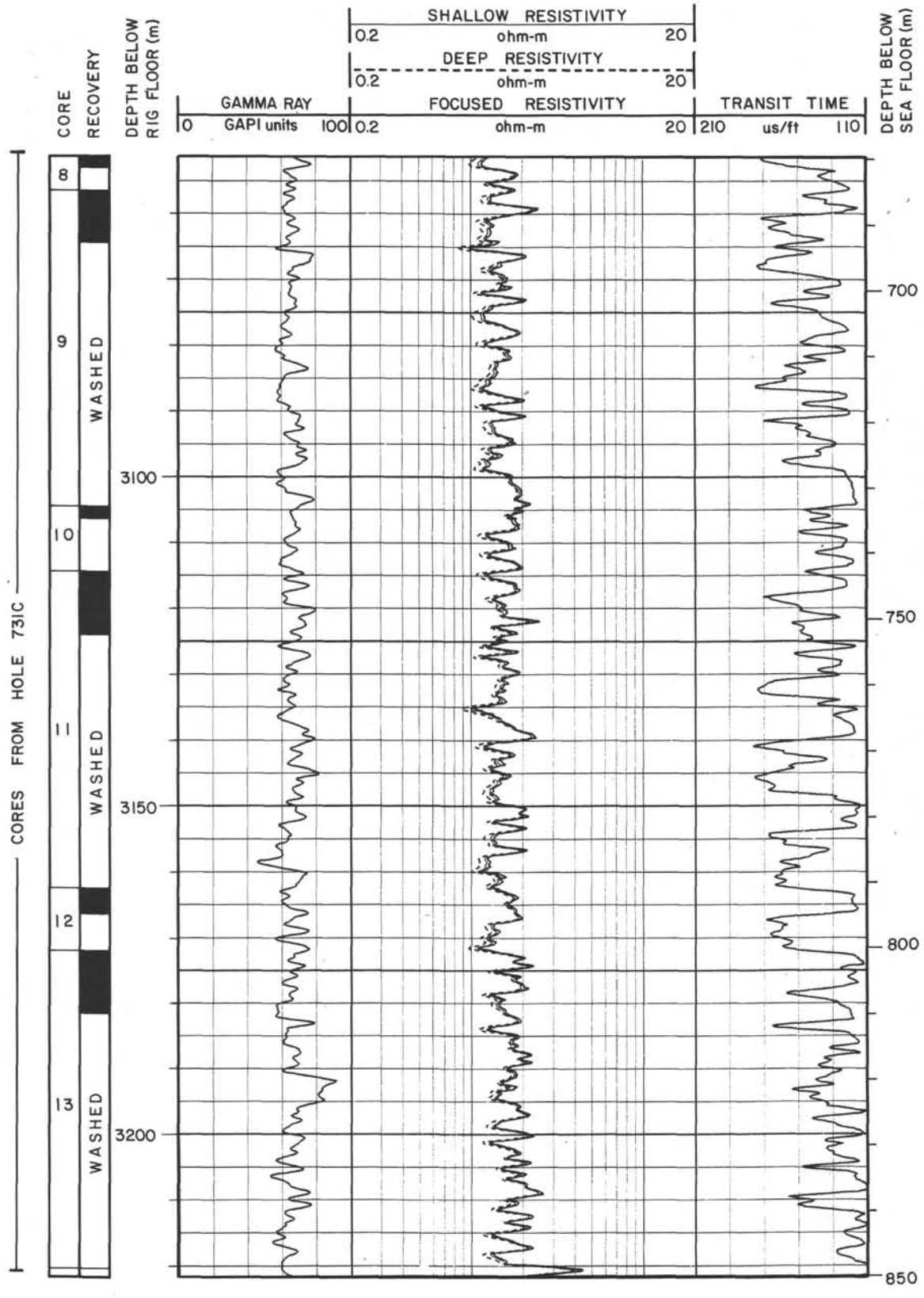

Summary Log for Hole 731C (continued)

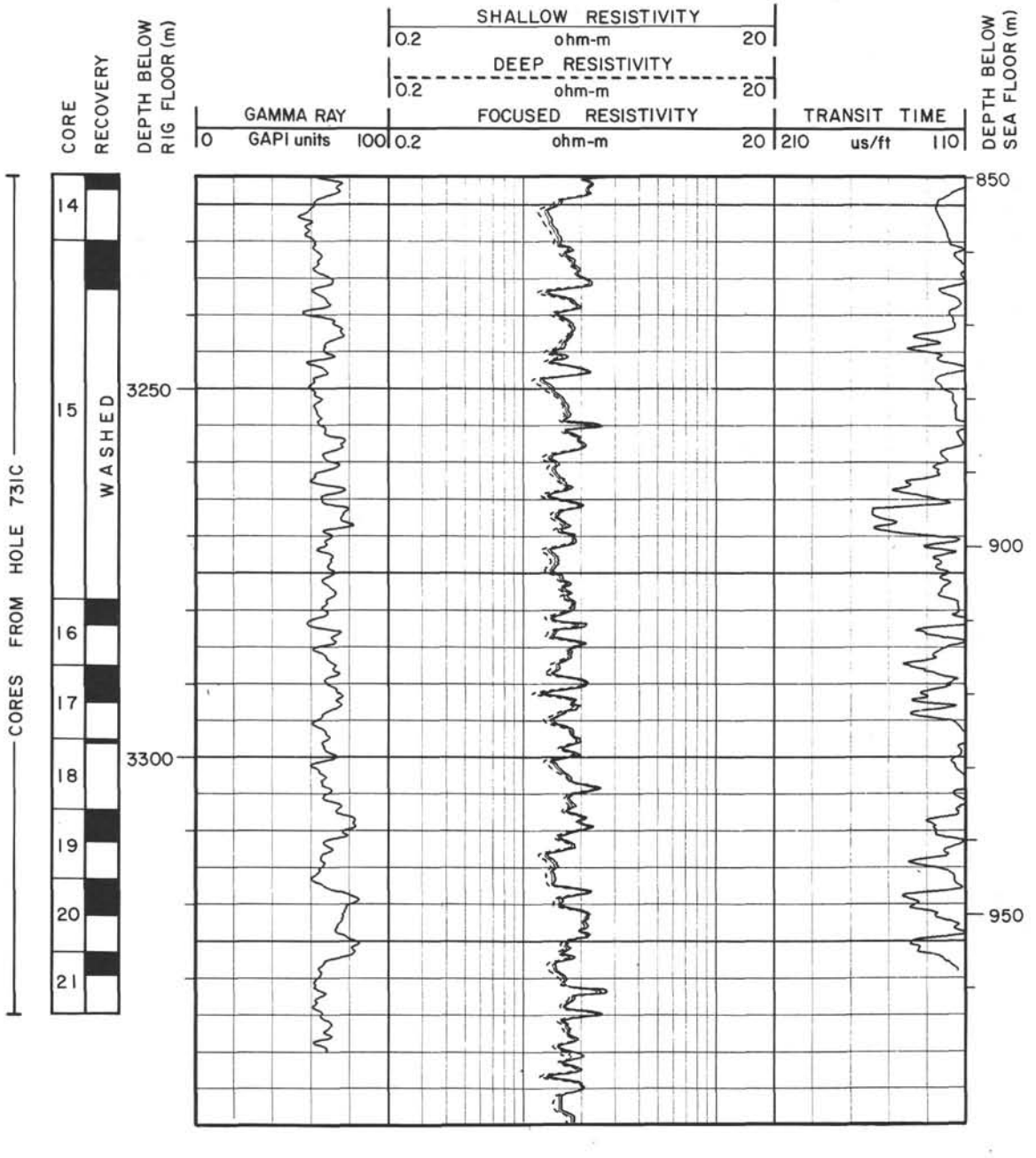

Summary Log for Hole 731C (continued)

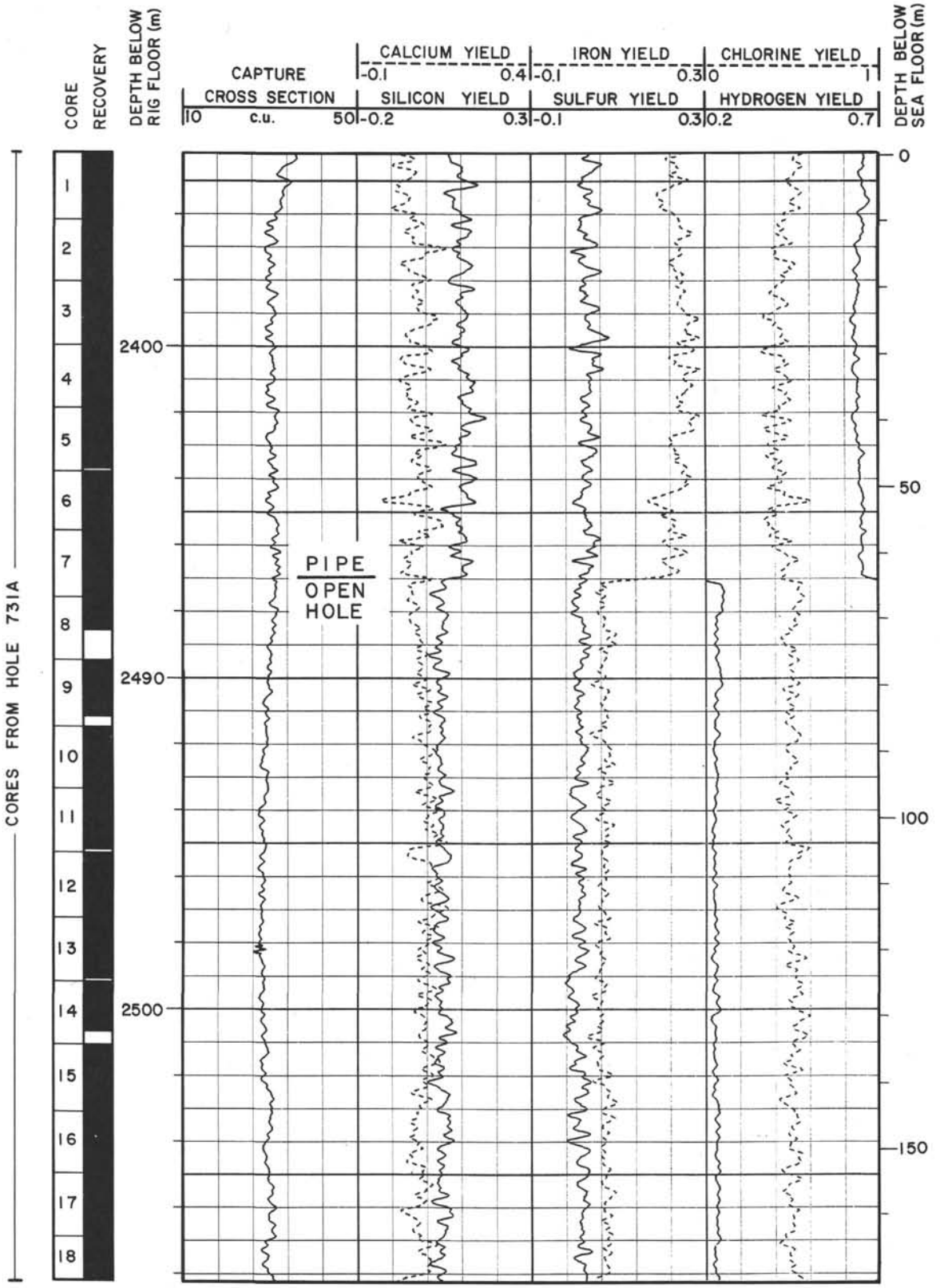

Summary Log for Hole 731C (continued)

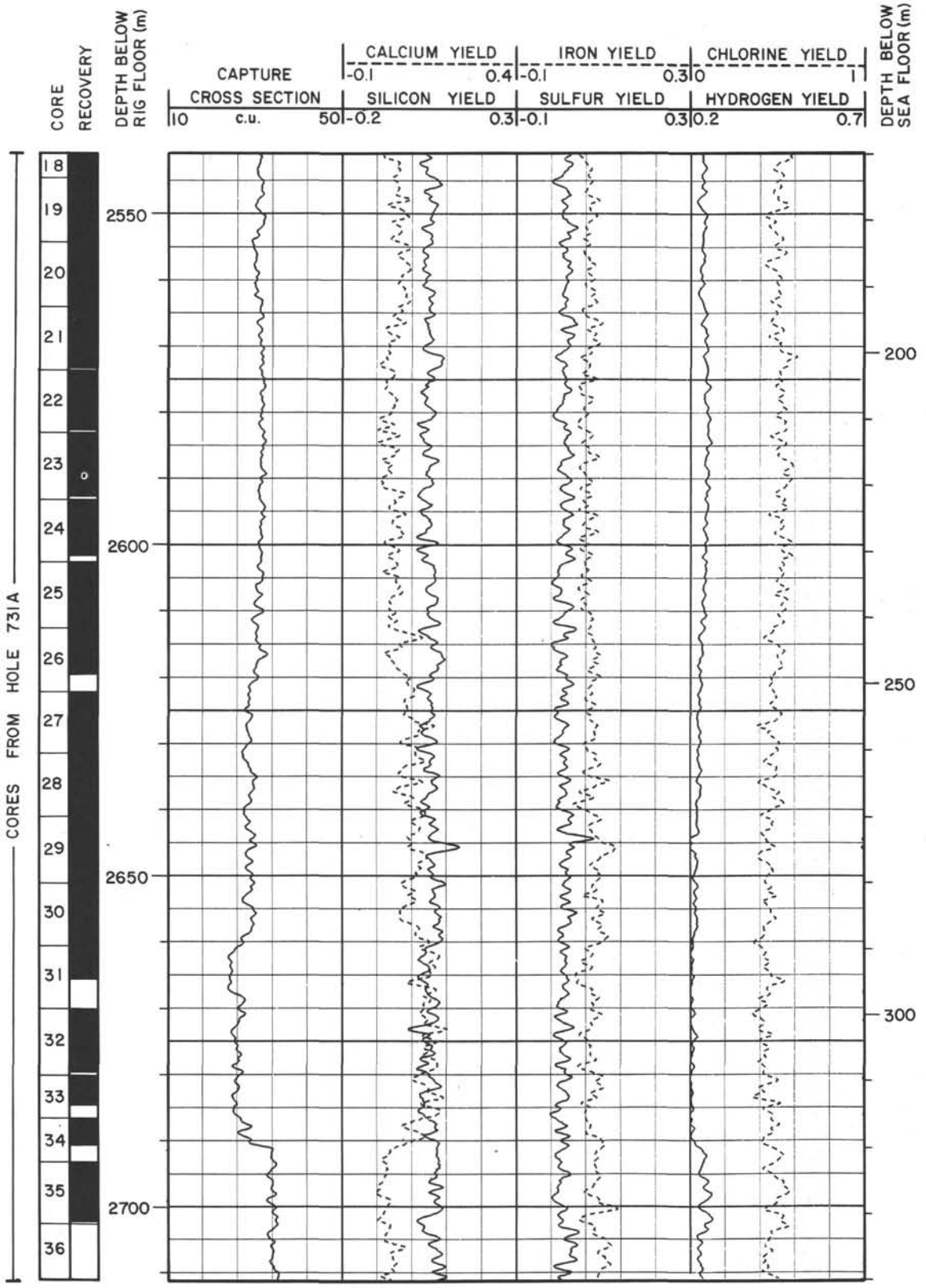

Summary Log for Hole 731C (continued)

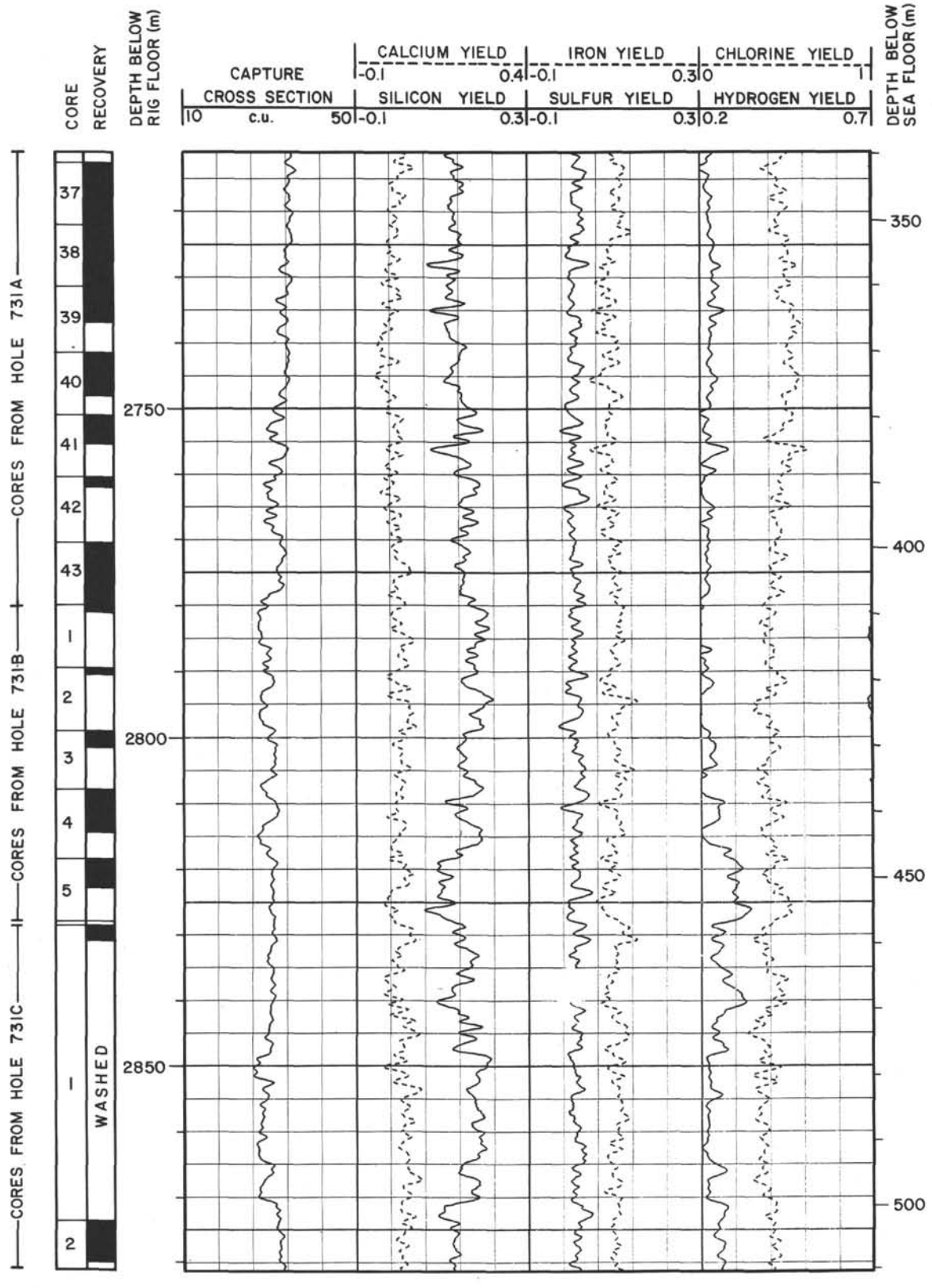

Summary Log for Hole 731C (continued)

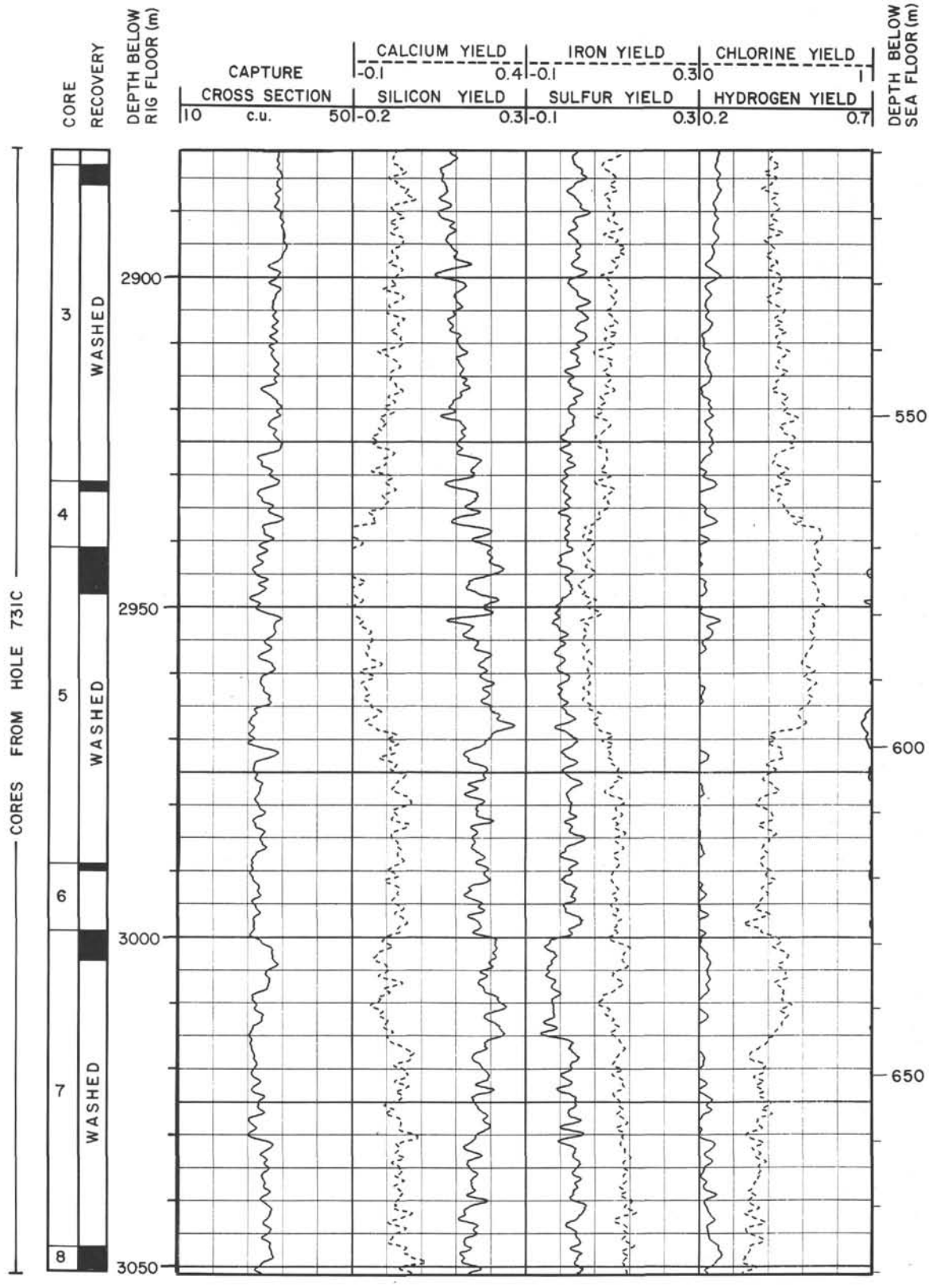

Summary Log for Hole 731C (continued)

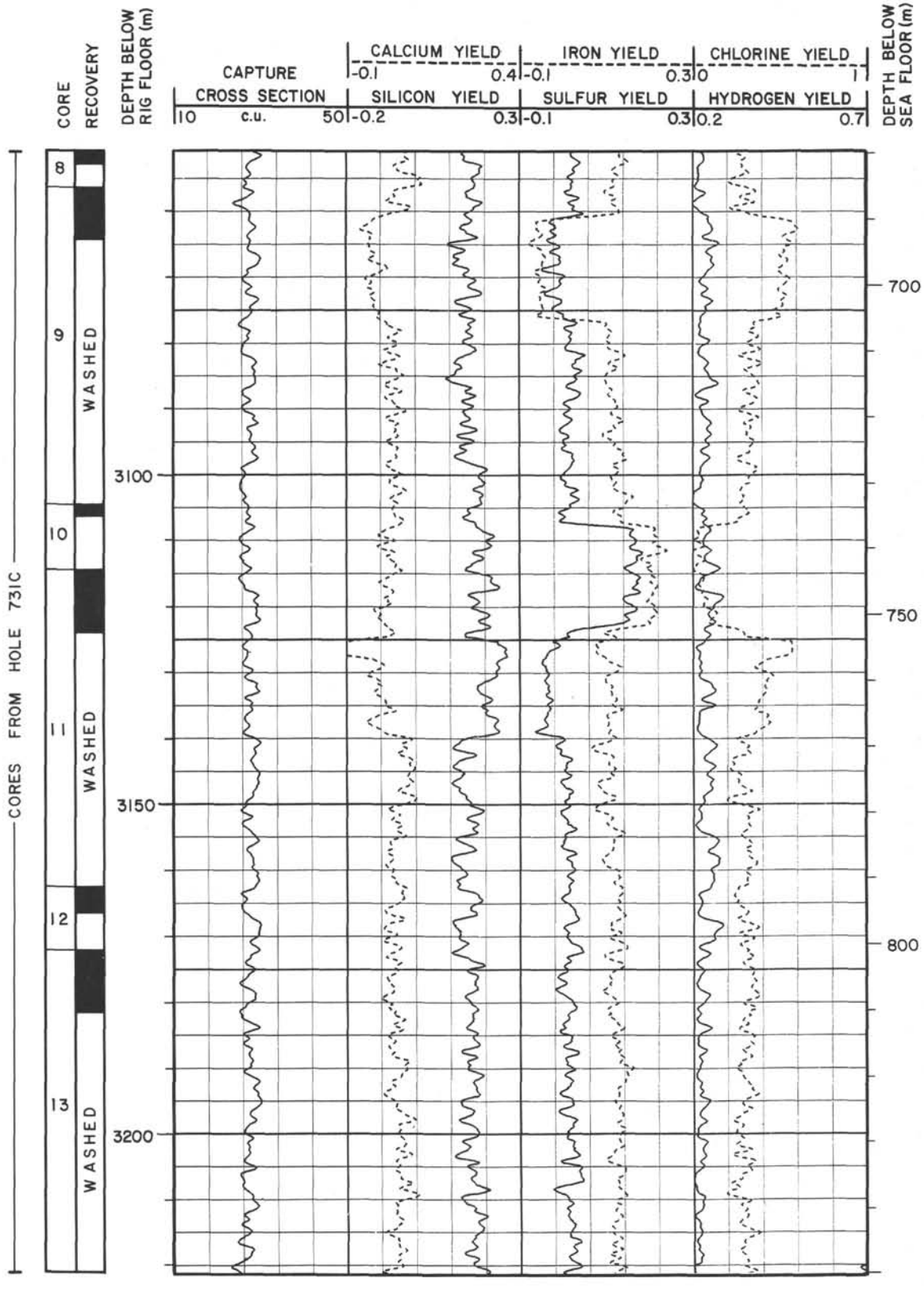

Summary Log for Hole 731C (continued)